Dynamic Control of Translation During Adult Neurogenesis

Dissertation

submitted to the

Combined Faculties for the Natural Sciences and for Mathematics of the Ruperto-Carola University of Heidelberg, Germany

for the degree of

Doctor of Natural Sciences

Presented by
Avni Baser

Dissertation

submitted to the

Combined Faculties for the Natural Sciences and for Mathematics of the Ruperto-Carola University of Heidelberg, Germany

for the degree of

Doctor of Natural Sciences

presented by

M.Sc. Avni Baser

born in Cayiralan/Turkey

Oral Examination: 18.05.2017

Dynamic Control of Translation During Adult Neurogenesis

Referees:
Prof. Dr. Ana Martin-Villalba
Dr. Aurelio Teleman

Abstract

Neurons are highly compartmentalized into specific functional units including dendrites, axons and somas. While most messenger RNAs (mRNAs) are constantly used to produce proteins, a subset will remain translationally silent and targeted to aforementioned subcellular structures in order to be available "on demand" upon intra- and extracellular signals. This uncoupling of general availability of mRNAs from actual translation into proteins facilitates immediate response to environmental changes without involving signaling to the soma, which may be far away from axon endings. Furthermore, this way cells avoid excess production of proteins, which is the most energy consuming process within the cell.

Adult neural stem cells (NSCs) reside in a thin layer lining the lateral ventricles of the brain and constantly produce progeny that migrates to the olfactory bulb and differentiates into several subtypes of interneurons. Their gene expression has been intensively studied using RNA-based technologies, assuming that mRNA availability readily translates into protein abundance. Whether there is indeed a linear relationship and to which level it is maintained during state transitions throughout neurogenesis has been elusive.

Here we studied both global- and transcript-specific translation over multiple stages of neurogenic differentiation. We uncovered dynamic changes of global protein synthesis peaking at stages of proliferation and neuronal integration. Further, using RiboTag mouse models, we showed that transcript abundance and its ribosome-binding shows highest linearity in NSCs that becomes increasingly divergent with the progression of differentiation. NSCs' transition to early neuroblasts involves translational repression of a subset of mRNAs including both multiple members of the protein synthesis machinery as well as the key pluripotency factor Sox2. *In silico* motif analysis within this cluster of transcripts led to identification of a pyrimidine-rich motif (PRM) that predicts sensitivity of their translation to the activity of mammalian target of rapamycin complex 1 (mTORC1). Indeed, pharmacological inhibition of mTORC1 reduced ribosome binding of PRM-containing transcripts, while PRM-free transcripts were not affected.

Together, this data provides a comprehensive view on the dynamic control of translation during neurogenic differentiation *in vivo* and uncovers a post-transcriptional mechanism that allows fast and robust repression of pluripotency factors in NSCs as they differentiate.

Zusammenfassung

Während die Mehrheit der messenger RNAs (mRNAs) in Neuronen kontinuerlich zu Proteinen translatiert wird, gibt es einen Teil der "auf Abruf" bereit steht. Diese mRNAs werden zu subzellulären Strukturen (z.B. Axonen) transportiert um spezifisch als Reaktion auf intra- und extrazelluläre Signale translatiert zu werden. Diese Entkopplung von mRNA-Verfügbarkeit und Translation ermöglicht zelluläre Reaktion ohne die Notwendigkeit von Signalen zum Zellkörper, welcher fernab der Axon-Enden sein kann. Zudem wird so die Überproduktion von Protein verhindert, was wichtig ist, da der Prozess der Proteinsynthese den höchsten Energieverbrauch innerhalb der Zelle aufweist.

Adulte neurale Stammzellen (NSCs) befinden sich in der subventrikulären Zone der lateralen Ventrikel innerhalb des Gehirns. Sie produzieren kontinuierlich Vorläuferzellen welche zum Bulbus olfactorius wandern um sich dort in Interneurone zu differenzieren. Die Genexpression von NSCs wurde intensiv mithilfe von RNA basierenden Technologien studiert, in der Annahme dass mRNA-Verfügbarkeit stark mit Protein Translation korreliert. Inwiefern es dahingehend wirklich ein lineares Verhältnis in NSCs gibt und ob es während neuronaler Differenzierung aufrechterhalten bleibt ist unbekannt.

In dieser Studie wurde die globale- und Transkript-spezifische Translation während mehrerer Stadien neuronaler Differenzierung untersucht. Level globaler Proteinsynthese waren dynamisch und erreichten ihren Höhepunkt in Stadien hoher Proliferation und neuronaler Integration. Mithilfe von RiboTag-Mausmodellen konnte gezeigt werden dass mRNA-Verfügbarkeit und Ribosom-Assoziation in NSCs eine starke Korrelation aufweisen, die jedoch mit zunehmender Differenzierung kontinuierlich abnimmt. Der Übergang von NSCs zu Neuroblasten wies translationale Repression einer Gruppe von mRNAs auf, welche unter anderem den wichtigen Stammzell-Faktor Sox2 beinhaltet. *In silico* Motivanalyse innerhalb der reprimierten Transkripte führte zur Identifizierung eines Pyrimidin-reichen Motivs (PRM), welches die Empfindlichkeit ihrer Translation gegenüber mTORC1-Aktivität bestimmt.

Zusammengefasst gibt diese Studie einen umfassenden Überblick über die dynamische Kontrolle von Proteintranslation während neurogener Differenzierung und identifiziert einen post-transkriptionellen Mechanismus, welcher schnelle und robuste Repression von Stammzell-Faktoren in differenzierenden NSCs ermöglicht.

Acknowledgements

While writing the last words of this thesis, I am still having a hard time to realize that this intense period is approaching an end. So many people have crossed my path and I am grateful for every single encounter. Every day was full of new challenges, which helped me to grow both personally and professionally. So many thanks to everybody who adviced me, allowed me to use their cell culture medium when I was too lazy to prepare it on a Sunday night or just simply enjoyed a beer with me after (or sometimes during) working hours. You all contributed to this work and I am proud of what we achieved together.

I want to thank my supervisor Ana Martin-Villalba for coaching, mentoring and supporting me in any possible way. You always believed in me and our project and kept everything on track. Thanks for being strict when you needed to be, but providing the space and freedom that we all need to develop as scientists.

I would like to thank Bernd Fischer for all the work we did together in the last year. It makes me very sad that you will not be around to harvest the fruits of our efforts. You will be missed.

I would also like to thank the members of my thesis committee Aurelio Teleman, Matthias Hentze and Georg Stoecklin for their valuable suggestions during this project, as well as Lazaro Centanin for taking the time to join my examination committee.

Thanks to everybody in the lab for creating a welcoming, supportive and fun environment. Most of you became close friends with whom I enjoyed working, discussing and sometimes argueing, knowing that at the end of the day nobody will hold grudges. I am sure that our friendship will last beyond this chapter of our lifes.

Thank you Enric for sharing your passion for science with me. Our endless discussions kept me motivated and helped me to become a better scientist. I feel lucky that I had the opportunity to work with you. Thank you Damian for always being excited about my experiments and constantly reminding me about the importance of proper controls. Thanks George for being supportive in any life situation, for being an honest friend, for not being mad at me for longer than necessary after our little disputes and fixing the office basketball whenever it was broken. Thank you Si for helping wherever you can and softening my worries whenever I was overthinking something again. Not to forget about your great efforts to get our money back from Lufthansa and taking care of Lab presents

when I got tired of it. Thanks Wilson for all the late-night discussions, encouraging me whenever experiments did not work and sharing your wisdom about the fractionator. Thanks to Liang for setting high standards, which I tried hard to meet. Thanks Manari for the delicious Greek food and being there as a friend. Thank you Sascha for your positive energy entertaining everybody with your hilarious laughter. Thank you Alex for your experimental support, your immense motivation and all the football talk. Thanks Maxim for not hesitating to share your huge knowledge on translation and always being honest about what you are thinking about my experiments. Thanks Gülce for giving me an opportunity to practice my Turkish on daily basis. Thank you Sheng for your bioinformatic support and keeping up your professional attitude until the very last working day. Big thanks to Steffi, Klara and Katrin for never hesitating to help wherever you can and kicking my a** when it was necessary. Thanks to Yonglong for finishing what I have started. I wish you all the best for this and I am sure you will do fine. Thanks Kiko for beating George at office basketball, it was fun to watch him lose. Thanks to Janina for probably the best chocolate brownies I ever had. Big thanks to Irmgard and Suse who helped in any organizational matter, making this part of our job very easy. I also want to thank Robert, Frederik, Alvaro, Gonzalo, Melanie, Nadine, Marko, Sabrina, Desiree, David, Moritz, Manuel, Daniel and Jan for their contributions.

I am deeply thankful to my family who has always supported me unconditionally and motivated me to reach my goals. Thank you for giving me the freedom I needed and always having trust in my decisions.

Last, but most importantly, I want to thank Melli. For being the person, who knows me the best. For day by day listening to the same Lab stories without complaining a single time. For always being supportive even when you thought I was wrong. For being so patient with me in any matter. I feel so lucky to have you in my life and I am looking forward to be by your side, every day.

Table of Contents

1. Introduction **1**
1.1 Neural stem cells in the adult brain 1
1.2 Eukaryotic translation 3
1.3 Stem cells, the role of protein synthesis and the relation to cellular metabolism 4
1.4 Ribosome biogenesis and global translational control in stem cells 5
1.5 Specific translation of cell fate regulators by RNA-binding proteins 7
1.6 Translational control in neurons 8
1.7 Role of mTOR signaling in global- and transcript specific protein translation 10
1.8 Novel methods to study protein synthesis *in vivo* 12
1.9 Objectives of this study 15

2. Materials & Methods **16**
2.1 Materials 16
2.1.1 Chemicals and reagents *16*
2.1.2 Buffers, solutions and media *18*
2.1.3 Antibodies and related products *20*
2.1.4 Primers and Probes *21*
2.2 Methods 22
2.2.1 Animal experiments *22*
2.2.2 Histology and cell biology *25*
3.2.3 Molecular biology *27*
2.2.4 Cell culture *31*
2.2.5 Imaging *31*
2.2.6 Statistics *32*
2.2.7 Computational analysis *32*

3. Results **34**
3.1 Measuring protein synthesis during adult neurogenesis 34
3.1.1 Systemic administration of OPP *34*
3.1.2 Direct administration of OPP to the brain *37*
3.1.3 In vitro application of OPP *41*
3.1.4 Quantification of protein synthesis during neurogenesis using OPP *42*
3.2 Measuring transcript-specific protein synthesis during adult neurogenesis 45
3.2.1 RiboTag strategy for parallel assessment of cell-type specific transcriptome and translatome *45*
3.2.2 Histological characterization of target populations *47*
3.2.3 Detailed composition of TiCRY labeled NSCs *50*
3.2.4 HA-tag incorporation into translating ribosomes of isolated NSCs *51*
3.2.5 FACS-mediated isolation of cells for total RNA sequencing *54*
3.2.5 RiboTag-mediated isolation of ribosome-associated transcripts *56*
3.2.6 Assessment of transcriptome and translatome by next generation sequencing *58*
3.2.7 Integrated Analysis of Transcriptome vs. Translatome During Lineage Progression *61*
3.2.8 SOX2 expression is post-transcriptionally repressed in ENBs *64*
3.2.9 Temporal repression is mediated by 5' pyrimidine-rich motifs and mTORC1 activity *68*
3.2.10 Translational uncoupling in NSCs upon brain injury *72*
3.2.11 Contribution of RNA-binding proteins to translational uncoupling *74*

4. Discussion **78**
4.1 Global protein synthesis in stem cells and their progeny 78
4.1.1 Cellular differences in protein synthesis – what does it matter? *78*
4.1.2 Proliferation and protein synthesis – like the chicken and the egg? *80*
4.1.3 Translational arrest in neuroblast – initiating differentiation? *80*

4.1.4 Protein synthesis in neurons – subtype dependent? ... *81*
4.2 Transcript-specific regulation of protein synthesis ... 82
4.2.1 Advanced RiboTag strategy unveils translational control ... *82*
4.2.2 Translation in NSCs – homeostasis vs. brain injury ... *83*
4.2.3 Progressive uncoupling with maturation – translational control as a neuronal feature? ... *85*
4.2.4 Definitive exit from pluripotency – by mTORC1 and PRMs? ... *86*
4.2.5 Translational block and release of Sox2 – roles outside of stem cells? ... *87*
4.2.6 The role of RNA-binding proteins within the neural lineage ... *88*
4.3 Concluding remarks ... 90

5. Supplements ... **91**
5.1 *De novo* motif analysis ... 91

6. References ... **93**

List of Figures

Figure 1 Adult neurogenesis in the subventricular zone

Figure 2 Process of protein biosynthesis in eukaryotes with main regulatory nodes

Figure 3 Overview of translational regulation taking place in the NSC lineage

Figure 4 Localized translation uncouples RNA abundance and protein synthesis

Figure 5 Links between mTORC1 signaling and the translation machinery

Figure 6 Classical and novel tools to address transcript-specific protein translation

Figure 7 OPP does not cross the blood brain barrier after intraperitoneal injection

Figure 8 Alternative routes of administration for OPP

Figure 9 Low OPP diffusion when injected directly into the CNS

Figure 10 Whole mount staining of the SVZ after intraventricular OPP injection

Figure 11 OPP incorporation of primary NSCs after acute exposure to IFN-γ

Figure 12 Global protein synthesis is highly dynamic during neurogenesis

Figure 13 Protein synthesis continuously drops at late stages of neurogenesis

Figure 14 RiboTag mouse models target stages of neuronal differentiation

Figure 15 Labeled NSCs continuously develop to neuroblasts

Figure 16 Histological characterization of RiboTag mouse models

Figure 17 Composition of Tlx-labeled NSCs based on FACS

Figure 18 Incorporation of HA-tag into translating ribosomes

Figure 19 Sorting of cells based on eYFP expression

Figure 20 Evaluation of HA-tag-based RNA-IP by enrichment analysis

Figure 21 Analysis of transcriptome and translatome based on single marker genes

Figure 22 Differential expression analysis for RNAseq & RIBOseq over stage-transitions

Figure 23 Stage-specific repression and enhancement of transcripts

Figure 24 Temporal interplay of transcription & translation during lineage progression

Figure 25 SOX2 Is post-transcriptionally repressed in ENBs

Figure 26 SOX2 translation effiency progressively drops from NSCs over NPCs to ENBs

Figure 27 SOX2 is highly expressed in a subpopulation of olfactory bulb interneurons

Figure 28 Pyrimidine-rich motifs in the 5′ UTR predict translational repression

Figure 29 Sucrose gradient fractionation of NSCs after Torin1 treatment

Figure 30 IHC for phosphorylation of ribosomal protein S6 indicating mTORC1 activity

Figure 31 Transcriptional and translational response of NSCs to brain injury

Figure 32 Correlation of translational regulation and presence of RBP-binding sites

Figure 33 Summary of global- and transcript-specific translation during neurogenesis

List of Tables

Table 1 Chemicals and reagents

Table 2 Buffers/solutions/media and their composition

Table 3 Antibodies used for FACS

Table 4 FACS-associated reagents

Table 5 Primary antibodies for IHC/ICC, western blot and immunoprecipitation

Table 6 Secondary antibodies used for IHC/ICC

Table 7 Primers used for qRT-PCR

Table 8 Probes used for *in situ* hybridization

Table 9 Primers used for genotyping of transgenic mice

Table 10 Transgenic mouse lines used in this study

Table S1 Overrepresented motifs in transcripts repressed in ENBs

Abbrevations

Abbrevation	Description
aNSCs	active neural stem cells
BAC	bacterial artificial chromosome
BSA	Bovine serum albumin
CHX	cycloheximide
CLIP	crosslinking IP
CNS	central nervous system
CSF	cerebrospinal fluid
DCX	Doublecortin
DiCRY	Dcx-inducible Cre Rpl22 eYFP (mouse line)
DNA	deoxyribonucleic acid
dpi	days post induction
EDTA	ethylenediaminetetraacetic acid
EDU	5-ethynyl-2´-deoxyuridine
eIF	eukaryotic initiation factor
EN	early neuron
ENBs	early neuroblasts (SVZ)
ENCODE	Encyclopedia od DNA elements
eYFP	enhanced yellow fluorescent protein
FACS	fluorescence-associated cell sorting
FDR	False discovery rate
GO	gene ontology
ICC	immunocytochemistry
ICH	immunohistochemistry
IFN-γ	interferon-gamma
IP	immunoprecipitation
ISH	*in situ* hybridization
kDA	kilodalton
LNBs	late neuroblasts (OB)
mRNA	messenger RNA
mTOR	mammalian target of rapamycin
NBs	neuroblasts
NPCs	neurogenic progenitor cells
NSCs	neural stem cells
OB	olfactory bulb
OPP	O-propargyl-puromyin
PFA	Paraformaldehyde
PRM	pyrimidine-rich motif
qNSCs	quiescent neural stem cells
RBP	RNA-binding protein
RMS	rostral migratory stream
RNA	ribonucleic acid
SVZ	subventricular zone

continued

TAM	tamoxifen
TiCRY	Tlx-inducible Cre Rpl22 eYFP (mouse line)
Tlx	Tailless
TOP	terminal oligopyrimidine motif
TPM	tags per million reads
TRAP	translating ribosome affinity purification
UTR	untranslated region
veh	vehicle-treatment
wpi	weeks post induction

1. Introduction

Parts of this introduction have been previously published (Baser et al., 2017) in an open-access journal and have been originally written by myself.

1.1 Neural stem cells in the adult brain

First postulated by Joseph Altman in the 1960s, neural stem cells (NSC) are today well established in maintaining brain homeostasis in multiple regions of the adult brain (Altman and Das, 1965). The subventricular zone (SVZ) represents the largest neurogenic niche, however NSCs are also present in the hippocampal dentate gyrus and to a lesser extent in the hypothalamus (Bond et al., 2015; Ming and Song, 2011).

The SVZ resides in the walls of the lateral ventricles and harbors radial glia like NSCs in a thin layer between ependymal cells (Figure 1). These cells constantly produce amplifying progenitors, which are mostly neurogenic and differentiate into neuroblasts (NBs) that migrate over a predetermined route, the rostral migratory stream, to the olfactory bulb. After arriving in the olfactory bulb, a fraction of these cells specifies into several classes of inhibitory interneurons, produces functional connections and ultimately integrates into the olfactory network. However, the majority of these cells do not survive, presumably due to the low levels of neuronal activity they receive (Petreanu and Alvarez-Buylla, 2002). The different stages of neuronal development are characterized by varying marker expression, which can be used to identify cells both *in situ* as well as after isolation from the tissue (Figure 1).

Position, morphology and multipotent potentials of adult NSCs closely resemble radial glia cells, the stem cells of the embryonic brain. It was suggested for a long time that adult NSCs might originate in embryonic cells, which last into adulthood. Performing elegant tracing experiments, two recent studies show that indeed a subset of neural progenitors become quiescent early during development and get reactivated postnatally (Fuentealba et al., 2012; Furutachi et al., 2015). Interestingly, loss of quiescent NSCs at embryonic stages impaired the maintenance of NSCs into adulthood (Furutachi et al., 2015). In adult life, quiescent (non-cycling) and activated (cycling) NSCs coexist both in the SVZ (Calzolari et al., 2015; Codega et al., 2014) as well as in the hippocampal dentate gyrus (Bonaguidi et al., 2011; Encinas et al., 2011).

While embryonic stem cells show unrestrained multipotency, their adult counterparts are characterized by very defined developmental programs, showing little plasticity during homeostasis. SVZ-NSCs are organized in domains and are restricted in their potential to create certain subtypes of neurons in the OB (Merkle et al., 2007; 2014). Only during dramatic environmental changes, demonstrated in several paradigms of brain injury, NSCs deviate from their original specifications and produce neuron subtypes which they do not produce under regular conditions (Arvidsson et al., 2002; Lindvall et al., 2004).

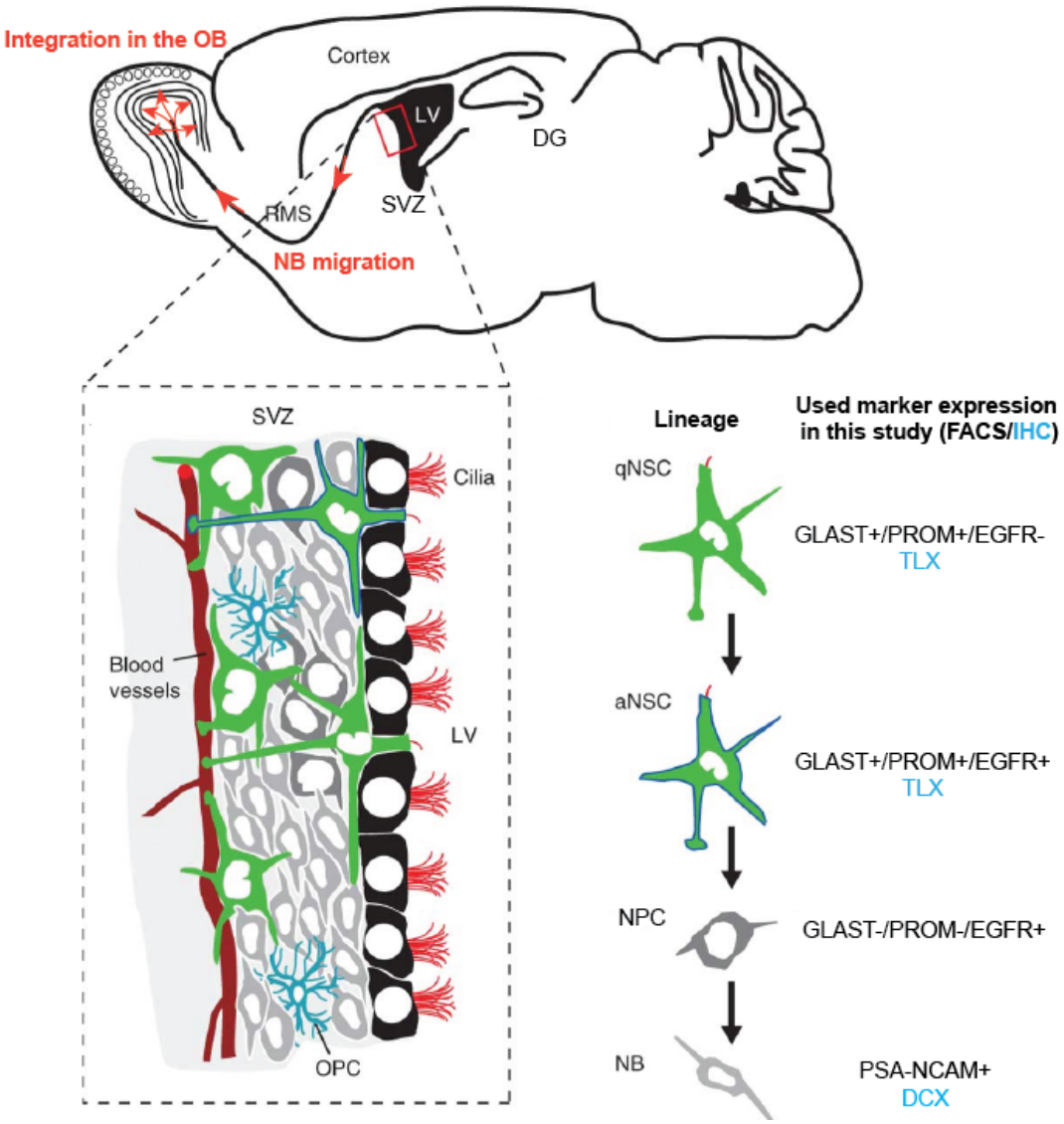

Figure 1: Adult neurogenesis in the subventricular zone. Quiescent- and active NSCs that reside in the SVZ produce amplifying neurogenic progenitor cells (NPCs), which differentiate into neuroblasts (NB) and supply the olfactory bulb (OB) with newborn interneurons. FACS: fluorescence-associated cell sorting, IHC: immunohistochemistry. LV: lateral venricle, OPC: oligodendrocyte progenitor cells, DG: dentate gyrus of the hippocampus. Modified from Fischer et al. (2011).

Taken together, SVZ-NSCs represent an excellent model system to study neuronal development both during homeostasis as well as brain injury.

1.2 Eukaryotic translation

The process of protein synthesis from existing messenger RNAs (mRNA), known as translation, is highly conserved over eukaryotic species and can be divided into the steps of initiation, elongation, termination and recycling. The initiation step is generally considered to be the rate-limiting step (Livingstone et al., 2010). Under homeostatic conditions, most protein synthesis is mediated over initial binding of the translation machinery to the 5′ cap of the untranslated region (UTR) of the messenger RNA (mRNA). This process is known as cap-dependent translation, in contrast to cap-independent translation, which bypasses scanning of the 5′ UTR.

Translation of each mRNA molecule starts with the formation of the 43S complex, comprising the 40S ribosomal subunit, the associated initiation factors eIF1, eIF1A, eIF3, eIF5, and the ternary complex formed by initiation factor eIF2, guanosine triphosphate and the initiator tRNA (eIF2-GTP-tRNA$^{Met}_{i}$, Figure 2). The 40S subunit is either directly recycled from the previous round of translation or generated from the pool of free subunits. Initiation factors eIF1, 1A and 3, upon association with 40S subunits, triggers the attachment of the ternary complex, thereby completing the 43S formation. The 5′ cap of the mRNA is prepared by addition of the initiation factor eIF4F via its cap-binding subunit eIF4E. Two other constituents of eIF4F are the scaffold protein eIF4G and the RNA helicase eIF4A. The 43S complex binds the cap of the mRNA and scans the 5′ UTR till it encounters the start codon that is usually the first AUG in a particular context (so-called Kozak context: GCC(A/G)CCAUGG). Upon recognition of the correct AUG by the initiator tRNA^{Met} anticodon, structural rearrangements of the 43S complex causes hydrolysis of eIF2-associated GTP and its dissociation, which leads to formation of the 48S complex. Another GTPase eIF5B, also activated by the start codon recognition, is responsible for the joining of the 60S subunit to the 48S and ultimately forming the 80S complex that begins synthesis of the encoded protein during elongation. Aminoacyl-tRNAs with anticodons complementary to corresponding codons in the A site of elongating ribosomes, are delivered by elongation factor eEF1A, while eEF2 stimulates ribosome translocation upon completion of the peptidyl-transferase reaction. Translation terminates when ribosomes reach the stop codon and two releasing factors eRF1 and eRF3 stimulate complete

dissociation of ribosomes from mRNAs. Recycled 40S subunits could again enter a new translation cycle at the 5′ end of the same or a different mRNA.

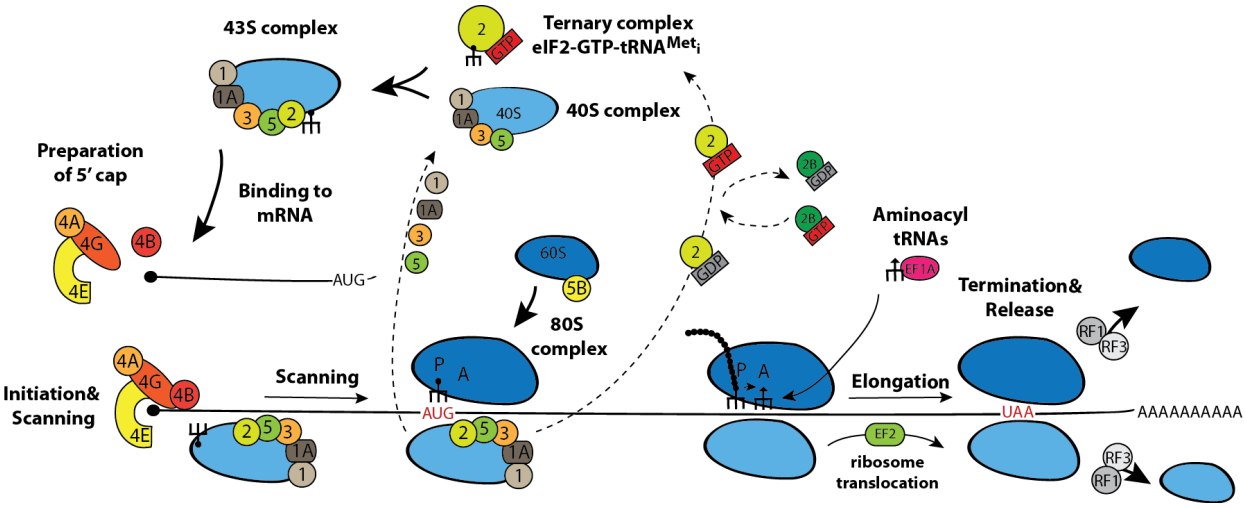

Figure 2: Process of protein biosynthesis in eukaryotes with main regulatory nodes. Basic steps of translation beginning from the formation of the ternary complex, formation of the 43S complex, which, after loading onto an mRNA, scans the untranslated region (UTR) until recognition of the start codon (AUG) resulting in the 48S complex assembly. 60S subunit joins and newly formed 80S ribosomes proceed to elongation moving along the coding sequence until the stop codon appears in the acceptor A site of the ribosomes. This starts up the process of termination and recycling, releasing 40S and 60S ribosomal subunits for a new round of translation on the same or another mRNA molecule. Numbered molecules indicate eukaryotic initiation factors (eIFs). From Baser et al. (2017).

1.3 Stem cells, the role of protein synthesis and the relation to cellular metabolism

Single cell transcriptomes of NSCs revealed that they are not clearly separated into distinct populations of quiescent and activated NSCs, but progress through multiple intermediate stages before amplification and differentiation (Llorens-Bobadilla et al., 2015; Shin et al., 2015). One major hallmark of NSC activation is transcriptional upregulation of factors critical for the protein synthesis machinery. Consequently, dormant NSCs (the most quiescent NSCs) show a particularly low level of protein translation, whereas progressive activation leads to increased global translation levels (Figure 3). Maintaining low protein synthesis levels was suggested to be of key importance for stem cell functions since deletion of PTEN, a negative regulator of PI3K/AKT signaling, in hematopoietic stem cells led to exhaustion of the stem cell pool and loss of stem cell-mediated reconstitution of the hematopoietic system after irradiation (Signer et al., 2014). Similarly, PTEN deletion in NSCs induces their terminal astrocytic differentiation and stem cell depletion in the hippocampal dentate gyrus (Bonaguidi et al., 2011).

Protein biosynthesis is the most energy consuming cellular process and its regulation has a considerable impact on the total cellular metabolism (Buttgereit and Brand, 1995; Rolfe and Brown, 1997). Neural stem cells mostly rely on glycolysis and the pentose phosphate pathway as their primary source of energy production, whereas mitochondria based oxidative phosphorylation emerges with differentiation (Candelario et al., 2013). Stem cells reside mostly in hypoxic niches, which restrict oxidative processes to avoid accumulation of reactive oxygen species (ROS). Activation and proliferation of NSCs promotes the generation of ROS, which can directly act as signaling molecules to activate the differentiation program (Khacho et al., 2016). Together, quiescent stem cells feature low levels of oxidative processes. This changes with proliferation and differentiation in order to adjust to the growing demand for energy.

1.4 Ribosome biogenesis and global translational control in stem cells

Ribosomes and other major components of the translation machinery are essential for even the most simple form of life (Hutchison et al., 2016). Due to the high abundance and conservation over all species, these factors are assumed to have mostly housekeeping functions and not to be involved in making cellular decisions. However, recent evidence points into a direction where the control of ribosome biogenesis and their effect on global translation levels can change cellular behavior. Particularly in the complex case of stem cells, which need to maintain a sensitive balance between quiescence, self-renewal and differentiation, this level of regulation is of utmost importance. Ribosomal DNA (rDNA) transcription produces ribosomal RNA (rRNA), which is the major component of ribosomes. A high level of rDNA transcription is a feature of stem cells and is downregulated in their progeny. Recently, a causal link between rDNA transcription and cellular behavior was shown in female drosophila germ line stem cells. Here, manipulation of rDNA transcription by upregulation of Pol1 delays differentiation, while reduction of rRNA production triggers cyst formation (=differentiation) (Zhang et al., 2014). Interestingly, translation rates in mammalian HSCs are lower than in any other more differentiated stage, independently of the rate of rDNA transcription (Signer et al., 2014). This indicates that generation of ribosomes can but does not necessarily lead to higher protein synthesis, demonstrating the need for additional components of the translation machinery.

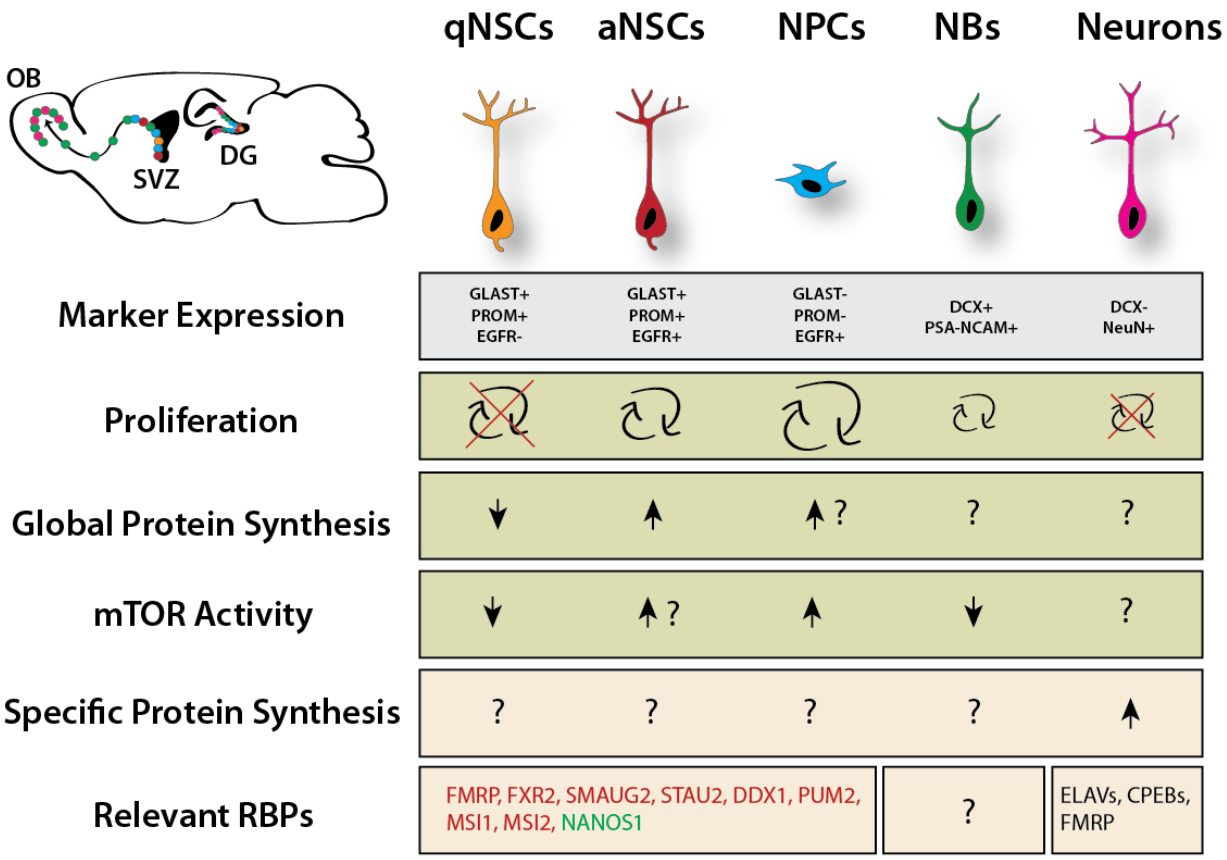

Figure 3: Overview of translational regulation taking place in the NSC lineage. Arrows represent relative estimation compared to other stages within the lineage. Question marks indicate unknown situation and are in part subject of this thesis. Question marks next to arrows indicate likely scenario based on proliferation rate, however not experimentally proven. Green colored RBPs are pro-neurogenic, red colored RBPs are anti-neurogenic. qNSC: quiescent NSC, aNSC: active NSC, NPC: neurogenic progenitor cells, NB: neuroblast. Modified from Baser et al. (2017).

As mentioned before, molecular characterization of NSCs on the single cell level groups them into four stages, which show varying levels of expression of ribosomal proteins (Llorens-Bobadilla et al., 2015; Shin et al., 2015). These four activation stages show progressive increase in transcription of ribosomal genes and global protein synthesis levels. Since activation ultimately leads to cell division, the question arises whether higher protein synthesis levels actually trigger division or are rather the consequence of cellular decision on a different level. For example, loss of the transcription factor Runx1 in HSCs leads to decreased protein synthesis and higher stress response, outcompeting wild-type HSCs (Cai et al., 2015). This study demonstrates a direct link between the regulation of transcription and translation.

Together, increased biogenesis of ribosomes by increased transcription of rRNA and ribosomal proteins often correlates with a proliferative status of stem cells (Figure 3). Whether there is a causal link placing regulation of the translation machinery on top of the

hierarchy of cell division decisions remains controversial and might be different between different stem cell systems.

1.5 Specific translation of cell fate regulators by RNA-binding proteins

Whereas the regulation of global translation levels for cell fate decisions is an emerging topic of interest, the translational control of specific cell fate modulators is a well-established concept for various molecules in multiple stem cell systems. Cells use a large repertoire of tools to post-transcriptionally control gene expression, including RNA-binding protein (RBPs) and microRNAs (miRNAs). RBPs are involved in a plethora of processes including alternative splicing, RNA processing, nuclear export, mRNA stability and translation (Ye and Blelloch, 2014). Particularly in highly polarized cells like neurons, RBPs help to locally and spatially regulate translation efficiency and successfully integrate environmental signals (Jung et al., 2012). The following examples illustrate the impact of RBPs on the development of neurons.

The best-studied RBPs in the NSC field are probably the family of musashi proteins (Msi). Musashi1 (Msi1) and its homolog Musashi2 (Msi2) play an important role in neural development across vertebrates and invertebrates (Okano et al., 2005). Both Msi proteins are highly expressed in the fetal and adult brain and enriched in the proliferative zones of the ventricular and subventricular zone. Single knockout of Msi1 only has a minor NSC phenotype while double knockout of Msi1/Msi2 significantly decreases neurosphere-forming capacity of NSCs (Sakakibara et al., 2002). There are multiple ways of action described for Musashi proteins. However, the most canonical function is mediated over two RNA recognition motifs. One of the most important targets is the Notch pathway component Numb. Musashi binds at certain motifs in the 3′ UTR (usually enriched for GUAG or UAG), leading to downregulation of Numb expression and subsequent activation of Notch signaling. Notably, Notch signaling is a well-known inhibitor of NSC differentiation (Pierfelice et al., 2011) and pharmacological inhibition of Notch signaling in freshly isolated quiescent NSCs leads to activation and increased protein synthesis (Llorens-Bobadilla et al., 2015).

In a hallmark study from 2014, Yang and colleagues describe a complex encompassing the well-known initiation factor eIF4E1, its binding partner 4E-T and multiple proneurogenic mRNAs, which regulates the generation of neurons in the embryonic brain (Yang et al.,

2014). The associated transcripts include the proneurogenic neurogenin and neurod family members. This complex is dynamically assembled and disassembled during development in order to avoid premature production of neurons. Disruption of the complex causes enhanced neurogenesis and precursor depletion. It is hypothesized that 4E-T most likely identifies target mRNAs for recruitment to cellular storages, including P body-like granules.

These examples illustrate that RBPs are usually negative regulators of NSC differentiation through repression of target transcripts, which is often driven by direct binding to regulatory motifs in the untranslated regions. Neural progenitors often use RBPs to fine-tune gene expression of factors critical for differentiation. This way, cells ensure proper balance between differentiated and undifferentiated cells and therefore correct expansion of the central nervous system. There is evidence that multiple RBPs have similar functions, just varying in their repertoire of target molecules. In fact, several of the aforementioned RBPs are found in P body-like granules, suggesting that RBPs might act cooperatively. In this line, it was shown that only an intact complex of the RBPs Staufen2, Pumilio2 and DDX1 regulates the balance of stem cell maintenance versus differentiation in the developing brain (Vessey et al., 2012).

1.6 Translational control in neurons

There are two ways to accomplish high abundance of proteins at specific cellular structures. Proteins can be actively transported after complete assembly and correct folding, or locally translated from mRNAs, which can be released from repressive complexes. The latter is providing economical advantages, since many copies of proteins can be made from a single mRNA. Additionally, proteins would not accumulate in other parts of the cell during transport, which could have undesirable consequences. Information about subcellular destination of mRNAs can be coded in their untranslated regions, providing another complex level of regulation.

Neurons are highly polarized cells characterized by large distances between the nucleus, the active site of mRNA transcription, and the axon terminals, which transmit information to neighboring neurons. Unlike the former view that axons are pure transmitters of signal, today it is well known that similar to dendrites, axons receive multiple signals from the environment (Figure 4). Developing axons integrate environmental signals for growth,

navigation and synapse formation, while in mature axons signals support maintenance of axonal integrity and repair after damage (Holt and Schuman, 2013; Jung et al., 2012).

Repression of mRNAs is often mediated by formation of RNA granules, intermediate RNA-protein complexes that harbor repressed mRNAs, together with their trans-acting components including RNA-binding proteins (RBPs) and micro RNAs (Kiebler and Bassell, 2006). RNA granule assembly and disassembly can be regulated by external cues, leading to release of mRNAs and subsequent translation by local ribosomes. Specificity of RBPs to target mRNAs is mediated by multiple mechanisms. Fragile X mental retardation protein (FMRP), a regulator of synaptic plasticity, recognizes target mRNAs by secondary structure (Melko and Bardoni, 2010), while repressors of the cytoplasmic polyadenylation element binding protein (Cpeb) family recognize a specific sequence element (Richter, 1999).

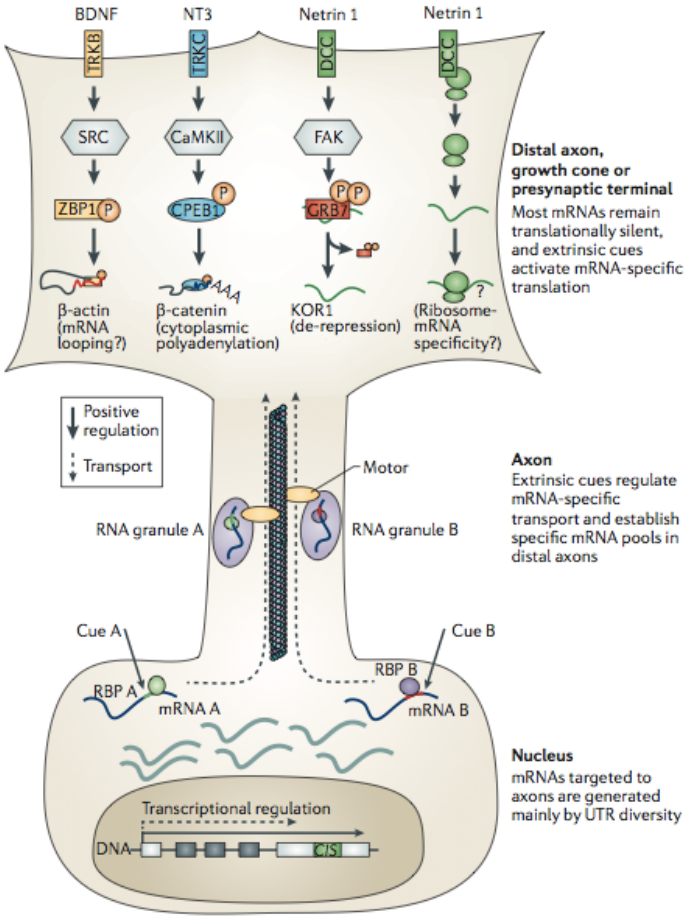

Figure 4: Localized translation uncouples RNA abundance and protein synthesis. Extrinsic cues, transmitted over membrane receptors, can activate translation of RNAs with specific properties. From Jung et al. (2012).

Together, multiple cis- and trans-acting elements control spatial- and temporal control of translation from mRNAs, allowing rapid reaction to environmental changes without involving signaling to the soma.

1.7 Role of mTOR signaling in global- and transcript specific protein translation

Protein synthesis is closely related to the nutritional status of cells. Growth-promoting or repressing signals are integrated by the mammalian/mechanistic target of rapamycin complex 1 (mTORC1), which controls protein synthesis via multiple downstream mediators (Dibble and Manning, 2013), Figure 5). The most important downstream effectors in the context of protein synthesis are the eukaryotic initiation factor 4E (eIF4E) binding proteins (4E-BPs) and the ribosomal S6 kinases (Ma and Blenis, 2009). Members of the 4E-BP family, when hypophosphorylated, interfere with the eIF4F complex assembly by binding to eIF4E and therefore preventing initiation of translation.

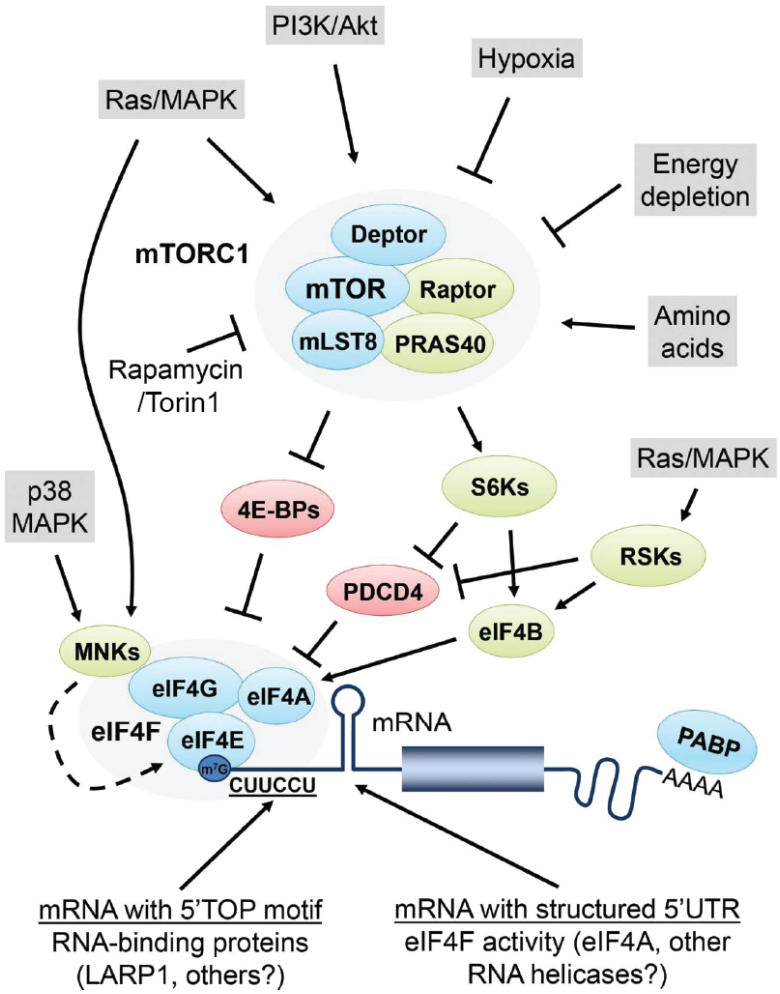

Figure 5: Links between mTORC1 signaling and the translation machinery. mRNAs with 5′ oligopyrimidine motifs (5′ TOP) or structured 5′ UTR are under special regulation. Modified from Nandagopal et al. (2015).

In active cells, mTORC1 phosphorylates 4E-BPs, releasing them from eIF4E and promoting initiation (Pause et al., 1994). Interestingly, cells react differently to mTORC1 inhibition, which might originate in different ratios of eIF4E and 4E-BP expression (Alain et al., 2012). mTORC1 also phosphorylates and activates S6 kinases, which in turn phosphorylate the ribosomal protein S6 and eIF4B, stimulating general translation (Holz et al., 2005). On top, S6 kinases phosphorylate and inactivate the eukaryotic elongation factor 2 kinase (eEF2K) which negatively affects protein synthesis via eEF2 phosphorylation (Wang et al., 2001).

While affecting the translation of all mRNAs by aforementioned global mechanisms, mTORC1 activity also selectively affects the translation of mRNAs with special features. There are mRNAs that contain long and structured 5′ untranslated regions (UTRs) coding for proteins involved in cell survival and proliferation (Dowling et al., 2010). The structured 5′ UTR makes these transcripts dependent on the unwinding activity of initiation factor eIF4A, a component of the eIF4F complex, increasing the sensitivity to eIF4E levels within the cell. eIF4A activity has been shown to be additionally regulated by phosphorylation of programmed cell death protein 4 (PDCD4) by S6 kinases (Figure 5).

Another group of transcripts, which is under the special control of mTORC1 activity, contain a terminal oligopyrimidine (TOP) motif at their 5′ end, making them particularly sensitive to mTORC1 inhibition (Jefferies et al., 1994; Thoreen et al., 2012). These transcripts are highly enriched for members of the translation machinery, including ribosomal proteins and initiation factors (Meyuhas, 2000). The 5′ TOP motif contains a cytosine at the penultimate position, which is followed by 4-14 pyrimidines. The special regulation of 5′ TOP mRNAs depends on the regulation of eIF4E by 4E-BPs, since deletion of 4E-BPs abolished the special regulation of these transcripts (Thoreen et al., 2012). Nevertheless, the exact mechanism of how the presence of these motifs affects mTORC1 sensitivity remains elusive. Over the years, several RNA-binding proteins were suggested to interact with 5′ TOP containing mRNAs in a sequence dependent or independent fashion, including La-related proteins 1 and 3 (LARP1/LARP3, (Cardinali et al., 2003; Tcherkezian et al., 2014)) and the stress granule associated proteins TIA1 and TIAR (Damgaard and Lykke-Andersen, 2011). It is likely that multiple mTORC1-associated components regulate the special sensitivity of 5′ TOP mRNAs in a cooperative manner.

1.8 Novel methods to study protein synthesis *in vivo*

Analysis of both, the transcriptome and translatome, has been mostly restricted to population studies, neglecting that tissue heterogeneity might cover individual contribution to the cellular proteome. The upcoming of next generation sequencing, coupled to identification of individual cells using fluorescence-associated cell sorting (FACS) and the use of sophisticated transgenic mouse lines allow today dissection of ultimate gene expression at high resolution. The following paragraphs introduce some of the current advancements, which in part have been used throughout this thesis.

Global rates of protein synthesis have been characterized using sucrose gradient fractionation experiments, but also by usage of the translation inhibitor puromycin, a tRNA homologue that incorporates into nascent proteins (Nathans, 1964). Recently the Salic lab developed a modified puromycin to detect nascent proteins with key advantages over existing methods (Liu et al., 2012). O-propargyl-puromyin (OPP) is a modified version of conventional puromycin that bears a terminal alkyne group that can be efficiently detected by fluorescence-coupled azide molecules. OPP is easy to use, robust, sensitive and both applicable for *in vitro* and in *vivo* studies. OPP massively extended our knowledge about protein synthesis levels in multiple stem cell systems both under homeostasis and stress conditions (Blanco et al., 2016; Llorens-Bobadilla et al., 2015; Signer et al., 2014).

Traditionally, the translational efficiency of individual transcripts has been assessed by its loading onto multiple ribosomes (polysomes). Their separation by sucrose gradient centrifugation and analysis by cDNA arrays allowed for the first time the comparison of global changes in transcription versus translation (Zong et al., 1999). This so-called translational state array analysis (TSAA) was applied to investigate the translational changes during differentiation of murine embryonic stem cells (Sampath et al., 2008). This data demonstrated that differentiation causes an anabolic switch that involves increasing transcript abundance, ribosome loading and global protein synthesis. Interestingly, some genes were only regulated on the translational level, demonstrating that mRNA levels can be a misleading readout of gene expression in certain cellular contexts.

The recent development of next generation sequencing techniques allows efficient production of sequencing libraries from minute amounts of mRNA at affordable rates (Adiconis et al., 2013). Thus, TSAA studies are no longer limited to available probe sets as in microarrays and now have much higher resolution. However, TSAA is still difficult to apply

in vivo, since tissues harbor heterogeneous cell populations that hampers interpretation of results. The study of specific cell populations requires cell sorting that potentially introduces artifacts, since improper sample handling can easily cause ribosome dissociation.

In order to overcome these difficulties, several mouse models have been established over the last years to investigate the ribosome-bound mRNA, called translatome (Figure 6). Translating ribosome affinity purification (TRAP) makes use of bacterial artificial chromosomes (BACs) introduced into a transgenic mouse model, which expresses a GFP-tagged variant of the ribosomal protein L10a in a defined cell population (Doyle et al., 2008; Heiman et al., 2008). Using several TRAP mouse lines, where tagged L10a was expressed under different specific promoters, it could be shown that morphologically indistinguishable neuronal subtypes display massive differences in translated genes (Heiman et al., 2008). These studies provided a resource of 16 transgenic BAC mouse lines targeting 24 subtypes of neurons – a valuable dataset to study the broad molecular spectrum of neurons (Doyle et al., 2008). Over the last years, additional TRAP lines were generated for various applications (Brichta et al., 2015; Zhang et al., 2016; Zhou et al., 2013). The TRAP methodology was originally generated to overcome technical limitations of neuronal cell sorting. FACS-mediated cell sorting of solid tissues can be difficult, especially in case of adult neurons, which are highly myelinated and have extensive processes within the brain.

TRAP is mainly limited by the availability of mouse lines. For every cell type of interest, a new transgenic line has to be generated and characterized, where (in the best case) an exclusive marker gene of this population is driving the expression of the ribosomal tag. This is laborious and a hindrance to its application to study multiple cell types *in vivo*. A parallel approach makes use of preexisting Cre-recombinase driver lines. In RiboTag mice, the endogenous Rpl22 protein, a ribosomal large subunit protein, is replaced with a HA-tagged variant that is driven by cell-type specific Cre-recombinase expression and allows isolation of ribosome-associated mRNA (Sanz et al., 2009). Both TRAP and RiboTag have been mostly used to study rare types of neurons in the brain, which are challenging to isolate by conventional methods.

While TRAP and RiboTag offer the great advantage of targeting ribosome-associated transcripts of a defined cell population *in vivo*, these techniques cannot completely

recapitulate ongoing translation since ribosomes can also "sit" on transcripts without active peptide synthesis. This ribosome stalling is considered to take place under certain conditions and can be addressed in great detail by ribosome profiling (Ingolia et al., 2009; 2011). Ribosome profiling is the deep sequencing of ribosome-protected mRNA fragments that are revealed by nuclease digestion. This method revolutionized the way we can look at ongoing translation, allowing the identification of novel open reading frames, the investigation of the number of ribosomes on certain transcripts, and the speed at which they are moving along the transcript under different conditions (Ingolia et al., 2011; 2014). Due to the high demand of input material, application of ribosome profiling on mouse tissue has so far been challenging. Gonzalez and colleagues have extended the methodology by doing ribosome profiling in combination with RiboTag mouse models (Gonzalez et al., 2014). This allowed detailed cell-type specific analysis of translational changes during glioma initiation. There are efforts to improve library preparation methods in order to do ribosome profiling from low input material, which will be crucial to understand ribosome behavior in specific subpopulations of cells in the brain (Hornstein et al., 2016).

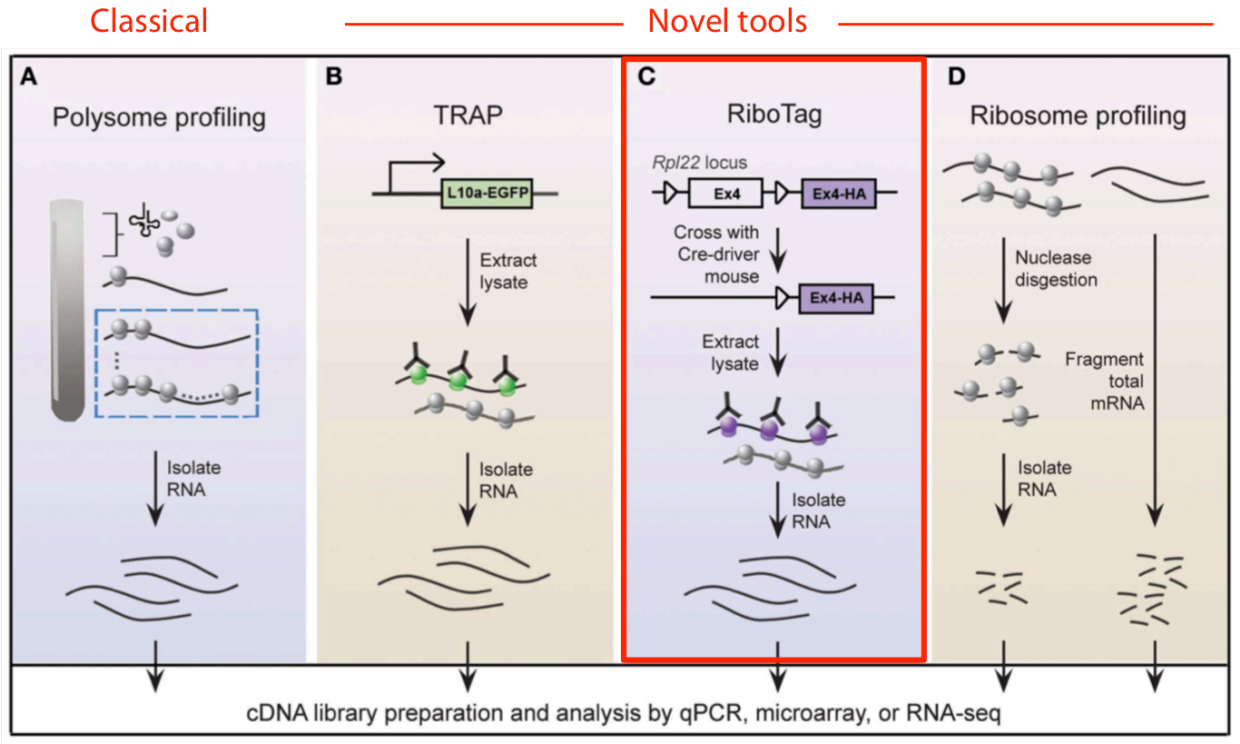

Figure 6: Classical and novel tools to address transcript-specific protein translation. RiboTag was marked since it is the prime method used in this thesis. Modified from Kapeli et al. (2012).

Together, these methods offer great potential to further dissect both mechanisms of global and specific control of protein synthesis in stem cells. Their application on carefully characterized subpopulations can help to understand the key post-transcriptional events taking place during activation and differentiation.

1.9 Objectives of this study

While several studies in the past addressed gene expression of NSCs and their progeny using microarray or RNAseq to quantify mRNA levels (Beckervordersandforth et al., 2010; Codega et al., 2014; Llorens-Bobadilla et al., 2015; Shin et al., 2015), there was little attention to the question whether these are actually translated into proteins. Neurons are characterized by local control of protein synthesis. At which stage of neurogenesis translational control emerges and how it is regulated during neuron production, remained elusive. Consequently, the main subjects of this thesis were to address: (i) to which level global translation varies between different stages of neurogenesis? (Part I); (ii) is there transcript-specific regulation of translation during neurogenesis, and if so, which mechanisms may coordinate selective translation of transcripts? (Part II).

2. Materials & Methods

2.1 Materials

2.1.1 Chemicals and reagents

Table 1: Chemicals and reagents

Chemical/Kit/Reagent/Tool	Manufacturer
Accutase	Sigma-Aldrich
Acid-Phenol:Chloroform, pH 4.5 (with IAA, 125:24:1)	Ambion
Agarose	Sigma-Aldrich
Agencourt Ampure XP Beads	Life Technologies
Agilent High-Sensitivity DNA Kit	Agilent
Agilent RNA 6000 RNA Pico Kit	Agilent
Agilent RNA 6000 RNA Nano Kit	Agilent
B27 Supplement	Life Technologies
bFGF	Relia Tech
Boric Acid	Fluka
C Tubes	Miltenyi
Click-IT Cell Reaction Buffer Kit	Life Technologies
cOmplete Protease Inhibitor Cocktail Tablets	Roche
Cycloheximide (CHX)	Sigma-Aldrich
Diethyl Pyrocarbonate (DEPC)	Sigma-Aldrich
Dithiothreitol (DTT)	Sigma-Aldrich
dNTP Mix (10mM)	Fermentas
D(+)-Glucose	Sigma-Aldrich
Dimethyl Sulfoxide (DMSO)	Sigma-Aldrich
Dulbecco's Modified Eagles Medium (DMEM)	Life Technologies
DNAfree DNAse Set	Qiagen
EdU (5-ethynyl-2-deoxyuridine)	Thermo Fisher Scientific
Ethylenediaminetetraacetic Acid (EDTA)	Thermo Fisher Scientific
Epidermal Growth Factor (EGF)	Promocell
Ethanol	Riedel de Haen
Fetal Bovine Serum (FBS)	Biochrom
Glycine	Sigma-Aldrich
Glycoblue	Ambion
Goat Serum	Chemicon
Hank's Balanced Salts Solution (HBSS)	Life Technologies
Ham´s F12	Life Technologies
Heparin Cell Culture Grade	Sigma-Aldrich
HEPES	Gibco
Hoechst 33342	Biotrend
Horse Serum	Biochrom
Hydrochloric Acid (HCl)	VWR
Interferon-Gamma	Millipore
Isoflurane	Baxter
Isopropanol (C_3H_8O)	Sigma-Aldrich
KAPA HiFi HotStart ReadyMix	KAPA Biosystems
Ketavet (100mg/mL)	Pfizer
Laminin	Sigma-Aldrich
L-Glutamine (100x L-Glutamine)	Life Technologies
Lab-Tek Chambers	Thermo
Magnesium Sulfate ($MgSO_4$)	Sigma-Aldrich
Mini-PROTEAN TGX Precast Gels	Biorad
mirVana miRNA Extraction Kit	Ambion
Neural Tissue Dissociation Kit, Trypsin	Miltenyi

Continued

Neural Tissue Dissociation Kit, Papain	Miltenyi
Neurobasal A Medium	Life Technologies
Nextera XT Sample Preparation Kit	Illumina
Nextera XT Index Kit	Illumina
Nonidet P-40 (NP-40)	Roche
Oligonucleotide Primers	MWG
O-Propargyl-Puromycin (OPP)	Jena Bioscience
Paraformaldehyde (PFA) Ampules (16%)	Thermo
Paraformaldehyde (PFA) (4%)	Roth
PBS (without Mg^{2+}/Ca^{2+})	PAA
PCR H_2O	Braun
Penicillin Streptomycin	Life Technologies
PicoPure RNA Isolation Kit	Arcturus
Pierce BCA Protein Assay Kit	Thermo Fisher Scientific
Pierce IP Lysis Buffer	Thermo Fisher Scientific
Pierce Protein G Magnetic Beads	Thermo Fisher Scientific
Poly-L-lysine hydrobromide (PLL)	Sigma-Aldrich
Potassium Chloride (KCl)	Applichem
Potassium Phosphate Monobasic (KH_2PO_4)	Gerbu
Precellys Ceramic Kit 1.4 mm small	Peqlab
Quantitect Primers	Qiagen
Qubit dsDNA High-Sensitivity (HS) Kit	Life Technologies
RNASCOPE Multiplex Fluorescent Assay Kit	Advanced Cell Diagnostics
RNase-Free H_2O	Ambion
RNasin Plus RNase Inhibitor (RNAsin)	Promega
RNeasy Mini Kit	Qiagen
Rompun (2%)	Bayer
Sodium Dodecyl Sulfate (SDS)	Roth
Sodium Azide (NaN_3)	Merck
Sodium Acetate ($C_2H_3NaO_2$)	Ambion
Sodium Chloride (NaCl)	Fluka
Sodium Chloride 0.9% Sterile (NaCl)	Braun
Sodium Dihydrogen Phosphate Monohydrate (NaH_2PO_4)	Roth
Sodium Hydroxide (NaOH)	Sigma-Aldrich
Sodium Phosphate Dibasic Heptahydrate ($Na_2HPO_4 \cdot 7H_2O$)	Sigma-Aldrich
Sodium Pyruvate ($C_3H_3NaO_3$)	Life Technologies
Sodium Tetraborate (Borax, $Na_2B_4O_7{\cdot}10H_2O$)	Merck
Sucrose	Sigma-Aldrich
Sunflower Oil	Sigma-Aldrich
SuperFrost Slides	Roth, Germany
Superscript II First-Strand Synthesis SuperMix	Life Technologies
SuperScript VILO cDNA Synthesis Kit	Life Technologies
SYBR Green PCR Master Mix	Applied-Biosystems
Tamoxifen	Sigma-Aldrich
Target Retrieval Solution	DAKO
Tools for Mouse Surgery	Fine Science Tools
Torin 1	Biomol
Trichloroacetic Acid (Cl_3CCOOH)	Sigma-Aldrich
Tris Base ($C_4H_{11}NO_3$)	Sigma-Aldrich
Triton X-100	Sigma-Aldrich
Trypsin-EDTA (0.05%)	Life Technologies
TSO Oligonucleotide	Exiqon
Tween-20	Merck
Ultracentrifuge Tubes	Beckman Coulter

2.1.2 Buffers, solutions and media

Table 2: Buffers/solutions/media and their composition

Experimental Paradigm	Buffer/Solution/Media	Composition
Animal Experiments	Perfusion Solution	5.71mg/mL Ketavet 2.8mg/mL Rompun in NaCl 0.9%
	Tamoxifen Solution	Tamoxifen, 10mg/mL (intraperitoneal) Tamoxifen, 50mg/mL (oral, heat at 50°C to dissolve) in a 9:1 mixture of sunflower oil and EtOH.
Histology and Immunofluorescence	Phosphate Buffered Saline (PBS), 20x	160g/L NaCl 23g/L Na_2HPO_4 28.84g/L NaH_2PO_4 4g/L KCl 4g/L KH_2PO_4 Adjust pH to 7.4 with HCl and fill up to 1L with dH_2O.
	0.1M Phosphate Buffer	69mL 0.2M monobasic stock (13.9g/500mL NaH_2PO_4) 231mL 0.2M dibasic stock (53.65g/L Na_2HPO_4 $7H_2O$) Bring volume up to 600mL (pH 7.3).
	Tris-Buffered Saline (TBS), 10x	24.23g/L Trizma base 80.06g/L NaCl Mix in 800mL ultra pure H_2O, adjust pH to 7.6 with HCl and fill up to 1L.
	Tris-Buffered Saline Supplemented (TBS++), 1x	100mL TBS 3mL Horse or goat serum 0.25mL Triton X-100
	Permeabilization Buffer	0.5% Triton X-100 Dissolve in PBS.
	Blocking Buffer	5% (vol/vol) BSA Dissolve in PBS.
	Alkyne-Azide Reaction Buffer	2mM $CuSO_4$ 20mg/mL Click it cell buffer additive 1/200 Alexa-coupled Azide (1mg/mL) Prepare in 1x Click it reaction buffer.
Cell Culture	Neurobasal A Medium (NBM, supplemented)	500mL Neurobasal A medium 10mL B27 supplement (50x) 5mL L-Glutamine (200mM) 5mL Pen-Strep, (Pen: 10,000units/mL; Strep: 10,000µg/mL) 2µg/mL Heparin *When growth factors were used:* 20ng/mL bFGF 20ng/mL EGF
	DMEM/F12	245mL DMEM 245mL Ham's F12 5mL L-Glutamine (200mM) 5mL Pen-Strep
	Borate Buffer	1.24g boric acid 1.9g sodium tetraborate (Borax) Adjust to 400mL with H2O, adjust pH to 8.5 and sterile filter.
	PLL Coating Solution	1mg/mL Poly-L-Lysine Prepare in borate buffer and sterile filter.
	Laminin Coating Solution	50 µg/mL Laminin Dilute in NBM. (Usually pre-coated with PLL)
	O-Propargyl-Puromycin (OPP)	Dissolve 0.5mg in 50µL (5% DMSO, 95% PBS)=20mM

	Solution	solution, use 1.5µL *in vivo* or 2.5µL/mL medium *in vitro* (50µM final).
	Interferon-Gamma Solution	Dissolve 100µg in 100µL phosphate buffer (stock; -80°C). Dilute 1/50 including 0.1% BSA (working solution: 20ng/µL, -20°C). Use 2.5µL/mL medium.
	Torin1 Solution	Dissolve 10mg in 5.5mL DMSO (100%)= 3mM stock (-80°C). Dilute 1/30 in PBS= 100µM working solution. (-20°C), Use 1/400 in medium (final: 250nM).
Sucrose Gradient Fractionation	DEPC H_2O	1:1000 DEPC Prepare in H_2O, leave overnight and autoclave.
	Gradient Buffer (2x)	30mM Tris-HCl pH7.4 30mM MgCl2 600mM NaCl 200µg/mL cycloheximide (CHX) 2mM dithiothreitol (DTT) Prepare in DEPC H_2O and sterile filter.
	Supplemented Polysome Lysis Buffer (PLB+)	5mL Gradient buffer (2x) 4.9mL DEPC H_2O 100µL Triton X-100 *Add freshly:* 100µL CHX (10mg/mL) 50µL c0mplete protease inhibitor (=1 tablet) 50µL RNAsin 10µL b-mercaptoethanol
	Light Sucrose Gradient Solution (17.5%)	8.67g sucrose 25mL 2x Gradient buffer Fill up to 50mL with DEPC H_2O.
	Heavy Sucrose Gradient Solution (50%)	25g sucrose 25mL 2x Gradient buffer Fill up to 50mL with DEPC H_2O.
RiboTag Immunoprecipitation	Homogenization Buffer (HB)	50mM Tris-HCl pH7.4 100mM KCl 12mM $MgCl_2$ 1% NP-40 Prepared in DEPC H_2O.
	Homogenization Buffer supplemented (HB+)	4.77mL HB 50µL DTT (100mM) 100µL c0mplete protease inhibitor (50x) 25µL RNAsin 50µL CHX (10mg/mL) 50µL Heparin (100mg/mL)
	High Salt Buffer	50mM Tris-HCl pH7.4 300mM KCl 12mM $MgCl_2$ 1% NP-40 1mM DTT 100µg/mL CHX final Prepare in DEPC H_2O.
	Extraction Buffer	PicoPure Extraction Buffer Supplement with 10µL/mL b-mercaptoethanol.

2.1.3 Antibodies and related products

Table 3: Antibodies used for FACS

Target Protein	Clone	Isotype	Conjugate	Manufacturer	Dilution
Anti-GLAST	ACSA-1	Mouse IgG2a	PE	Miltenyi	1:20
Anti-CD45	30-F11	Rat IgG2b	APC-Cy7	BD	1:200
Anti-O4	O4	Mouse IgM	APC	Miltenyi	1:50
Anti-PROM-1	13A4	Rat IgG1	PerCP-eFluor710	eBioscience	1:75
Anti-PSA-NCAM	2-2B	Mouse IgM	PE-Vio770	Miltenyi	1:50

Table 4: FACS-associated reagents

Name	Manufacturer	Dilution
EGF-Alexa488	Life Technologies	1:100
Fc Blocking Reagent	Miltenyi	1:20
Sytox Blue	Life Technologies	1:1000

Table 5: Primary antibodies for IHC/ICC*, western blot** and immunoprecipitation***

Target Protein	Clone/Name	Isotype/Species	Manufacturer	Dilution
Anti-4EBP1**	53H11	Rabbit IgG	Cell Signaling	1:1000
Anti-Calretinin*	Polyclonal/ab702	Rabbit IgG	Abcam	1:1000
Anti-β-Catenin*	Polyclonal	Rabbit IgG	Sigma	1:300
Anti- β-Catenin*	14	Mouse IgG1	BD	1:500
Anti-DCX*	Polyclonal/C-18	Goat IgG	Santa Cruz	1:300
Anti-DCX*	Polyclonal	Guinea Pig	Merck Millipore	1:1000
Anti-GFAP*	GA5	Mouse IgG1	Millipore	1:1000
Anti-GFAP*	Polyclonal	Rabbit IgG	Millipore	1:1000
Anti-GFP*	Polyclonal	Chicken IgY	Aves Labs	1:1000
Anti-GLAST*	Polyclonal	Guinea Pig	Frontier Science	1:1000
Anti-Hemagglutinin (HA)*/**/***	16B12	Mouse IgG1	Covance	1:1000 (IHC) 1:100 (IP)
Anti-Ki67*	SP6	Rabbit IgG	Novus	1:100
Anti-Ki67*	Ki-S5	Mouse IgG	Millipore	1:500
Anti-Mash1*	301733	Rat IgG2a	RDI Fitzgerald	1:500
Anti-NeuN*	A60	Mouse IgG	Millipore	1:300
Anti-p70 S6K**	Polyclonal	Rabbit	Cell Signaling	1:1000
Anti-p-H3*	3H10	Mouse IgG1	Millipore	1:500
Anti-p-4EBP1 (Thr37/46)**	236B4	Rabbit IgG	Cell Signaling	1:1000
Anti-p-S6 (Ser240/244)*/**	Polyclonal	Rabbit	Cell Signaling	1:1000
Anti-p-p70 S6K (Thr389)**	1A5	Mouse IgG2a	Cell Signaling	1:1000
Anti-RFP*	Polyclonal	Rabbit IgG	Rockland	1:1000
Anti-Rpl22**	Polyclonal	Mouse	Custom (D. Wiest)	1:500
Anti-S6 Ribosomal Protein**	5G10	Rabbit IgG	Cell Signaling	1:1000
Anti-Sox2*	EPR3131	Rabbit IgG	Abcam	1:1000
Anti-Sox2*	Polyclonal/ Y-17	Goat IgG	Santa Cruz	1:500

Table 6: Secondary antibodies used for IHC/ICC

Antibody	Conjugate	Host	Manufacturer	Dilution
Anti-mouse	Alexa405 and 633	Goat	Life Technologies	1:500
Anti-mouse	Alexa405 and 633	Donkey	Life Technologies	1:500
Anti-chicken	Alexa488	Goat	Life Technologies	1:500
Anti-chicken	DyLight488	Donkey	Dianova	1:500
Anti-chicken	Alexa633	Goat	Life Technologies	1:500
Anti-guinea pig	CF™ 405S	Donkey	Sigma-Aldrich	1:500
Anti-guinea pig	DyLight488	Donkey	Dianova	1:500
Anti-guinea pig	Alexa546	Goat	Life Technologies	1:500
Anti-goat	Alexa546	Donkey	Life Technologies	1:500
Anti-goat	DyLight647	Donkey	Dianova	1:500
Anti-rabbit	Alexa488 and 555	Donkey	Life Technologies	1:500
Anti-rabbit	Alexa488 and 555	Goat	Life Technologies	1:500

2.1.4 Primers and Probes

Table 7: Primers used for qRT-PCR

Target Gene (Protein)	Primer (QuantiTect primer assay)	Manufacturer
Nre21 (Tlx)	Mm_Nr2e1_1_SG	Qiagen
Nestin	Mm_Nes_1_SG	Qiagen
Gfap	Mm_Gfap_1_SG	Qiagen
Rbfox3 (NeuN)	Mm_Rbfox3_1_SG	Qiagen
Ascl1/Mash1	Mm_Ascl1_1_SG	Qiagen
Doublecortin	Mm_Dcx_1_SG	Qiagen
Cd24a	Mm_Cd24a_1_SG	Qiagen
Pax6	Mm_Pax6_1_SG	Qiagen
Rpl18	Mm_Rpl18_2_SG	Qiagen
Rps17	Mm_Rps17_1_SG	Qiagen
Rps20	Mm_Rps20_1_SG	Qiagen
Sox2	Mm_Sox2_1_SG	Qiagen
Actin B	Mm_Actb_1_SG	Qiagen
Gapdh	Mm_Gapdh_3_SG	Qiagen
Sox9	Mm_Sox9_1_SG	Qiagen

Table 8: Probes used for *in situ* hybridization

Target Transcript	Probe	Manufacturer
Sox2	Probe - Mm-Sox2	Advanced Cell Diagnostics
Sox2	Probe - Mm-Sox2-C2	Advanced Cell Diagnostics
DapB	Negative Control Probe-DapB-C3	Advanced Cell Diagnostics
Ppib	Advanced Cell Diagnostics	Advanced Cell Diagnostics

Table 9: Primers used for genotyping of transgenic mice

Mouse Line (short)	Transgene	Primer Sequences (forward/reverse, 5'->3')	Outcome
DiCRY	Dcx-CreER	GTCAGGCTATGGATTCATTTACAACTGTTAGTC/ CAGCTCTCATGTCACCGGCCATG	Cre+: 650bp Cre-: no band
TiCRY	Tlx-CreER	TTTTCCCGACTGTTTCGTTC/ CGGTCACACCACATACGTTC	Cre+: 338bp Cre-: no band
Continued			

TiCROMATO	Tomato-flox	AAGGGAGCTGCAGTGGAGTA/ CCGAAAATCTGTGGGAAGTC (WT) GGCATTAAAGCAGCGTATCC/ CTGTTCCTGTACGGCATGG (Mutant)	WT: 297bp Mutant: 196bp
DiCRY/TiCRY	eYFP-flox	AAGACCGCGAAGAGTTTGTC/ AAAGTCGCTCTGAGTTGTTAT/ GGAGCGGGAGAAATGGATATG	WT: 600bp Homozygous: 300bp Heterozygous: 300/600bp
DiCRY/TiCRY/ TiCROMATO	Rpl22-HA	GGGAGGCTTGCTGGATATG/ TTT CCAGACACAGGCTAAGTACAC	WT: 243bp Homozygous: 290bp Heterozygous: 290/243bp

2.2 Methods

2.2.1 Animal experiments

a) Animals

Animals were housed under standard conditions and fed *ad libitum*. All procedures were in accordance to the DKFZ guidelines and approved by the Regierungpräsidium Karlsruhe. C57BL/6J mice, hereinafter referred to as 'wildtype (WT)', were bred in house at the DKFZ Center for Preclinical Research facility. All transgenic mouse lines used in this thesis are summarized in Table 10.

TlxCreER- and Tomato-flox mice were kind gifts of Prof. Hai-Kun Liu. TlxCreER-mice were bred to R26-LSL-EYFP and Rpl22-HA mice, both purchased from The Jackson Laboratory, to generate TlxCreER-eYFP-Rpl22-HA (TiCRY) offspring. Some experiments required stronger endogenous fluorescence expression. To achieve this eYFP was replaced by Tomato creating TiCROMATO offspring. DcxCreER mice were a kind gift of Prof. Markus Schwaninger. Similar to TiCRY mice, DcxCreER were bred to R26-LSL-EYFP and Rpl22-HA mice to obtain DcxCreER-eYFP-Rpl22-HA (DiCRY) offspring. Genotyping of transgenic mice was performed within the Molecular Neurobiology department of the DKFZ using primers that are described in Table 9.

Cre-mediated recombination was induced by oral gavage of Tamoxifen (dissolved in a 9:1 sunflower oil- ethanol mixture) at a dose of 200mg/kg bodyweight (e.g. 5mg Tamoxifen in 100µL per dose for a 25g mouse) for two (in TiCRY mice) or three doses (for DiCRY mice) each with an interval of twelve hours. Unless otherwise stated, all experiments started when mice were 8-12 weeks old.

Table 10: Transgenic mouse lines used in this study

Full Name	Short Name	Description	Reference
B6-Tg(Nr2e1-Cre/ERT2)1Gsc	Tlx-CreER^{T2}	Tamoxifen-inducible Cre recombinase under the regulatory element of Tlx.	Liu et al., 2008
B6-Tg(Dcx-creERT2)#Mrks	Dcx-CreER^{T2}	Tamoxifen-inducible Cre recombinase under the regulatory element of Dcx.	Werner et al., 2012
B6.129X1-Gt(ROSA)26Sortm1 (EYFP)Cos/J	R26-LSL-EYFP	Cre-reporter line based on a loxP-flanked stop cassette followed by eYFP.	Srinivas et al., 2001
B6-Gt(ROSA)26Sortm14(CAG-tdTomato)Hze	Tomato-flox	Cre-reporter line based on a loxP-flanked stop cassette followed by tdTomato.	-
B6.129-Rpl22tm1.1Psam	Rpl22-HA	loxP-flanked exon 4 of Rpl22 followed by HA-tagged exon 4 of Rpl22 before Rpl22 stop codon.	Sanz et al., 2009

Cisterna magna injection of OPP was performed by S. Kleber (Molecular Neurobiology, DKFZ) as previously described (Furlan et al., 2003) in 10µL total volume (90% PBS/10% DMSO, total of 0.1mg). PBS-injected mice served as negative controls. For intraperitoneal injections, OPP was dissolved in 100µL (60% PBS/40% DMSO, 1mg) and injected into a single mouse. EDU injection (220µL of 20mg/1.1mL stock solution solved in 90% PBS/10% DMSO; final: 150mg/kg) served as positive control. Injection of PBS/DMSO served as negative control. Intravenous (IV) injection of OPP was performed by L. Gao (Molecular Neurobiology, DKFZ) at a dose of 100µL (60% PBS/40% DMSO, 1mg) into the tail vein.

b) Global forebrain ischemia (performed by K. Zwadlo, Molecular Neurobiology, DKFZ)

Global ischemia was performed on male mice using the bilateral common carotid artery occlusion (BCCAO) model essentially as previously described (Speetzen et al., 2013; Yoshioka et al., 2011a; 2011b). Prior to surgery, mice received a 200mg/kg subcutaneous injection of metamizol to alleviate the pain associated with the operation. Anesthesia was induced by exposure to a mixture of air and 3% isoflurane until the pedal reflex disappeared and respiration had stabilized. Anesthesia was maintained at approximately 1.5% isoflurane exposure. A sagittal skin incision of approximately 0.5cm was made above the parietal skull and a laser Doppler probe holder (Perimed) was glued at approximately the following position zeroed at the bregma and the skull surface: -1/-1.3/0mm. Mice were placed in a supine position and a sagittal skin incision of approximately 1cm was made in the neck along the midline to expose the trachea. Both common carotid arteries (CCAs) were then carefully exposed using fine forceps. For sham operations, the procedure stopped here and mice were sutured and returned to their home cages. Special attention was paid to prevent the damage of the neighboring vagal nerve while preparing the CCAs,

as this can cause severe parasympathetic dysfunction and death. Once arteries were exposed, a thread of silk of about 4cm was passed underneath them to facilitate later clamping. The laser Doppler fluorimetry probe (PeriFlux System 5000, Perimed) was next inserted into the probe holder to measure the regional cerebral blood flow (rCBF). Both CCAs were clamped using vascular microclamps (Fine Science Tools) for a period of 22 minutes prior to reperfusion. Only animals with an ischemic rCBF after 1 minute smaller than 13% of the pre-ischemic value were used. rCBF values were constantly monitored during clamping. After removing the clamps for reperfusion, the silk and the probe holder were removed and the wounds were sutured. Temperature was monitored during the complete duration of the surgical procedure using a thermometer connected to a rectal probe (Bioseb) and maintained at 36.5±0.5°C using a heating pad and an infrared lamp.

c) Stereotactic injection of OPP

To measure protein synthesis rates in the SVZ, OPP (1.5µL of 20mM solution dissolved in 5% DMSO/PBS) was loaded into a 10µL Nanofil syringe (World PrecisionInstruments, WPI) equipped with a 33G needle (WPI). Analgesia was achieved by injecting a 200mg/kg dose of metamizol intraperitoneally before surgery. Anesthesia was induced using 3% isoflurane, which was later reduced to 1.5% for maintenance. Deeply anesthetized mice were placed in a motorized stereotactic frame (Stoelting) equipped with an injection pump. A sagittal incision of approximately 1cm was made along the midline to expose the skull. After locating the bregma, the injection coordinates were marked in the skull and a small hole was prepared using a 25G needle. Following coordinates allowed targeting the lateral ventricle: -0.5/1.2/-2mm. The solution was injected at a 150nL/min rate. Waiting additional 10 minutes after completion of injection prevented backflow of the solution. Mice were sacrificed 30 minutes later.

d) Cell sorting

Animals were sacrificed by cervical dislocation and brains were immediately placed on ice. The subventricular zone (SVZ) was microdissected as a wholemount as previously described (Mirzadeh et al., 2010), further the olfactory bulbs (OB) were dissected. Tissue of a single mouse was used per replicate (SVZ and/or OB) for sequencing experiments, while up to five mice were pooled per sample for OPP experiments. Tissue was digested with trypsin and DNase according to the Neural Tissue Dissociation kit in a Gentle MACS

Dissociator (Miltenyi). For sequencing experiments endogenous eYFP fluorescence was used to identify cells of interest. For OPP experiments cells were sorted as previously described (Llorens-Bobadilla et al., 2015) using the antibodies listed before (Table 3). During cell sorting, Sytox blue (Thermo Fisher Scientific, 1:1000) was used to exclude dead cells.

For transcriptome analysis, 200-500 $eYFP^+$ or $eYFP^-$ (control) cells per sample were sorted directly into 100µL Picopure lysis buffer (Thermo Fisher Scientific).

e) RiboTag immunoprecipitation and sequencing

RiboTag immunoprecipitation was conducted essentially following the original protocol (Sanz et al., 2009) with minor modifications. Animals were perfused with Hank's Balanced Salt Solution (HBSS) supplemented with the translation inhibitor cycloheximide (CHX, 200 µg/mL) for stabilization of RNA-ribosome complexes. Tissue of interest was dissected and placed in tubes containing 1.4mm ceramic beads (PEQLAB). Homogenization buffer was added to a weight per volume ratio of 3% (e.g. 0.015g in 500µL) and tissue was homogenized using Minilys Personal Homogenizer (Bertin Instruments). Samples were centrifuged and supernatant was used for immunoprecipitation. Five percent of the lysate was kept as input control for later enrichment analysis. Anti-HA antibody (Covance, 1:100) was added for four hours (indirect conjugation) following addition of Protein G magnetic beads (100µL, prewashed with homogenization buffer, Thermo Fisher Scientific) and overnight incubation (all steps at 4°C). Supernatant was discarded and beads were washed three times for ten minutes in high salt buffer. Finally, beads were resuspended in Picopure lysis buffer (supplemented with β-mercaptoethanol) and RNA was isolated by Picopure RNA isolation kit (Thermo Fisher Scientific) following the manufacturer's protocol.

2.2.2 Histology and cell biology

a) Immunohistochemistry

Animals were anesthetized by an overdose of Rompun (14mg/kg bodyweight; Bayer) and Ketavet (100mg/kg bodyweight; Pfizer) in 0.9% NaCl (Braun) and transcardially perfused with 20mL Hank's Balanced Salt Solution (HBSS, Life Technologies) followed by 10mL of 4% paraformaldehyde (PFA) in PB-buffer (Roth). Brains were removed and postfixed overnight in 4% PFA. Tissue was washed twice with PBS and then cut coronally in 50-70µm thick

coronal or 100µm sagittal sections using a Leica VT1200 vibratome. To cut sections from the olfactory bulb, the tissue was embedded in 2.5% agarose. Agarose was carefully removed while cutting using a brush. For long-term storage, floating sections were placed in 0.01% sodium azide-containing PBS. For immunofluorescence, brain sections were placed in net carriers in 12 well plates in 0.1M Tris Buffer pH7.4 supplemented with 8% NaCl (TBS). The sections were washed three times in TBS each 15min at RT on a shaker. Next, sections were blocked for 1h in TBS++ and transferred to 0.5ml Eppendorf tubes containing 200µL TBS++ and the diluted primary antibodies (see Table 5). Samples were incubated at 4°C on a shaker for 24 hours. Afterwards sections were transferred back to net carriers in 12 well plates, washed three times with TBS, and after additional blocking in TBS++ for 30 min transferred back to 0.5ml Eppendorf tubes containing the diluted secondary antibody mix in TBS++ (see Table 6). Sections were incubated in secondary antibodies at RT on a shaker for 2h. Hoechst 33342 was used to counterstain DNA. Finally, sections were placed back into net carriers in 12 well plates washed three times for 15 min with TBS and one additional time in 0.1M PB. Sections were floated in 0.1M PB in a petri dish, mounted on glass slides and embedded with Fluoromount G (Southern Biotech).

To stain SVZ wholemounts, mice were transcardially perfused first with HBSS and then with 4% paraformaldehyde (PFA). SVZ wholemounts were microdissected as previously described (Mirzadeh et al., 2010). Tissue was post-fixed overnight in 4% PFA, blocked and permeabilized in PBS containing 10% serum and 0.5% Triton X-100 (PBS++) and incubated with primary antibodies for 2 days under continuous rotation at 4°C. Next, tissue was washed three times in PBS++ for at least 30 min each. After washing, tissue was incubated overnight with secondary antibodies at 4°C. Finally the tissue was washed three times with PBS++ for at least 30 min each and once more with 0.1M PB before getting mounted as previously described.

b) Immunocytochemistry

Cells were plated in poly-D-lysin- (PDL) and laminin- coated Lab-Tek chambers until they adhered or the duration of the respective treatment. Coating was performed using 100µg/mL PDL (overnight at RT) and 50µg/mL laminin (2 hours, 37°C). Cells were washed with PBS and fixed for 20 minutes at RT with 2% PFA added directly into the medium from a 16% stock. For staining, cells were permeabilized for 10 minutes using 0.25% Tx-100 in PBS. After two washes with PBS, unspecific binding was blocked by 30 minute incubation

in blocking buffer (5% BSA in PBS). Primary antibodies were then added in blocking buffer and incubated for 1 hour at RT. Chambers were then washed three times using 0.1% Tween-20 in PBS (wash buffer), each time for at least 5 min. Appropriate secondary antibodies and Hoechst33342 were diluted in blocking buffer, added to the chambers and incubated for 1 hour at RT. Samples were washed 3 times in wash buffer and one more time in PBS prior to mounting using Fluoromount G.

c) OPP/EDU detection by click chemistry

To detect the alkyne group in O-Propargyl-puromycin (OPP) or 5-ethynyl-2'-deoxyuridine (EDU) treated samples, an Alexa488- or Alexa647-coupled azide was mixed with supplemented reaction buffer according to the Click-iT Cell Reaction Buffer Kit (Thermo Scientific) and added for 30 minutes after immunostaining for marker proteins. Samples were washed two times in PBS and mounted as previously described. Samples which were not treated with OPP or EDU, respectively, served as controls to estimate background signal.

d) RNA *in situ* hybridization

RNA *in situ* hybridization was performed using RNASCOPE Multiplex Fluorescent Assay (Advanced Cell Diagnostics) with one major modification of the protocol: To allow subsequent protein staining, suggested pretreatment steps were skipped and replaced by an extended (15min, 95°C) heat-based target retrieval using a modified citrate buffer (Target Retrieval Solution, Dako). This decreased the damage of proteins and allowed subsequent detection using immunofluorescence.

Immunofluourescence was performed following the RNA detection as described previously, but protected from light to avoid bleaching of the RNA signal. DapB (bacterial transcript) served as a negative control and Ppib (ubiquitous transcript) served as a positive control while setting up the technique.

3.2.3 Molecular biology

a) RNA isolation

To isolate the total RNA from freshly sorted cell populations, 200-500 cells from each population were directly sorted into 100µL of Picopure Extraction buffer and RNA was

isolated according to the manufacturer's instructions including a DNAse digestion step, done using 5µL of enzyme. RNA was finally resuspended in 11µL PCR-grade water.

For the isolation of RNA from cultured cells, RNA was isolated according to the MirVana RNA isolation kit, also including a DNAse digestion step. Occasionally, cells were stored on RNAlater solution upon harvesting and RNA was isolated not later than 5 days.

For high throughput RNA-isolation (over 50 samples), Acid-Phenol:Chloroform, pH 4.5 (with IAA, 125:24:1, Thermo Fisher Scientific) was used. Shortly, one volume of Acid-Phenol: Chloroform was added to the sample (at least 200µL, if smaller volume fill up with water). Samples were heated for 10 minutes at 65°C and the pressure was released by opening the tubes under a fume hood. The aqueous phase was transferred to a fresh tube and supplemented with 1.1 volumes isopropanol and 1µL GlycoBlue (Thermo Fisher Scientific). RNA was precipitated overnight at -20°C (alternatively 2h at -80°C). Samples were centrifuged for 20min at 4°C at full speed. Pellets were washed once with ice cold 70% ethanol and dried under the fume hood. Dry pellets were resuspended in PCR-grade water and were ready for further downstream applications.

b) Reverse transcription and quantitative real time polymerase chain reaction (qRT-PCR)

To perform qRT-PCR, 100-500ng of total RNA were reverse transcribed to cDNA using the Superscript Vilo cDNA Synthesis kit (Thermo Fisher Scientific) according to the manufacturer's instructions.

qRT-PCR was performed using Power SYBR Green PCR Master Mix (Thermo Fisher Scientific) in a 384 well plate with a CFX384 Touch Real-Time PCR Detection System (Biorad). Reactions were prepared the following way: 1µL of cDNA was mixed with 1µL Quantitect Primer Assay (Qiagen, containing forward- and reverse primer), 5µL SYBR Green PCR Master Mix and 3µL water (total 10µL reaction). All reactions were performed in 3 technical replicates. Replicates which differed more than one cycle from the other two replicates were excluded from the analysis.

c) Enrichment analysis

A fraction of isolated RNA was reverse transcribed to cDNA and analyzed for correct enrichment of targeted cell populations.

For RiboTag immunoprecipitation (IP) correct enrichment was assessed by comparison of cell type specific marker expression in input samples (5% of lysate, taken before addition of antibody) and IP samples using qRT-PCR.

Similarly, correct enrichment by cell sorting was assessed by comparison of cell-type specific marker expression between eYFP-positive cells and eYFP-negative control populations.

Final enrichment was depicted as fold enrichment (IP over input) between HA-tag positive samples (often referred to as Cre^{+}) and HA-tag negative samples (often referred to as Cre^{-}) or, after cell sorting, as fold enrichment of marker expression betwen eYFP positive- and negative populations.

d) Sequencing library preparation

RNA samples from RiboTag immunoprecipitation (RIBO) and cell sorting (total RNA) were first analyzed using RNA 6000 Pico/Nano chips (Agilent) on a 2100 Bioanalyzer system (Agilent) to assess quality of isolated RNA and to estimate total amounts. Samples were discarded when obvious signs of degradation were visible. Further, samples were assessed for correct enrichment of cell-type specific markers (see 3.2.3d). Again, samples without significant enrichment were discarded.

RNA-seq libraries were prepared using Smart-seq2 technology as previously described (Picelli et al., 2014). Samples which passed strict quality control were subjected to reverse transcription using an oligo(dT) primer and a locked nucleic acid (LNA)-containing template-switching oligonucleotide. Full-length cDNAs were amplified by 15-18 cycles of PCR using KAPA HiFi DNA polymerase. cDNA libraries were purified using two rounds of AMPure XP (Beckman Coulter) purification at 0.8x (bead to solution ratio). cDNAs were then quantified using Qubit (Thermo Fisher Scientific) and run on a High Sensitivity Bioanalyzer chip (Agilent). Samples where cDNA appeared degraded were excluded from further processing. 500pg of cDNA from each sample was then converted into uniquely barcoded libraries for Illumina sequencing according to the Nextera XT Sample Preparation protocol with minor modifications. Specifically, we extended the tagmentation step to 8 minutes and performed a double cleanup with 0.8X AMPure XP beads after PCR amplification for 9 cycles. 5ng of each library were used for multiplexing. The multiplex was finally cleaned and concentrated using Ampure XP beads (1x ratio),

measured again by Qubit and run on a bioanalyzer chip to calculate the final molarity. Samples were sequenced in an Illumina HiSeq 2000 to an average depth of 20-30 million reads per sample.

e) Sucrose gradient fractionation of NSCs

Before the actual fractionation sucrose gradients were prepared at the day of the experiment. Heavy (50%) and light (17.5%) sucrose gradient solutions were prepared and 5.5mL were added to the corresponding chambers of a Hoefer SG Series Gradient Maker (Fisher Scientific) with magnetic stirrers. The gradient maker was placed on a stir plate on an elevated platform and the output was connected to a glass capillary (20-40µL, Blaubrand) placed at the bottom of an ultracentrifuge tube (14mL, Beckman Coulter). The valves were opened to allow the sucrose solutions to mix and flow into the tube via gravity, starting with light sucrose. The sucrose solution that comes out becomes denser over time displacing the lighter sucrose upwards to generate a gradient in the tube. The gradients were prepared at least 1 hour before fractionation and kept at 4°C until use.

A 70-90% confluent 150cm^2 flask (≈20x10^6 cells) was treated with cycloheximide (CHX, 100µg/mL) to immobilize ribosomes. After 5 minutes incubation at 37°C, cells were collected and washed with ice-cold PBS+ (containing CHX). Cells were transferred to eppendorf tubes and washed one more time with PBS+. Cells were lysed in 500µL supplemented polysome lysis buffer (PLB+) and incubated 10 minutes at 4°C. Samples were centrifuged (full speed, 4°C) for 10 minutes to remove the nuclei. Supernatant was transferred to a fresh tube. Whenever necessary, an input sample containing 5% of the lysate was kept for later comparison. The rest was added to freshly prepared sucrose gradients. Tubes were filled up to the rim with PLB+ and transferred to ultracentrifuge buckets. Buckets were balanced and centrifuged for 2.5 hours 4°C and 35.000rpm using a SW40Ti rotor in a L8M Ultracentrifuge (Beckman).

Samples were fractionated in 12 fractions containing one mL sample using an Isco fractionator (Brandel) while monitoring absorption at 254nm wavelength. To each individual fraction or pooled fractions, 10% SDS was added to a final concentration of 1% to unfold proteins and dissociate ribosomes. RNA isolation was performed using acidic Phenol-Chloroform-Isoamylalcohol (PCI, 25:24:1, Thermo Fisher Scientific). Alternatively, proteins were precipitated using trichloroacetic acid (TCA).

f) Protein purification from sucrose fractions

Fractions were thawed up on ice for 30 minutes and centrifuged at full speed for 10 minutes at 4°C. Pellets were washed by 10% trichloroacetic acid (Sigma-Aldrich, diluted in H_2O). The supernatant was removed, the pellets were air-dried and resuspended in 15µL sample buffer (0.5M Tris HCl pH7.4, 0.5M NaCl). After addition of 4x Laemmli sample buffer containing b-mercaptoethanol (Biorad), samples were denatured for 5 minutes at 95°C and stored at -20°C or directly analyzed by SDS-Page.

2.2.4 Cell culture

a) Isolation and culture of primary NSCs

For isolation of primary NSCs, mice were sacrificed and brains were dissected into ice-cold dissection buffer. Wholemounts of the SVZ were microdissected as described before and were processed according to the papain Neural Tissue Dissociation kit in a Gentle MACS dissociator (Miltenyi). After digestion, cells were washed twice in Neurobasal medium, resuspended in 5mL of growth factor-containing Neurobasal medium and cultured at a density of one mouse per 25cm^2 flask for the first week. Afterwards, spheres were dissociated using Accutase and transferred into 75cm^2 flasks. Confluent cultures were then passaged at a 1:3 ratio two or three times per week.

Torin1 was added to cells at a final concentration of 250nM. PBS containing 3.3% DMSO served as control treatment (vehicle).

For culture after cell sorting (see 3.2.1d) cells were incubated in the absence of growth factors in Neurobasal medium supplemented with B27, Glutamine and Pen/Strep. OPP (Jena Biosciences) was added to the cells at 50µM for one hour prior to fixation.

2.2.5 Imaging

Confocal images were acquired using a Leica TCS SP5 confocal microscope. Image J was used for processing and images were only adjusted for brightness and contrast. For OPP quantifications, all images within compared groups were acquired with identical settings. Analysis was performed in ImageJ software using a custom-written macro for unbiased segmentation and quantification of pixel intensity and cell size. OPP quantifications are depicted as the integrated pixel intensity within a cell and normalized to a reference group

within the same experiment. In graphs, mean and standard deviation are shown. Illustrator CS5 (Adobe) was used for figure assembly.

2.2.6 Statistics

The statistical tests used varied with the type of input data and they were specified in the respective figure. All analyses were performed in Graphpad Prism 6.0 (Graphpad) or in R.

2.2.7 Computational analysis

All computational analyses were done in collaboration with Bernd Fischer from the Computational Genome Biology group at the DKFZ, Heidelberg.

a) Processing and analysis of RNAseq and RIBOseq data

Sequence reads from both RNAseq and RIBOseq samples were aligned to the mouse reference genome (ENSEMBL Release 80) and the ENSEMBL gene annotation (Release 80) using the STAR alignment algorithm version 020201 (Dobin et al., 2013) with the proposed the ENCODE settings to generate gene-specific raw count values. Expected gene counts and TPM values (transcripts per million) were computed using RSEM (version 1.2.21) with bowtie2 (version 2.2.6)(Li and Dewey, 2011) with the same genome and version and annotation. Differential gene expression analysis between developmental stages of the RNAseq data was conducted by the R/Bioconductor package DESeq2 (Love et al., 2014). Thereby p-values were computed by fitting a negative binomial distribution and subsequent testing by a Wald test. P-values were corrected for multiple testing by controlling the false discovery rate applying the method of Benjamini-Hochberg. For RIBOseq data the same analysis was applied to analyse the differential abundance of ribosome bound RNA.

To assess the translation efficiency, genes with an average log2 read count of at least 10 were considered. At first, a linear model was fitted for each replicate individually to explain the RIBOseq data by a linear combination of RNAseq data (representing efficient translation) and RIBO- (representing background expression). Analysis of variance of this part provides the proportion of variance that is explained by RNAseq and by RIBO- in each replicate separately. The RIBOseq signal that cannot be explained by RNAseq or RIBO- can be explained by either enhanced or repressed translation. To assess, if the detected enhanced or repressed translation was statistically significant, we compared the two

replicates and tested, if the remaining signal is different from zero by applying a moderated t-test implemented in the R/Bioconductor package limma (Ritchie et al., 2015). P-values were corrected for multiple testing by the method of Benjamini-Hochberg. At this stage the analysis of variance provides the proportion of variance that can be explained by translation efficiency (correlated signal) and the remaining unexplained variance (uncorrelated signal) that is most likely of technical source.

b) *De Novo* motif analysis

3'UTR, 5'UTR and protein coding sequences of all protein coding genes were tiled in 6-mer nucleotide sequences. For each developmental stage separately, for translationally repressed and enhanced genes separately, and for 3'UTR, 5'UTR and coding sequence separately, an unbiased motif analysis was performed. For each possible 6-mer, the number of genes containing the tested 6-mer in the set of repressed (enhanced) genes and in the remaining genes was computed. A p-value was computed by a binomial test and corrected by the method of Benjamini-Hochberg. All over- or underrepresented motifs at a false discovery rate of 10% were reported.

3. Results

3.1 Measuring protein synthesis during adult neurogenesis

It has been traditionally challenging to determine protein synthesis rates in complex living systems. Here, protein synthesis of neural stem cells (NSCs) and progeny was quantified using a novel, modified version of the tRNA homologue puromycin, called O-Propargyl-Puromycin (OPP)(Liu et al., 2012). A series of experiments have been conducted in order to determine optimal experimental setup for robust quantification, which are summarized in the following paragraphs.

3.1.1 Systemic administration of OPP

Puromycin is frequently used as an antibiotic reagent since it effectively blocks protein synthesis in prokaryotes and eukaryotes. It does so by mimicking an aminoacyl-tRNA molecule and binding to the acceptor site of active ribosomes, which ultimately leads to premature termination of the polypeptide chain. This mechanism has been used in the past to assess the rate of specific protein synthesis using radioactive labels (Isaacs and Fulton, 1987). By combination with fluorescent molecules (Starck et al., 2004) and the application of antibodies against puromycin (Schmidt et al., 2009) it became popular to use puromycin to monitor general protein synthesis within the cell. However, low signal-to-noise ratio as well as contradictions to previous findings relating to subcellular localization of the signal raised doubts over discoveries using the classical puromycin approaches. To overcome this, the Salic group recently improved labeling of nascent proteins by introducing O-Propargyl-Puromycin (OPP), a puromycin analog that bears a terminal alkyne group (Liu et al., 2012). OPP maintains puromycin properties but allows covalent binding to fluorescent azide molecule (for microscopy) or biotin-azide (for affinity-based isolation). This system makes use of the copper(I)-catalyzed alkyne-azide cycloaddition (CuAAC) “click” reaction which is robust, rapid and highly sensitive (Kolb et al., 2001).

One of the aims of this thesis was to investigate protein synthesis rates of multiple cell populations within the subventricular zone of the adult brain. Administration of substances to the central nervous system (CNS) is highly challenging and the major burden of treating neurological disorders. This relies mostly in the presence of the blood-brain-barrier (BBB), a specialized system that prevents the leakage of plasma into the CNS.

Puromycin is known to be a substrate of P-glycoprotein, one of the major efflux transporters, which is highly expressed by brain endothelial cells and in fact used to purify brain capillary endothelial cell cultures (Perrière et al., 2005). Therefore, it was expected that systemic application of OPP would likely not lead to significant enrichment within the CNS. However, since data on the bioavailability of puromycin after different routes of administration is highly limited, systemic administration and investigation in different organs was the starting point of a series of experiments to determine the best use of OPP to investigate CNS components.

Mice were injected intraperitoneally and sacrificed one hour after injection. Parallel to the experimental group, which received OPP, two control groups were used: mice that received vehicle injection (PBS/DMSO) controlling for background signal and mice that received a shot of 5-ethynyl-2´-deoxyuridine (EDU), a modified nucleoside, which detects cell proliferation and is visualized by "click"-chemistry similar to OPP (serving as a positive control). After sacrifice, liver, small intestine and brain were collected, fixed and sectioned for detection of OPP and EDU. Azide-coupled Alexa 488 (Azide-488) was used detect OPP and EDU.

Tissue samples of PBS-injected mice did not show fluorescence in any tissue, indicating high specificity of the alkyne (OPP/EDU) – azide (Azide-488) reaction (Figure 7A,B). Liver sections did not show EDU incorporation, which is in line with low proliferation in liver, while small intestine sections showed a characteristic pattern of proliferating EDU^+ cells at the bottom of the intestinal crypts, where stem- and progenitor cells are present (Figure 7A). Both liver and small intestine exhibited high OPP signal. While being homogeneous in the liver, the OPP signal was more heterogeneous in the small intestine where again cells at the bottom of the crypts showed higher signal indicating that the proliferative cells exhibit higher protein synthesis than others (Figure 7A). No OPP signal could be detected in the brain, while scattered EDU^+ cells lining the wall of the lateral ventricles indicated that the staining procedure was successful (Figure 7B). Prolonged incubation after injection (up to 12h) did not change the results (data not shown).

Together, this data showed that intraperitoneal injection of OPP does not lead to incorporation in the brain, making it impossible to use it over this route of administration.

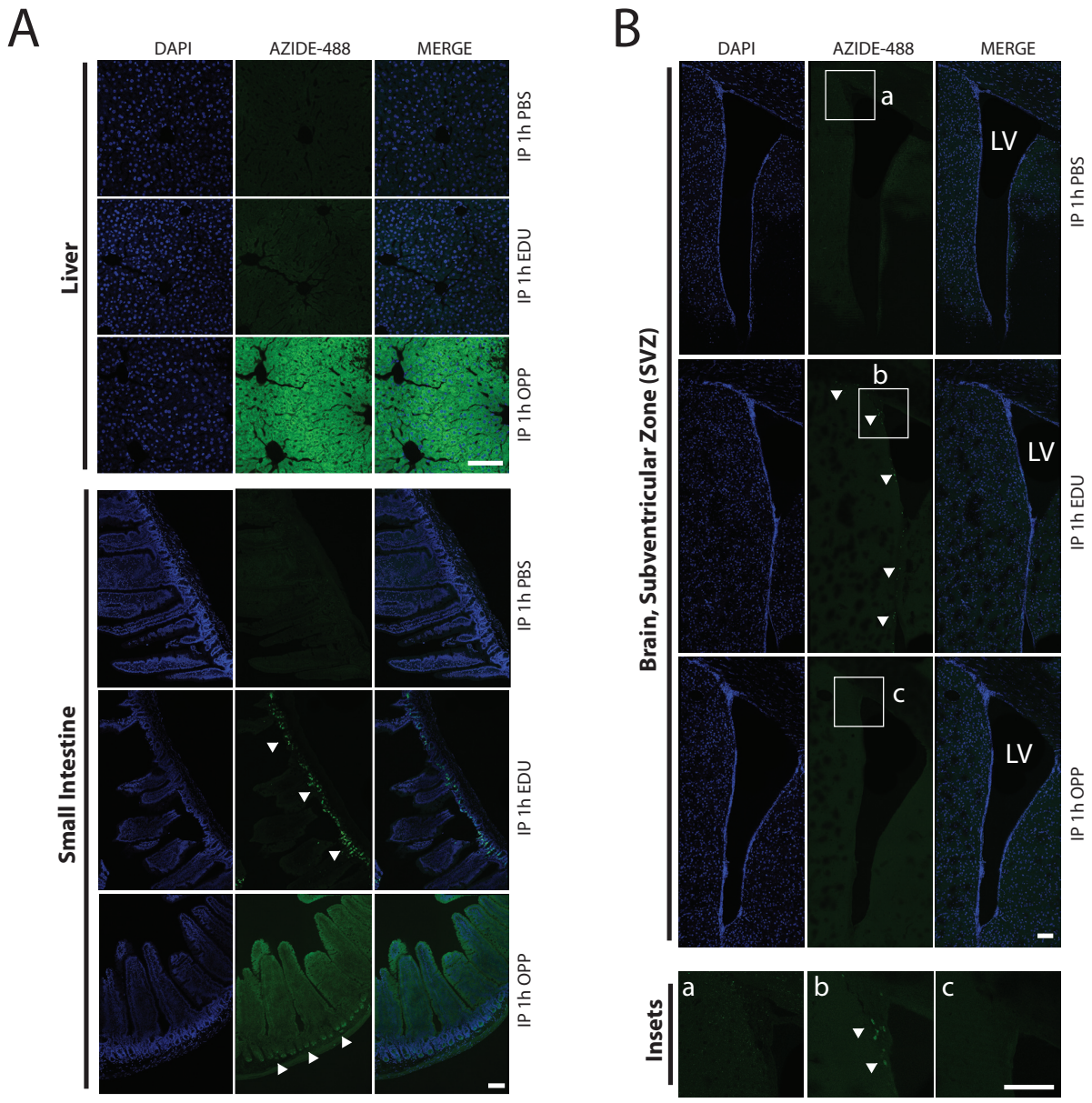

Figure 7: OPP does not cross the blood brain barrier after intraperitoneal injection. **A** Control tissues (top: liver, bottom: small intestine). Azide-488 signal one hour after PBS (-ctr), EDU (+ctr) or OPP injection. **B** Brain tissue (around lateral ventricle) shows no OPP signal. Some EDU^{+} cells (see inset b) lining the ventricular wall indicate successful detection by "click" chemistry. Scale bars: 100µm. LV: lateral ventricle.

In order to exclude poor absorption rate an additional experiment was conducted administrating OPP intravenously (IV) into the tail vein. IV injections are considered to be more efficient than IP injections since the substance is directly introduced to the blood system (Turner et al., 2011). In order to exclude the factor of short timing, injected animals were sacrificed 24h after administration. Similar to the IP administration, no specific signal could be detected in the brain, which would indicate any regions of higher translational activity (Figure 8A). With these results, systemic administration of OPP was excluded as a potential strategy and alternative methods came to focus.

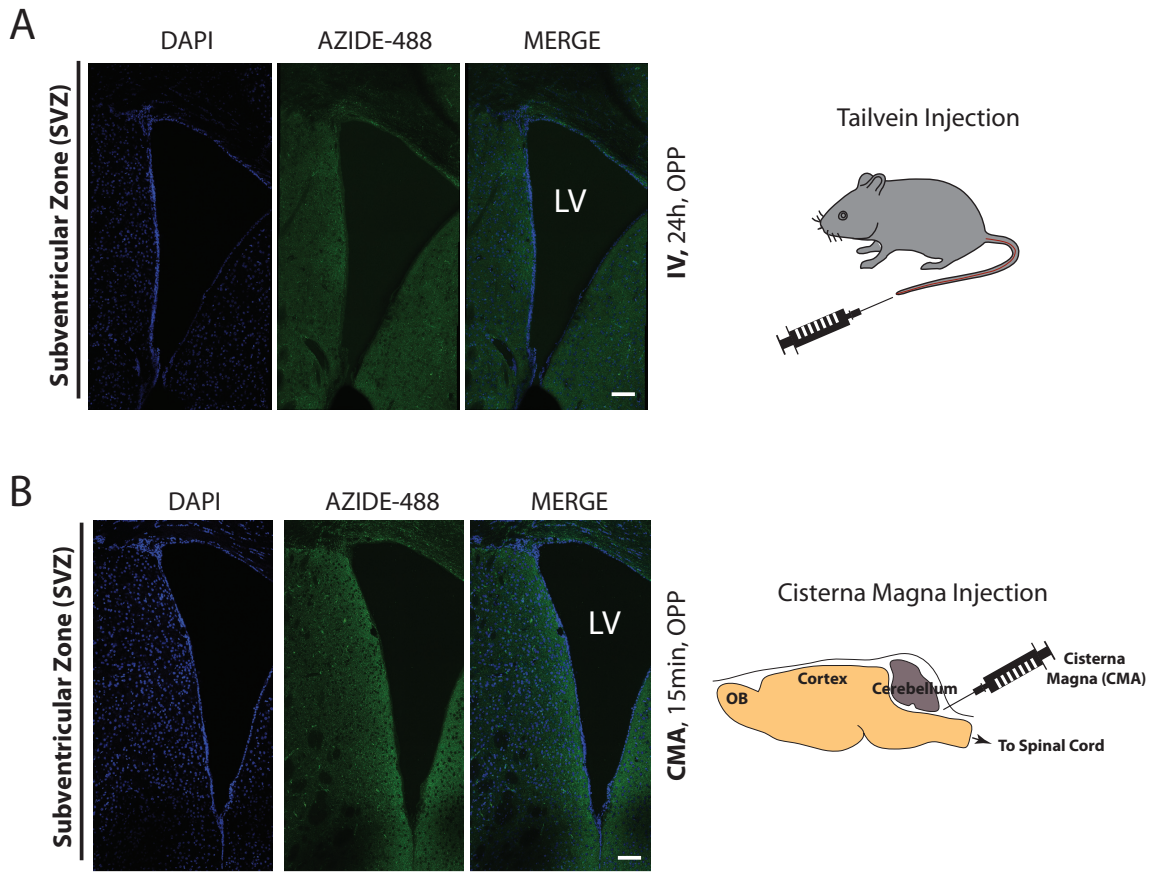

Figure 8: Alternative routes of administration for OPP. **A** Intravenous injection (IV) to the tail vein following 24h period does not enrich for OPP in the brain. **B** Cisterna Magna (CMA) injection of OPP to overcome blood brain barrier. No OPP signal around lateral ventricles, areas, which should get in contact with OPP assuming efficient distribution over the cerebrospinal fluid (CSF). Scale bars: 100µm. LV: lateral ventricle.

3.1.2 Direct administration of OPP to the brain

Homogenous exposure of cells to OPP is key to exclude technical artifacts. To achieve this within the brain, OPP was directly injected into the Cisterna Magna (CMA). The CMA allows direct access to the cerebrospinal fluid (CSF), which is connecting various parts of the brain over the ventricular system. It is one of three openings of the subarachnoid space located between the cerebellum and the dorsal surface of the medulla (Figure 8B) and is often used for collection of CSF for diagnostic purposes (Liu and Duff, 2008). Here it was used to administer minute volumes of OPP to the CNS, expecting that OPP would be evenly distributed over the entire brain and allow quantification of OPP incorporation. Mice were sacrificed shortly after CMA injection (15min) in order to exclude prolonged OPP accumulation within the brain. Again, no OPP signal could be detected around the lateral ventricles, the primary region of interest that contains the neurogenic region of the subventricular zone indicating that OPP does not spread efficiently over the CSF (Figure

8B). To figure out whether OPP was uptaken by any brain tissue the entire brain was screened for OPP signal. Indeed, two hot spots of OPP incorporation could be found: the hypothalamus and the lateral walls of the third ventricle (Figure 9A). The third ventricle is bounded by the thalamus and the hypothalamus on both sides. Additionally, this region is in close proximity to the injection site indicating that OPP gets quickly immobilized at certain structures within the brain. Interestingly, a series of experiments using intranasal injection of OPP did not lead to any accumulation in the brain, also supporting poor diffusion of OPP (data not shown).

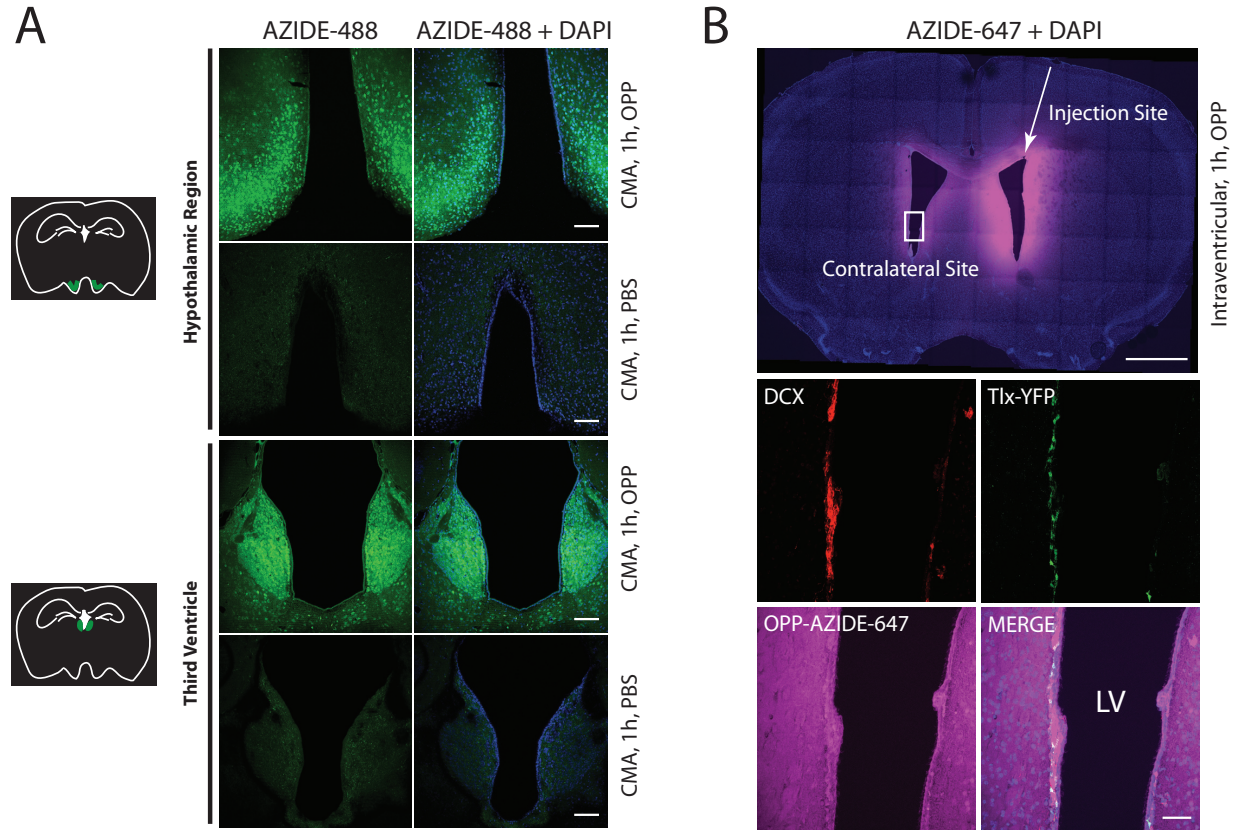

Figure 9: Low OPP diffusion when injected directly into the CNS. **A** Cisterna Magna (CMA) injected OPP gets immobilized at regions close to the injection site. Scale bar: 100µm. **B** Intraventricular injected OPP spreads around lateral ventricle and is transported to contralateral ventricle over the CSF. Saturation at the injection site does not allow comparison of cells. Contralateral side was analyzed showing regional differences. However, comparison of NSCs (Tlx-YFP^{+}) and neuroblasts (DCX^{+}) is not conclusive in coronal view. Scale bars: 1mm (overview); 50µm (insets). CMA injections (A) were perfomed by Susanne Kleber (Molecular Neurobiology, DKFZ, Heidelberg).

Overall, this data suggests that CMA injection is not a favorable technique to introduce OPP to the CNS. Next, intraventricular injection of OPP was performed in order to assess protein synthesis rates of neural stem cell niche components. As described before, a drawback of this method is that cells closer to the injection site unavoidably take over more of OPP, which could result in artifactual conclusions. To overcome this scenario, the

contralateral side of injection was analyzed primarily. A transgenic mouse line (Tlx-CreER^{T2}-YFP) was used for this experiment, which in combination with staining for doublecortin (DCX) allowed identification of neural stem cells (Tlx-YFP^{+}) and neuroblasts (DCX^{+}). OPP signal was saturated around the injected ventricle. As expected, signal was significantly weaker on the contralateral ventricle (Figure 9B). The OPP signal was homogenous around the contralateral ventricle indicating that by this mode of administration, OPP is equally distributed in the ventricular system. However, the fact that the signal became consistently weaker with increasing distance to the ventricle indicated that it might be difficult to compare cells with varying distance to the ventricular wall. Interestingly, the cell layer directly contacting the CSF, which typically consists of ependymal cells was not brighter than layers further away which suggests that the translational activity certainly contributes to the OPP signal and ependymal cells might feature relatively low levels. Comparison of the labeled cell types (NSC and neuroblasts) was rather inconclusive since OPP signal was homogenous over the entire SVZ. Together, intraventricular injections allowed robust detection of OPP both at the side of injection as well as at the contralateral ventricle and offered a promising starting point for investigation of neighboring cell types within the subventricular zone.

Further OPP experiments were conducted using subventricular zone whole mount sections, which compared to traditional sectioning techniques, preserve the complete architecture of the SVZ and offer higher cellular resolution (Mirzadeh et al., 2010). OPP was injected into the lateral ventricle as previously and the SVZ of the contralateral ventricle was dissected and prepared for analysis. Parallel to OPP detection, immunohistochemical stainings for the NSC marker glutamate aspartate transporter (GLAST), ß-catenin (to visualize cell bodies) and the proliferation marker Ki-67 were performed. ß-catenin staining reveals the unique architecture of the SVZ surface, which is characterized by the presence of numerous pinwheels (created by ependymal cells) in whose center GLAST^{+} NSCs reside (Mirzadeh et al., 2008).

The hypothesis was that active NSCs, characterized by Ki-67 expression (indicating proliferation), would show higher OPP signal and therefore translational activity when compared directly to neighboring Ki-67^{-} quiescent NSCs (considering that cell division requires protein synthesis). Indeed, this analysis showed that GLAST^{+} NSCs in the center of the pinwheels that are actively proliferating feature highly increased OPP incorporation when compared to the non-proliferating counterpart (Figure 10A).

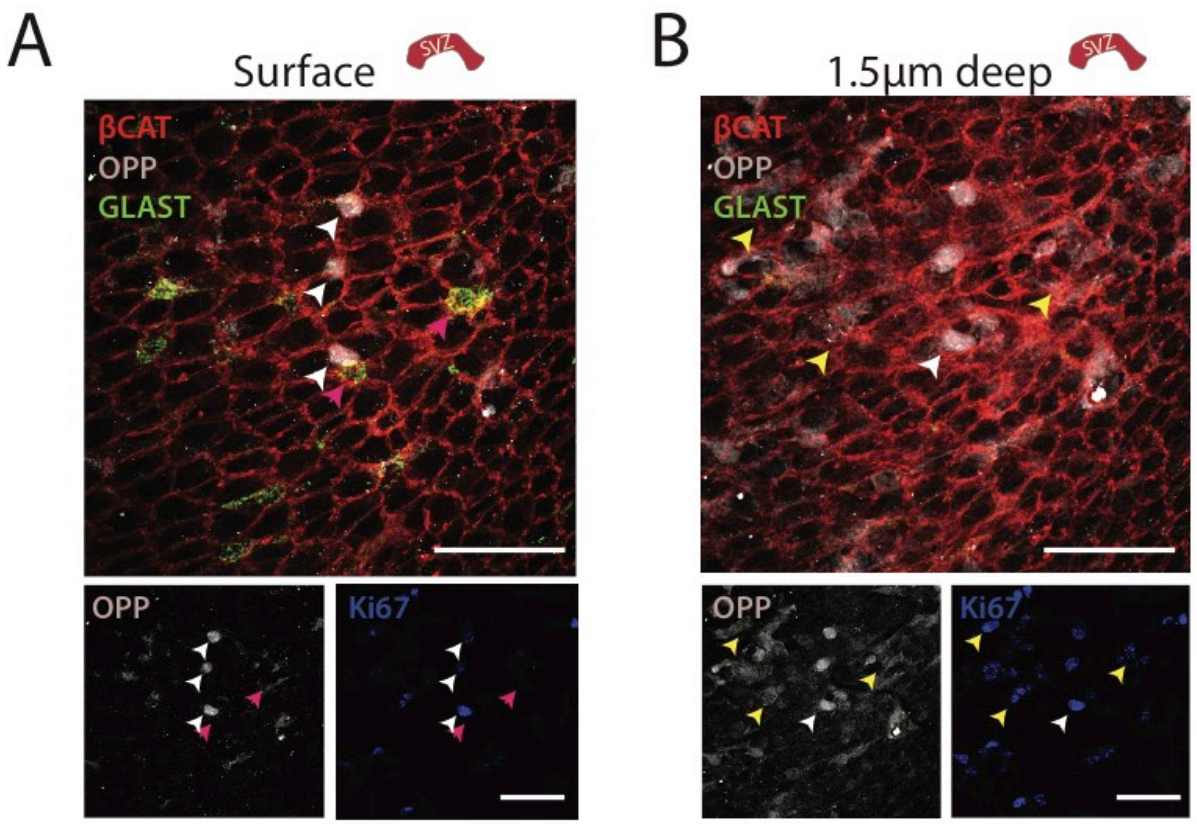

Figure 10: Whole mount staining of the SVZ after intraventricular OPP injection. **A** Surface view of the SVZ featuring GLAST^{+} NSCs in the center of the pinwheels built by ßCAT+ ependymal cells. Some GLAST^{+} cells feature high OPP signal and coexpression of the proliferation marker Ki-67 (active NSCs, see white arrowheads). GLAST+ cells which are Ki-67^{-} feature low levels of OPP (purple arrowheads, quiescent NSCs). **B** View of the SVZ at 1.5µm depth. Many more OPP^{high}/Ki-67^{+} cells appear, which are most likely neural progenitor cells (NPCs, yellow arrowheads). Scale bars: 50µm. Experiments conducted and data analyzed in collaboration with Enric Llorens Bobadilla (Molecular Neurobiology, DKFZ, Heidelberg). A modified version of this figure has been published in Llorens Bobadilla et al., Cell Stem Cell (2015) and the PhD thesis of Enric Llorens Bobadilla (Molecular Neurobiology, DKFZ, Heidelberg).

Interestingly, when looking deeper into the tissue, many more OPP^{high} cells appeared which were not always positive for the proliferation marker Ki-67 (Figure 10B). Many of these cells likely resemble neural progenitor cells (NPCs), the progeny of the GLAST^{+} NSCs.

Together, this section demonstrated that intraventricular injection resembles the best route of administration of OPP to the CNS in order to study the neurogenic zone of the SVZ. However, poor diffusion of OPP through solid tissue represented a major limitation of the system, allowing only quantitative comparison of cells that reside at a similar distance to the ventricular wall. For any other case, OPP allowed only crude estimates about the relative translational activity. Therefore, subsequent experiments focused on defining stable and controlled conditions in order to use OPP for accurate measurements of protein synthesis in defined cell populations.

3.1.3 *In vitro* application of OPP

Since equal exposure of cells to OPP is of utmost importance for accurate quantification of its incorporation, following experiments were conducted using culture systems. Primary NSCs of the SVZ were used to study OPP incorporation *in vitro*. In order to investigate to which extent inflammatory signals are affecting protein synthesis rates, we exposed NSCs to Interferon-γ (IFN- γ), one of the major cytokines, whose receptor is upregulated in NSCs after brain injury (Llorens-Bobadilla et al., 2015). One hour after exposure to IFN-γ, OPP was added to the culture well and cells were fixed after one additional hour (Figure 11A). OPP incorporation was assessed by both FACS and microscopy. Cycloheximide (CHX) is a highly potent protein synthesis inhibitor, which was added to some samples after 30 minutes of OPP exposure and served as a control. FACS analysis showed that almost all cells took up OPP in the OPP treated samples, while PBS treated samples did not show any signal. Interestingly, an equal fraction of cells (almost 100%) took up OPP in CHX-treated cells indicating rapid incorporation of OPP after exposure. While the fraction of OPP^+ cells did not differ between conditions, signal intensity varied and could be assessed both by microscopy and medium fluorescence intensity (MFI) using FACS analysis (Figure 11C-E). While CHX dropped OPP signal in average by more than half, IFN-γ treatment did not effect OPP incorporation of NSCs (Figure 11E). Interestingly, speckles with high OPP signal could be detected at higher magnification within cells, which might represent hotspots of translation (Figure 11F). Together, this experiment demonstrated that OPP is efficiently incorporated after exposure to primary NSCs and that differences in global translation caused by treatment with the translation inhibitor CHX can be readily detected. Further, acute exposure to the inflammatory agent IFN-γ did not cause changes of global translation rates.

Unlike the *in vivo* exposure, results here were easy to quantify and highly reproducible. We next applied this system to freshly isolated cells of the SVZ in order to answer the question, whether certain stages of neurogenesis are characterized by global changes of protein synthesis.

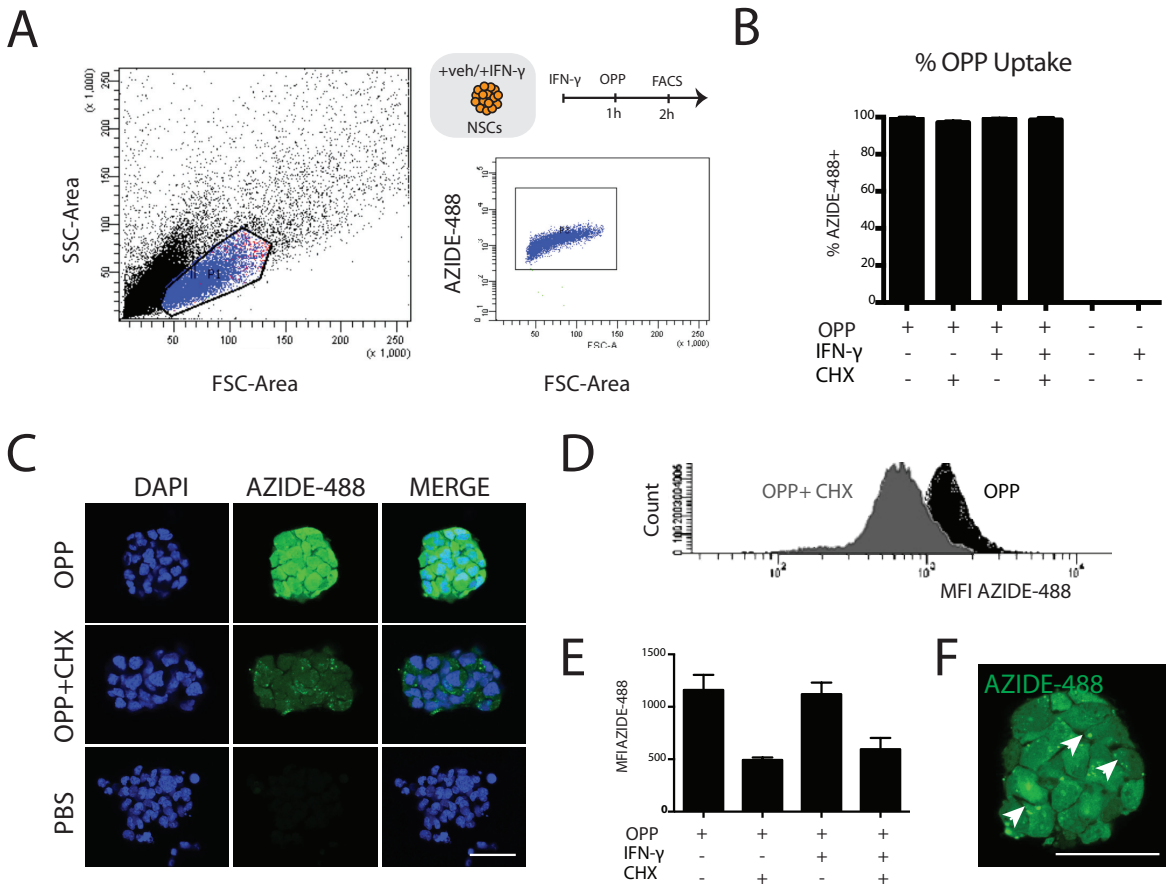

Figure 11: OPP incorporation of primary NSCs after acute exposure to IFN-γ. **A** Experimental setup and representative FACS gates. Primary NSCs isolated from the SVZ were acutely exposed to recombinant IFN-γ. Changes of protein synthesis rates were investigated by OPP incorporation (detected by Azide-488). Analysis was primarily done by FACS. **B** Rate of OPP uptake for different conditions. All OPP exposed samples show almost 100% OPP incorporation rate, even when added CHX, indicating that OPP is efficiently and quickly taken up by cells. **C** Representative images of NSC spheres under different conditions. PBS exposed cells do not show any signal. OPP exposed cells show strong and homogenous OPP incorporation. OPP and CHX exposed cells show much weaker signal. **D** Histogram representing medium fluorescence intensity (MFI) for OPP-Azide-488 under OPP and OPP+CHX condition. **E** Quantification of MFI under different conditions. CHX negatively affects OPP signal, while IFN-γ has no effect. **F** Representative OPP exposed neurosphere at higher resolution. Speckles (arrows) indicate hot spots of protein translation. Scale bars: 25µm. NSCs: neural stem cells, veh: vehicle treatment (PBS), FSC: forward scatter, SSC: sideward scatter.

3.1.4 Quantification of protein synthesis during neurogenesis using OPP

In order to investigate global protein synthesis at different stages of neurogenesis, multiple cell populations from the subventricular zone (SVZ) and olfactory bulb (OB) were isolated based on their surface expression of previously reported marker proteins (Codega et al., 2014; Llorens-Bobadilla et al., 2015). This way, quiescent NSCs (qNSC, GLAST$^+$PROM$^+$), active NSCs (aNSC, GLAST$^+$PROM$^+$EGFR$^+$), neural progenitor cells (NPC, only EGFR$^+$), early neuroblasts (ENB, PSA-NCAM$^+$ from SVZ) and late neuroblasts (LNB, PSA-NCAM$^+$ from OB) were isolated (Figure 12A). Cells were plated for a short resting period and subsequently

treated with OPP. Incorporation of OPP was detected by fluorescence and quantified for each population (Figure 12B,C).

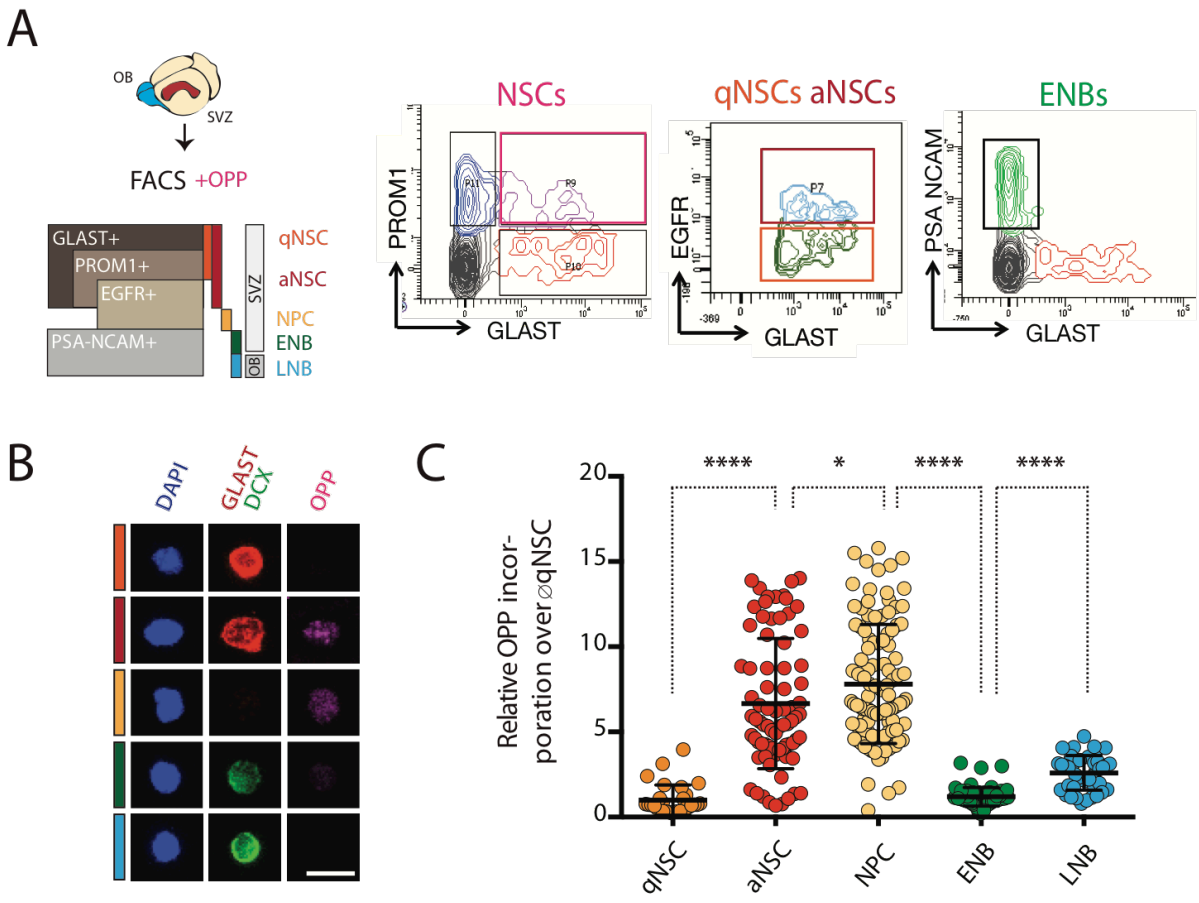

Figure 12: Global protein synthesis is highly dynamic during neurogenesis. **A** Sorting strategy for different stages of NSC differentiation with representative gates. **B** Representative images of OPP incorporation with specific marker expression, GLAST for NSCs, DCX for neuroblasts. **C** Quantification of OPP incorporation relative over qNSCs. Every circle represents a single cell. Scale bar: 10µm. Statistical significance by students t-test (Mann-Whitney). qNSC: quiescent NSC, aNSC: active NSC, NPC: neural progenitor cell, ENB: early neuroblast (SVZ), LNB: late neuroblast (OB), OPP: O-Propargyl-puromycin, OB: olfactory bulb, SVZ: subventricular zone. Experiments conducted in collaboration with Enric Llorens Bobadilla (Molecular Neurobiology, DKFZ, Heidelberg).

This data indicated that protein synthesis rates greatly vary between the different stages of neural differentiation. A very low level of translation characterized quiescent NSCs (qNSCs), as it was previously reported (Llorens-Bobadilla et al., 2015). Active NSCs (aNSCs; 6.7xqNSC) greatly upregulated protein synthesis, which further increased in neural progenitor cells (NPCs, 7.8xqNSC).

At the stage of early neuroblasts of the SVZ (ENBs,1.2xqNSC) protein synthesis reduced to the level of qNSCs. Interestingly late neuroblasts of the olfactory bulb (LNBs) showed

higher levels of protein synthesis (2.6xqNSC), potentially related to the complex process of integration to the neuronal network.

To further complete the picture, protein synthesis of olfactory bulb stages ranging from LNBs to neurons were determined. Since neurons are morphologically complex and their FACS purification is rather challenging, later stages were isolated by simple tissue dissociation of the OB where cells of interest were identified afterwards based on their marker expression (Figure 13A,B). OPP was added to the single cell suspension after a resting period and cells were fixed and analyzed as previously described. Again levels greatly varied between stages gradually decreasing from LNBs (DCX^+, 7.96xneuron) to early neurons (EN, DCX^+NeuN^+, 3.68xneuron) to mature, fully integrated neurons (NeuN+ only, 1), which finally showed very low levels of OPP incorporation (Figure 13C).

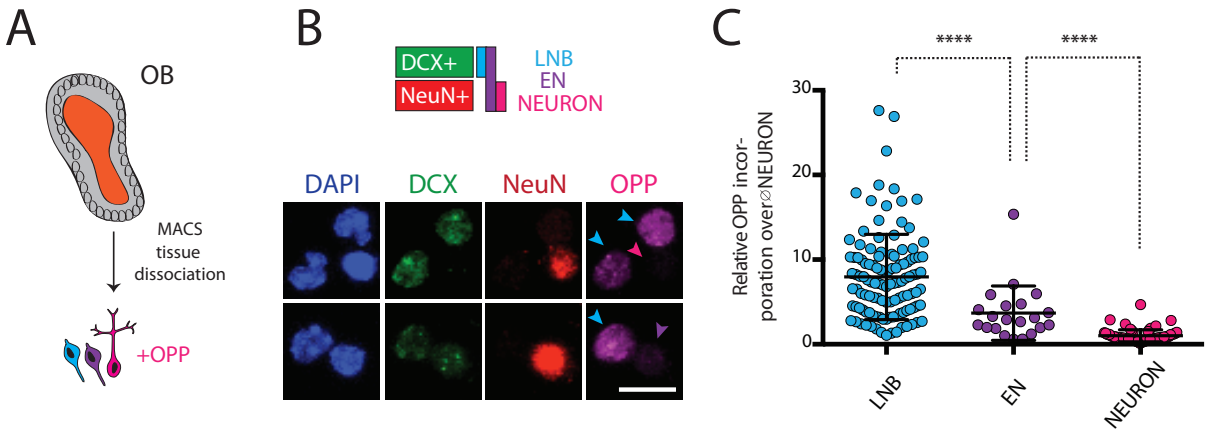

Figure 13: Protein synthesis continuously drops at late stages of neurogenesis. **A** Strategy to compare protein synthesis of olfactory bulb neuroblasts (LNB; DCX^+NeuN^-) to early neurons (EN; DCX^+NeuN^+) and mature neurons (DCX^-NeuN+). **B** Representative images of OPP incorporation of LNBs, ENs and mature neurons. **C** Quantification of OPP incorporation of LNBs, ENs and neurons (relative to neurons). Every circle represents a single cell. Scale bar: 10µm. Statistical significance by students t-test (Mann-Whitney). EN: early neuron, OPP: O-Propargyl-puromycin, OB: olfactory bulb, SVZ: subventricular zone.

Together, this data demonstrated highly dynamic regulation of global protein synthesis over the process of SVZ neurogenesis with peaks during active proliferation in aNSCs and NPCs as well as during integration of LNBs into the neuronal network of the olfactory bulb.

The second part of this thesis focused on the questions of how much transcript-specific translation efficiency (translation-dependent changes of protein expression) changes over the process of neurogenesis, which messenger RNAs (mRNAs) are particularly affected and which mechanisms contribute to the translational uncoupling.

3.2 Measuring transcript-specific protein synthesis during adult neurogenesis

It is well known that epigenetic modifications as well as regulation of transcription factors are closely associated to cellular identity, highly distinguishing between the pluripotent and committed status of cells. However, little is known about the importance of changes at the posttranscriptional level. Here, a system to monitor ribosome-association of individual transcripts at individual stages of the neuronal lineage was established. Both important steps during the establishment as well as interesting observations using this technique were summarized in the following paragraphs.

3.2.1 RiboTag strategy for parallel assessment of cell-type specific transcriptome and translatome

In order to investigate the transcript-specific translation efficiency we developed a system for parallel assessment of the transcriptome and translatome (the fraction of mRNAs which are bound to ribosomes) of NSCs and their progeny *in vivo*. In RiboTag mice, exon four of the large ribosomal subunit protein RPL22 gets replaced by a hemagglutinin (HA) tagged variant (RPL22-HA) due to Cre-recombinase activity (Sanz et al., 2009). In parallel, recombination labels cells with a fluorescent reporter (eYFP), which facilitated isolation by cell sorting (Figure 14A). Previously established inducible and cell type specific Cre-driver lines (CreERT2) were used, in order to target NSCs (Tlx-inducible-Cre-Rpl22.HA-eYFP, referred as TiCRY) and progeny (Dcx-inducible-Cre-Rpl22.HA-eYFP, referred as DiCRY). Varying mouse model, time point after induction of recombination by tamoxifen and region of dissection (SVZ or OB) allowed investigation of four populations ranging from NSCs to neurons (Figure 14A). HA-tag expression was limited to the cell types of interest: using TiCRY short time after labeling, HA-tag$^+$ cells were limited to the walls of the lateral ventricles, coexpressing glial fibrillary acidic protein (GFAP), a widely used NSC marker. Only few of the labeled cells were positive for the mitotic marker phospho-histone 3 (pH3) indicating no bias for amplifying cells (Figure 14B). The DiCRY mouse model was used to recombine the RPL22 locus in neuroblasts.

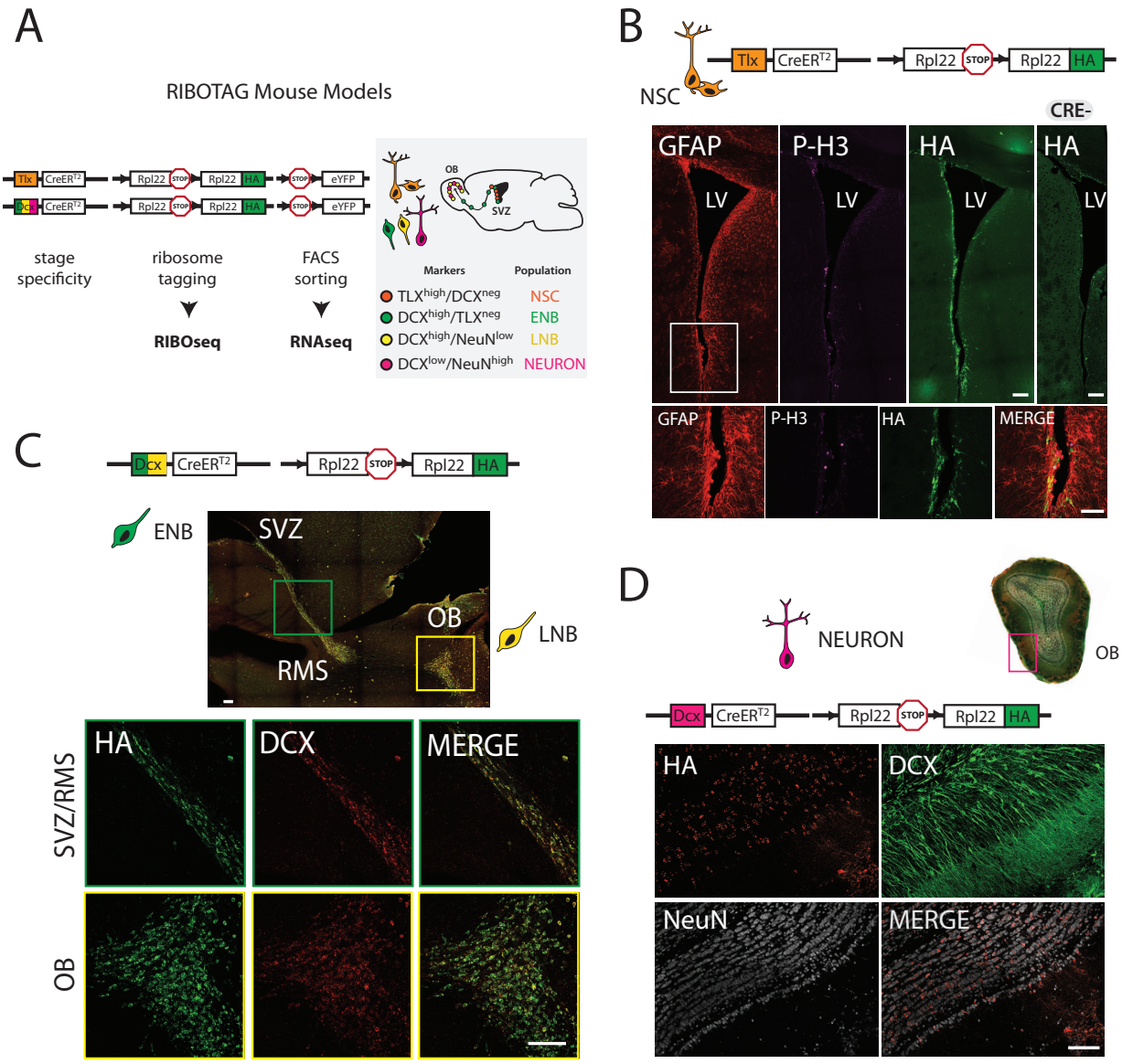

Figure 14: RiboTag mouse models target stages of neuronal differentiation. **A** Schematic representation of RiboTag mouse lines used for the study, HA-tag allows isolation of ribosome-associated mRNA, cell sorting based on eYFP expression allows isolation of total mRNA. **B** IHC confirming HA-tag expression in NSCs (controlled by the Tlx-promoter) of the SVZ, labeled cells are mostly GFAP^{+}pH3^{-}. Scale bars: 50µm. **C** IHC confirming expression of HA-tag in migrating neuroblasts (controlled by the Dcx-promoter) both in the SVZ/RMS (ENB, green box) as well as in the OB (LNB, yellow box). Scale bars: 100µm. **D** IHC confirming expression of HA-tag in NeuN+ neurons four weeks after initial labeling as DCX^{+} neuroblasts. Scale bar: 100µm. OB: olfactory bulb, RMS: rostral migratory stream, SVZ: subventricular zone, NSC: neural stem cell, ENB: early neuroblast (SVZ), LNB: late neuroblast (OB).

A short timepoint after labeling was used to investigate ENBs, neuroblasts of the SVZ, and LNBs, the neuroblasts of the OB. Here, HA-tag^{+} cells marked migrating neuroblasts, which coexpressed doublecortin (DCX) protein, confirming correct identity (Figure 14C). In order to address the gene expression of neurons, DiCRY mice were induced and sacrificed four weeks afterwards. After this time, all labeled cells migrated to the OB and lost expression of neuroblast markers and acquired markers of mature neurons (e.g. NeuN, Figure 14D).

Together, RiboTag models allowed cell-type specific expression of HA-tag in up to four stages of neurogenesis from subventricular zone neural stem cells. Next, composition of the target populations was investigated in more detail.

3.2.2 Histological characterization of target populations

RiboTag experiments until now were exclusively conducted using constitutively active Cre driver lines recombining in terminally differentiated cell types (Sanz et al., 2009; 2013; Shigeoka et al., 2016). Complete ribosome turnover in the brain is estimated to account for up to nine days (Retz and Steele, 1980). Consequently, when using inducible mouse models an adequate time after activation has to pass ensuring high level of tagged RPL22 protein in ribosomes. One major concern was that, in the highly dynamic process of neurogenesis, labeled cells would proceed into the next stage during this period. Therefore, significant efforts have been spent to minimize latency after recombination. To allow rapid clearance and avoid sustained long-term activation oral administration of Tamoxifen was used instead of former intraperitoneal injections, which leads to long-term exposure. Using few shots but high doses reduced the latency period. To assess NSC dynamics following oral Tamoxifen (TAM) administration, TiCRY mice were induced with two shots and sacrificed at different timepoints (3d, 4d, 5d). eYFP was used to identify recombined cells and their fate was monitored by coexpression of the neuroblasts marker DCX (Figure 15A). At these timepoints a negligible number of labeled cells showed proliferation by pH3 expression (which precisely marks G2/M-phase transition). Three days after the last shot of TAM almost 95% of labeled cells were negative for the neuroblast marker (94.8%). Four days after labeling this number only slightly dropped (93.3%±2.9), while five days after labeling the percentage of DCX-/eYFP+ cells dropped under 90% (87%±5, Figure 15B,C). In parallel, RNA IPs where performed at different timepoints after labeling for both mouse lines. In TiCRY mice, four days after labeling represented the first timepoint with significant and robust detection of ribosome-associated RNA from tissue of a single mouse. DiCRY mice were induced by three shots of TAM (recombination effiency is highly mouse line dependent) and showed robust enrichment of mRNA only three days after last TAM administration, most likely since labeled cells migrate out of the SVZ at later timepoints. Consequently, further experiments were conducted three (in DiCRY mice) or four days (in TiCRY mice) after TAM administration.

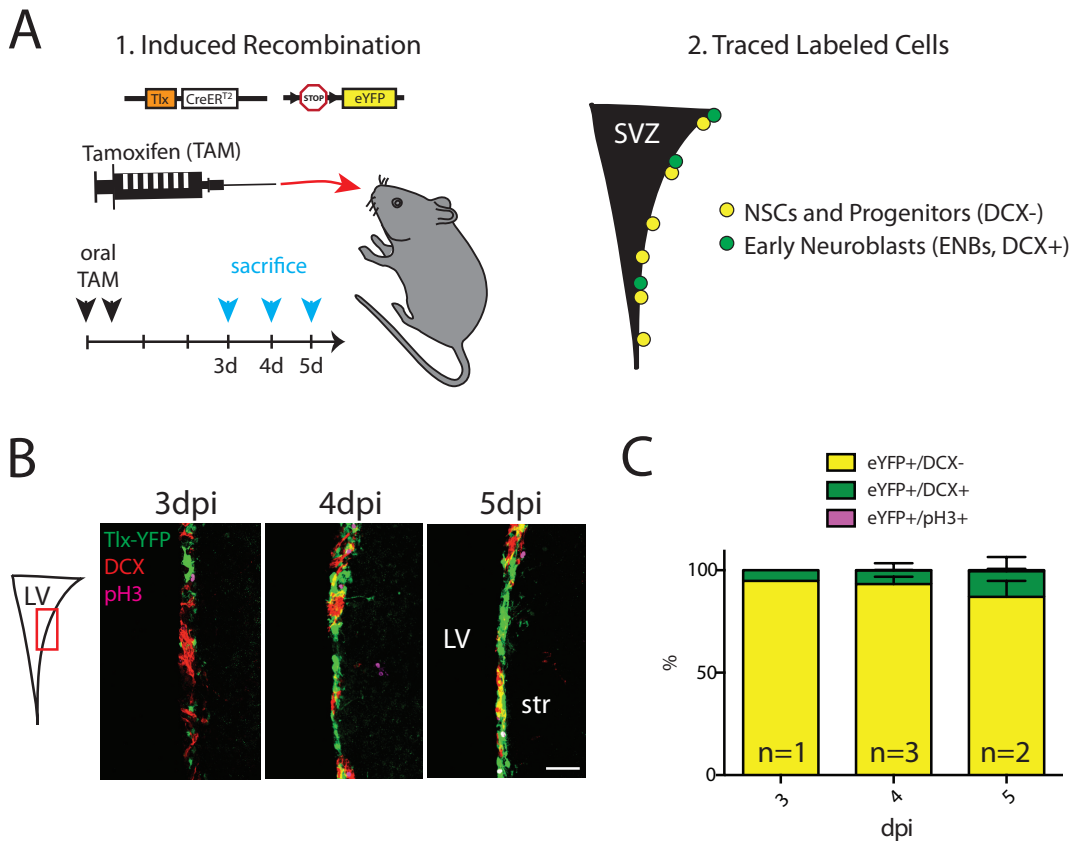

Figure 15: Labeled NSCs continuously develop to neuroblasts. **A** Experimental strategy: TiCRY mice got induced by two shots of oral TAM and identity of the cells was determined by costaining of eYFP and the neuroblasts marker DCX. **B** Representative images showing temporal development of labeled cells. Scale bar: 25µm. **C** Quantification of the overlap of eYFP, DCX and pH3. Very few labeled cells show pH3 expression, while increasing proportion of cells gain DCX expression. dpi: days post induction.

The process of generating mature neurons from SVZ neuroblasts takes at up to 22 days (Petreanu and Alvarez-Buylla, 2002). A timepoint of four weeks after TAM administration was chosen to ensure maximum differentiation into neurons. Together, NSCs were addressed by using the subventricular zone of TiCRY mice (4 days post induction, 4dpi), ENBs by using the SVZ of DiCRY mice (3dpi), LNBs by using the OB of DiCRY mice (3dpi) and neurons by using DiCRY mice (4 weeks post induction, 4wpi).

Next the composition of target populations was investigated in detail by looking at the marker expression and position of eYFP$^+$ cells individually for each mouse model. TiCRY cells were mostly NSCs and neurogenic progenitor cells (eYFP+/DCX-: 88.32%±1.8), some ENBs (eYFP+/DCX+: 7.75%±1.9) and few of unknown identity further away from the ventricle (eYFP+/DCX-: 3.94%±1.3; Figure 16A). DiCRY cells of the SVZ were mostly ENBs (eYFP+/DCX+: 90.52±1.3) and some DCX negative cells of unknown identity (eYFP+/DCX-: 9.49±1.3; Figure 16B).

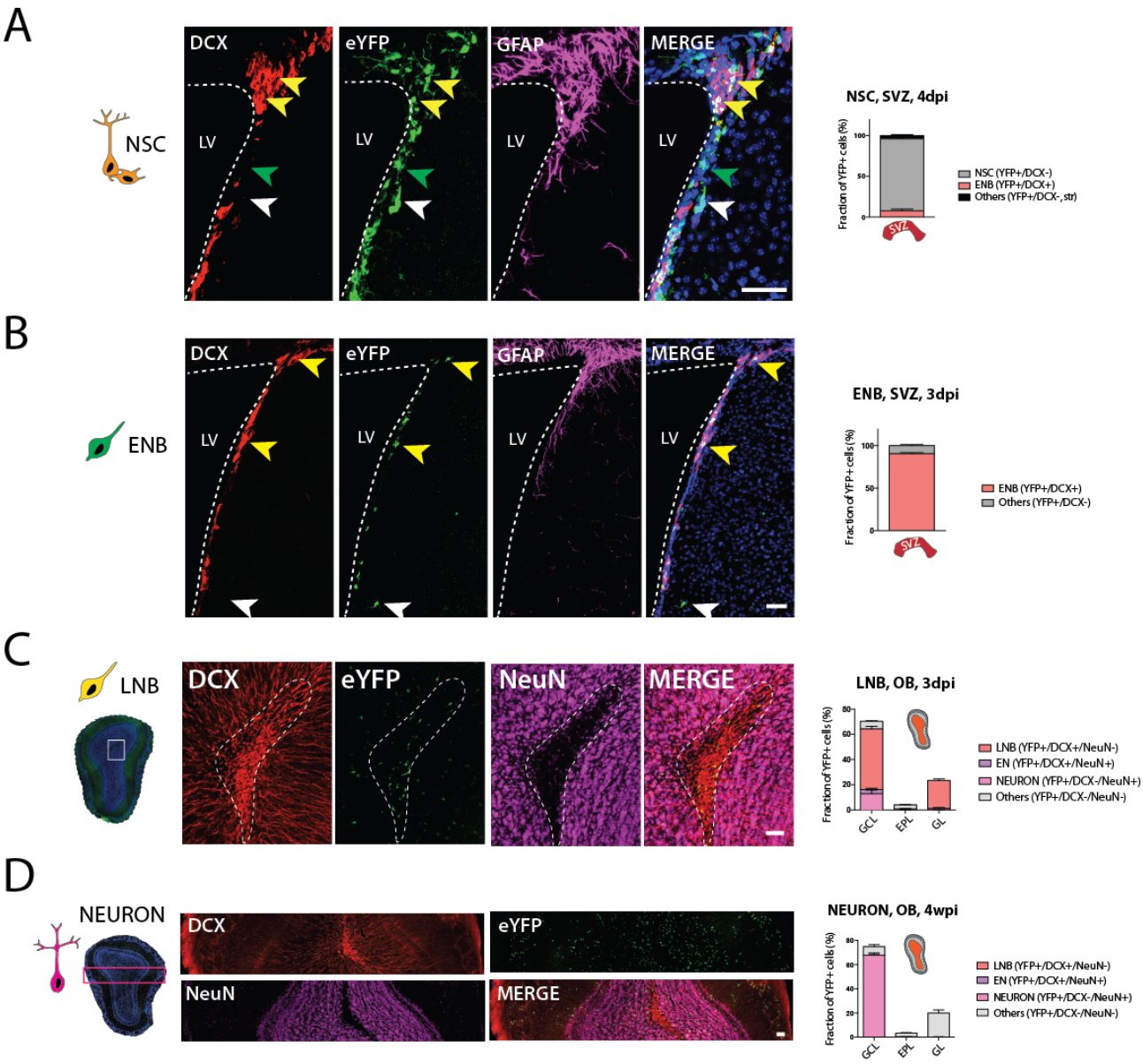

Figure 16: Histological characterization of RiboTag mouse models. Immunofluorescence estimating cell type composition based on eYFP expression and characteristic marker protein expression with quantification. **A** NSCs using TiCRY mice 4dpi, green arrow indicating NSCs, yellow arrows indicating ENB contamination, white arrow showing rare labeled cells outside the SVZ. **B** ENBs using SVZ of DiCRY mice 3dpi , yellow arrows pointing at ENBs and white arrow showing rare labeled cells outside the SVZ. **C** LNBs using OB of DiCRY mice 3dpi, core of the OB marked by dashed line, labeled cells are mostly in the core of OB expressing DCX protein. **D** Neurons using OB of DiCRY mice 4wpi, labeled cells throughout the OB mostly coexpressing NeuN protein. Scale bars: 50µm. SVZ: subventricular zone, OB: olfactory bulb, GCL: granular cell layer, EPL: external plexiform layer, GL: glomerular layer, dpi/wpi: days (weeks) post induction.

DiCRY cells of the OB (3dpi) could be found in all layers (GCL/MCL: 70.33%±1.3, EPL: 4.25%±0.3, PGL: 23,60%±1) indicating no regional bias. eYFP cells in the GCL/MCL were mostly LNBs (eYFP+/DCX+: 47.83%±2, % of all eYFP+ cells in OB), further ENs (eYFP+/DCX+/NeuN+: 3.4%±0.9), neurons (eYFP+/DCX-/NeuN+: 13%±2.9) and some of unknown identity (eYFP+/DCX-/NeuN-: 6.1%±0.5), which most likely consisted of NeuN-negative subtypes of neurons as assessed by morphology and position (Figure 16C). Few

labeled cells could be found in the EPL. These were mostly NeuN- negative neurons (eYFP+/DCX-/NeuN-: 3.33%±0.1), further LNBs (eYFP+/DCX+/NeuN-: 0.21%±0.1) and very few NeuN-positive neurons (eYFP+/DCX-/NeuN+: 0.03%±0.06). YFP cells in the PGL were mostly LNBs eYFP+/DCX+/NeuN-: 22.4%±1), some ENs (eYFP+/DCX+/NeuN+: 1%±0.9) and rarely fully mature neurons (eYFP+/DCX-/NeuN+: 0.2%±0.2). Four weeks after induction of DiCRY mice most YFP cells lost DCX expression indicating maturity (Figure 16D). GCL/MCL cells were mostly mature NeuN positive neurons (eYFP+/DCX-/NeuN+: 67.7%±2) or NeuN negative neurons (eYFP+/DCX-/NeuN-: 7%±1.7). Again, only few cells could be found in the EPL with similar characteristics compared to the three day timepoint (mostly eYFP+/DCX-/NeuN-: 3.1%±0.4). PGL cells were almost exclusively mature neurons (eYFP+/DCX-/NeuN+: 20%±2.5).

Together, this data demonstrated that usage of two inducible Cre-recombinase lines allows investigation of four stages of neuronal differentiation (NSC, ENB, LNB, Neuron) by temporal- (time after induction, 3/4dpi vs. 4wpi) and local control (region of dissection, SVZ or OB). Refinement of induction strategy allowed high purity of target populations with no obvious biases.

3.2.3 Detailed composition of TiCRY labeled NSCs

Subventricular zone NSCs are present in distinct activation states encompassing dormant primed-quiescent, active non-cycling and active cycling states (Codega et al., 2014; Llorens-Bobadilla et al., 2015). This discrete separation is based on molecular characterization of individual cells. Analysis based on single markers allows separation of quiescent- ($EGFR^-$) and active NSCs ($EGFR^+$).

When using transgenic mouse lines, there is the risk that labeled cells have biases for subpopulations and do not recapitulate the entire population. In order to exclude that when using the Tailless (Tlx) promoter as the driver of fluorescence labeling FACS analysis was performed four days after the last injection of TAM in Tlx-$CreER^{T2}$-Tomato cells, where NSCs were labeled by a red fluourescent protein ($Tomato^+$). Combination with staining for previously described surface markers allowed characterization of $Tomato^+$ cells (Figure 17A). Indeed, Tlx-recombined cells comprised all stages of NSCs. Approximately half of the cells were $GLAST^+$ (52.1%±0.6), a marker for NSCs and closely related astrocytes. It was

previously reported that the Tlx-promoter does not drive recombination in astrocytes (Liu et al., 2008), indicating that four days after recombination half of the cells were representing NSCs. Of the GLAST^{+} fraction, again approximately half were EGFR^{+}, active NSCs (51.7%±9.1) and the other half EGFR^{-} quiescent NSCs (46.7%±9.1). Of GLAST- cells 45.6%±0.3), the majority were EGFR+ neural progenitor cells (NPCs, 62.7%±1.6), while the rest represented PSA-NCAM+ neuroblasts (33.3%±2; Figure 17B). Interestingly, FACS based quantification estimated neuroblast contamination higher than the previous histology based analysis using eYFP as the fluorescent marker (15.2% over 7.8%).

Overall, this data demonstrated that Tlx-labeled NSCs comprised all stages of NSCs (quiescent NSC, active NSC, neural progenitors) to similar proportions as they appear in an unbiased approach (Llorens-Bobadilla et al., 2015).

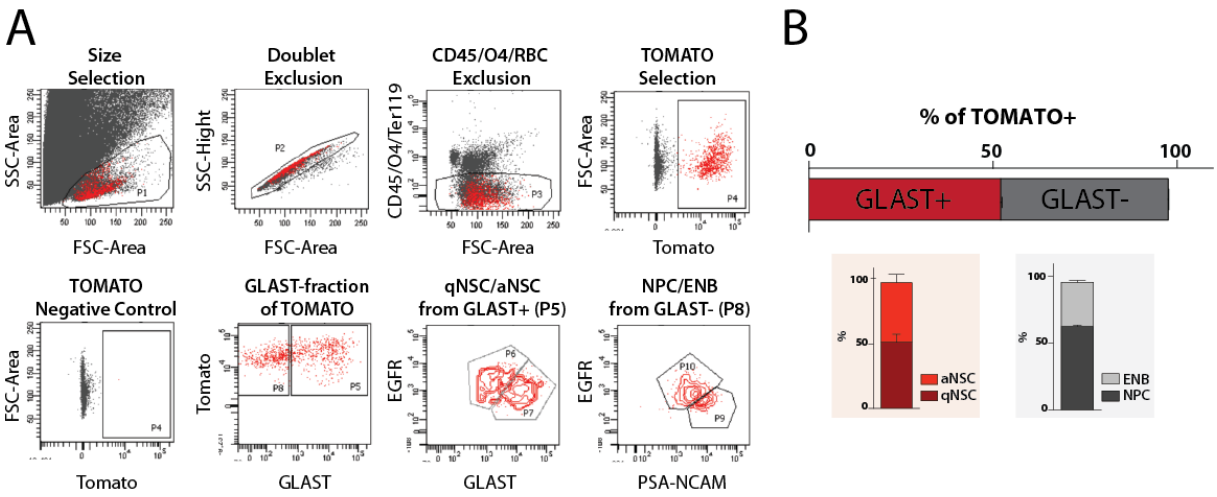

Figure 17: Composition of Tlx-labeled NSCs based on FACS **A** Representative FACS gates for NSCs labeled by Tlx-TOMATO four days post induction. NSCs that are labeled by recombination under the Tlx-promoter contain both quiescent (GLAST^{+}EGFR^{-}) and active NSCs (GLAST^{+}EGFR^{+}). Prom1 was not used in this experiment since it is known that Tlx does not drive recombination in astrocytes. **B** Composition of TOMATO^{+} cells four days after induction. The numbers do not sum up to 100% since some few cells lay between gates. Experiments conducted in collaboration with Enric Llorens Bobadilla (Molecular Neurobiology, DKFZ, Heidelberg).

3.2.4 HA-tag incorporation into translating ribosomes of isolated NSCs

To further characterize HA-tag expression, correct ribosome incorporation and isolation of ribosome-associated mRNAs, NSCs were isolated from TiCRY/NiCRY mice. In TiCRY lines replacement of endogenous RPL22 by RPL22-HA is driven by the stem cell-specific Tailless (Tlx) promoter, while in NiCRY mice recombination is driven by the Nestin promoter which

is active in NSCs and ependymal cells of the SVZ. Since culture conditions select for amplifying cells, only active NSCs and their progeny survive after multiple passaging. NSCs were first characterized by western blot (Figure 18A).

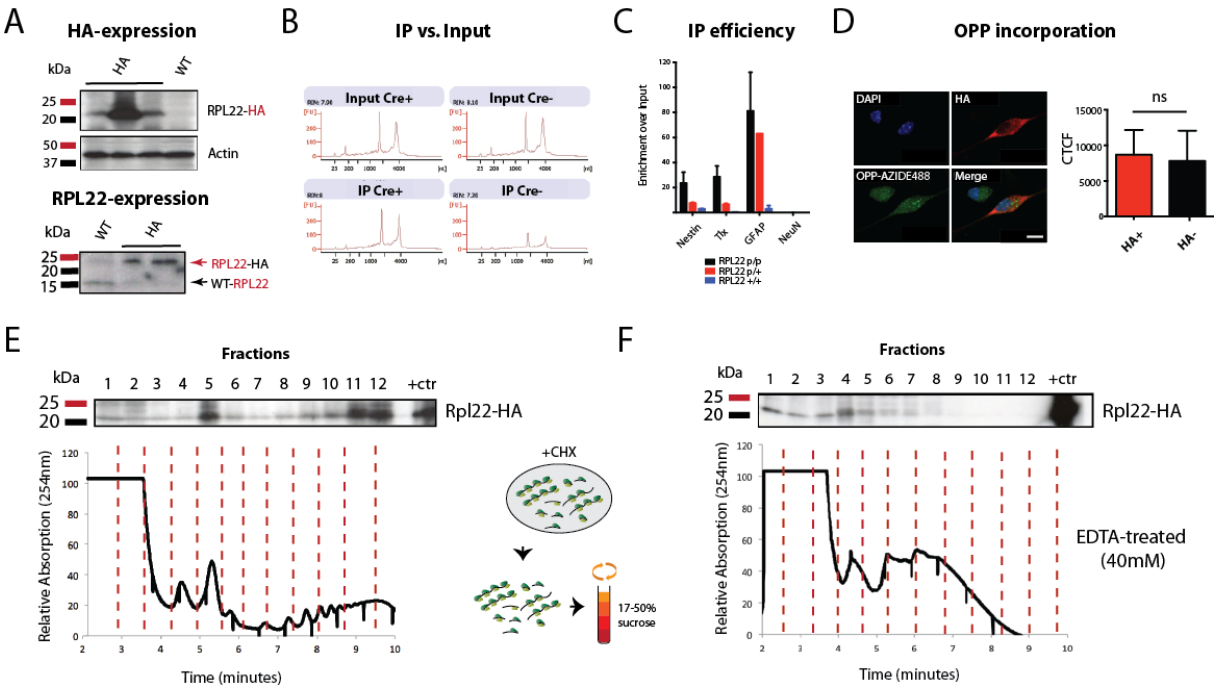

Figure 18: Incorporation of HA-tag into translating ribosomes **A** Top: NSCs isolated from TiCRY mice express HA-tag, replicates show different levels indicating variability based on induction efficiency. Cells of WT mice do not express HA-tag. Bottom: HA-tag is associated to RPL22 since staining shows characteristic 8kDa shift due to HA-tag (23kDa instead of 15kDa). Isolated TiCRY cells entirely replaced WT-RPL22 by RPL22-HA. **B** Representative Bioanalyzer profiles showing that input RNA levels do not vary between Cre^+ mice (expressing HA-tag) and Cre^- mice (no HA-tag), however samples from Cre^+ mice reveal approximately 3-fold more RNA over the background level of Cre^- mice after HA-immunoprecipitation. Data from TiCRY mice. **C** Enrichment of cell type specific transcripts by qPCR after HA-immoprecipitation. Efficiency by enrichment of IP- over input samples. Comparison of NSCs from mice homozygous for the RPL22-tag (p/p), heterozygous for the RPL22-tag (p/+) and WT mice indicates linear relationship between HA-tag expression and IP efficiency. NeuN serves as negative control. Cells isolated from NiCRY mice (Nes-inducible-Cre-Rpl22.HA-eYFP). **D** OPP incorporation does not vary between HA-tag expressing- and non-expressing cells indicating no major impact on global protein synthesis. Measured by corrected total cell fluorescence (CTCF). NSCs isolated from NiCRY mice. Scale bar: 10µm. n= 30 cells each. **E** Polysome fractionation using cultured NSCs indicates efficient incorporation of RPL22-HA (antibody against HA-tag) into actively translating polysomes (see fractions 8-12). Total lysate resembles positive control (+ctr). **F** Disruption of polysomes using EDTA leads to shift of RPL22-HA expression to light fractions indicating specific association to active ribosomes. Experiments in C and D were performed in collaboration with Alejandro Santos Lopez and were presented previously in his bachelor thesis (Molecular Neurobiology, DKFZ, Heidelberg).

While cells isolated from TiCRY mice showed variable amounts of HA-tag expression, wild-type (WT) cells did not show any HA-tag expression. Further, WT cells expressed RPL22 protein at the size of the endogenous protein (15kDA), while $HA\text{-}tag^+$ cells showed a characteristic 8kDA shift due to the size of the HA-tag. This data demonstrated correct RPL22-associated HA-tag expression in isolated NSCs. Next, RNA immunoprecipitation

(RNA-IP) was performed using HA-tag to pull down ribosomes and associated mRNAs. While total mRNA input levels did not vary between HA-tag expressing (Cre+, RPL22-HA) and WT (Cre-, RPL22) mice, immunoprecipitation allowed recovery of approximately 3-fold more RNA in RPL22-HA mice compared to the background (Figure 18B). However, still significant amounts of mRNA were bound even without HA-tag expression indicating high levels of unspecific binding to antibody and beads. Next, cultured cells were used to assess the relationship between HA-tag expression and mRNA recovery. RNA immunoprecipitation was performed using NSCs from WT mice ($RPL22^{+/+}$), heterozygous mice for RPL22-HA expression ($RPL22^{p/+}$) and homozygous mice ($RPL22^{p/p}$) with subsequent enrichment analysis of several genes over input RNA by quantitative PCR (Figure 18C). RNA IP using cells, which lack HA-tag expression did not enrich for any of the analyzed transcripts indicating that unspecific binding is occurring exclusively when performing IP experiments directly from tissue. Enrichment was stronger for cells from homozygous mice, which expressed higher levels of HA-tag, compared to cells from heterozygous mice. This suggested a linear relationship between RPL22-HA expression and immunoprecipitation (IP) efficiency.

Association of proteins with reporter tags can potentially interfere with its function. HA-tag caused a substantial shift in RPL22 size. To control that this modification does not affect its core function, global translation rates of HA^+ and HA^- NSCs were compared using OPP incorporation (Figure 18D). No differences in OPP incorporation could be observed suggesting that RPL22-HA activity is comparable to its endogenous counterpart.

Previous experiments showed association of HA-tag with RPL22 protein. The question remained whether modified RPL22 protein is incorporated into ribosomes as well as whether these ribosomes are actively translating or are potentially stalled. To test for this, sucrose gradient fractionation was performed for cultured NSCs, which allows precise allocation of ribosomal subunits, single ribosomes (monosomes) and multiple ribosomes (polysomes; Figure 18E). HA-tag expression could be found in free fractions but strongly enriched in the monosome- and polysome fractions, indicating association to actively translating ribosomes. To confirm that HA-tag is indeed associated to actively translating ribosomes and does not sediment unspecifically at a similar molecular weight, Ethylenediaminetetraacetic acid (EDTA), was used to disrupt polysomes and HA-tag expression was monitored afterwards. Synthesis of the polypeptide chain as well as

maintenance of polysomes is highly dependent on the availability of magnesium ions. EDTA is a magnesium-chelating agent, which efficiently dissociates polysomes and allows identification of ribosome-associated components. Indeed, HA-tag expression was shifted to lighter fractions after treatment with EDTA, indicating that HA-tag is actively engaged in translating ribosomes (Figure 18F).

Together, these experiments demonstrated that HA-tag is associated with RPL22 protein and this complex is incorporated into actively translating ribosomes with no obvious biases.

3.2.5 FACS-mediated isolation of cells for total RNA sequencing

In order to enrich NSCs, ENBs, LNBs and neurons for transcriptome analysis, RiboTag mice were induced as previously described (see paragraph 3.2.2). Three days (in DiCRY mice: ENBs and LNBs), four days (in TiCRY mice: NSCs) or four weeks (in DiCRY mice: neurons) after induction mice were sacrificed and the tissue containing the cells of interest (SVZ or OB) was isolated. A single-cell suspension was prepared and cells were sorted based on eYFP expression using fluorescence associated cell sorting (FACS). A dead cell marker was used to exclude highly autofluorescent dying cells. Additionally, immune cells were excluded based on expression of the surface marker CD45 (Figure 19A). This way, 200-500 cells of high eYFP expression were sorted directly into lysis buffer. To control for correct enrichment of targeted cells the same number of cells of the eYFP negative pool was sorted in parallel. RNA was isolated from sorted cells and a fraction was used to generate cDNA and analyze samples for correct enrichment. Comparison of eYFP-positive over eYFP-negative cells by quantitative PCR revealed enrichment for stage-specific marker genes (Figure 19B). In NSC samples, Tlx and Ascl1, marker genes for stem- and progenitor cells were highly enriched over control cells (>20 fold) while Nestin, a transcript shared by NSCs, progenitors and highly abundant ependymal cells was not enriched in the $eYFP^+$ cells, potentially since its expression is higher in non-targeted ependymal cells. Transcripts representing negative controls (Dcx for neuroblasts, NeuN for neurons) did not show any enrichment indicating high purity of sorted cells. Similarly, for ENB and LNB samples neuroblasts marker genes (CD24a and Dcx) were highly enriched in eYFP expressing cells in contrast to the astrocyte marker GFAP.

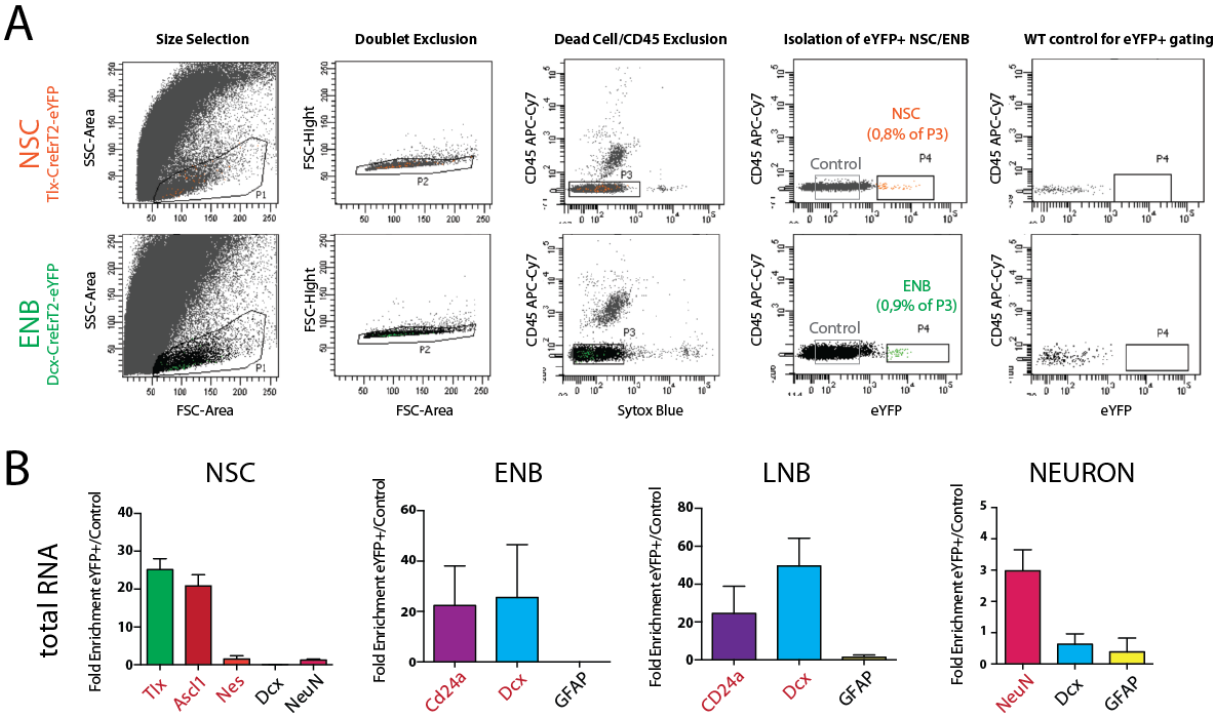

Figure 19: Sorting of cells based on eYFP expression **A** FACS sorting strategy for isolation of NSCs and ENBs based on eYFP expression. eYFP negative cells were collected and used as control samples for enrichment analysis. **B** Enrichment of cell type specific transcripts by comparison of eYFP+ and eYFP- cells by qPCR. Genes that expected to be strongly enriched after correct enrichment are marked in red. All samples were assessed by qPCR before submission for sequencing.

In sorted neurons, the neuronal marker NeuN was enriched over the control population in contrast to the neuroblast marker Dcx and the astrocyte marker GFAP, however to a much lower extent than previous levels enrichment (approximately 3-fold over 20-fold). This might come by the fact that the olfactory bulb is highly populated by neurons causing that random sorted cells in the control sample as well contain many neurons.

All samples were analyzed for enrichment of target genes to ensure high purity. Samples with no obvious enrichment were excluded from further processing. Of high confidence samples a minimum of two replicates were transformed to next generation sequencing libraries using a previously established protocol for low input amounts (Picelli et al., 2014). Together, eYFP based sorting using different mouse models and regions of dissection allowed isolation of NSCs, ENBs, LNBs and neurons of high purity. Enrichment analysis over samples from control populations allowed pre-selection of best samples for subsequent conversion into sequencing libraries.

3.2.5 RiboTag-mediated isolation of ribosome-associated transcripts

In order to assess the ribosome-associated fraction of mRNAs (so-called translatome) from NSCs and progeny, samples were processed similarly as described before for transcriptome analysis (see 3.2.4). Instead of the eYFP expression, HA-tagged ribosomal protein RPL22 was used for isolation of ribosomes with associated RNAs. RiboTag mice were induced as described before and tissue of interest was homogenized and the lysate was incubated with HA-antibody for immunoprecipitation (IP, Figure 20A). A fraction of the lysate (input) was kept for later enrichment analysis, since it contained RNAs from the entire tissue. The complex was isolated using affinity beads and ribosome-associated RNAs were purified subsequently. A fraction of both, input- and IP samples was converted into cDNA and analyzed by quantitative PCR (Figure 20B-E). In parallel HA-based immunoprecipitation was performed with Cre-negative mice, which did not express HA-tag (RIBO-). This way, enrichment could get normalized for background binding. Correct enrichment was assessed by comparing levels of cell-type specific transcripts between input- and IP fractions.

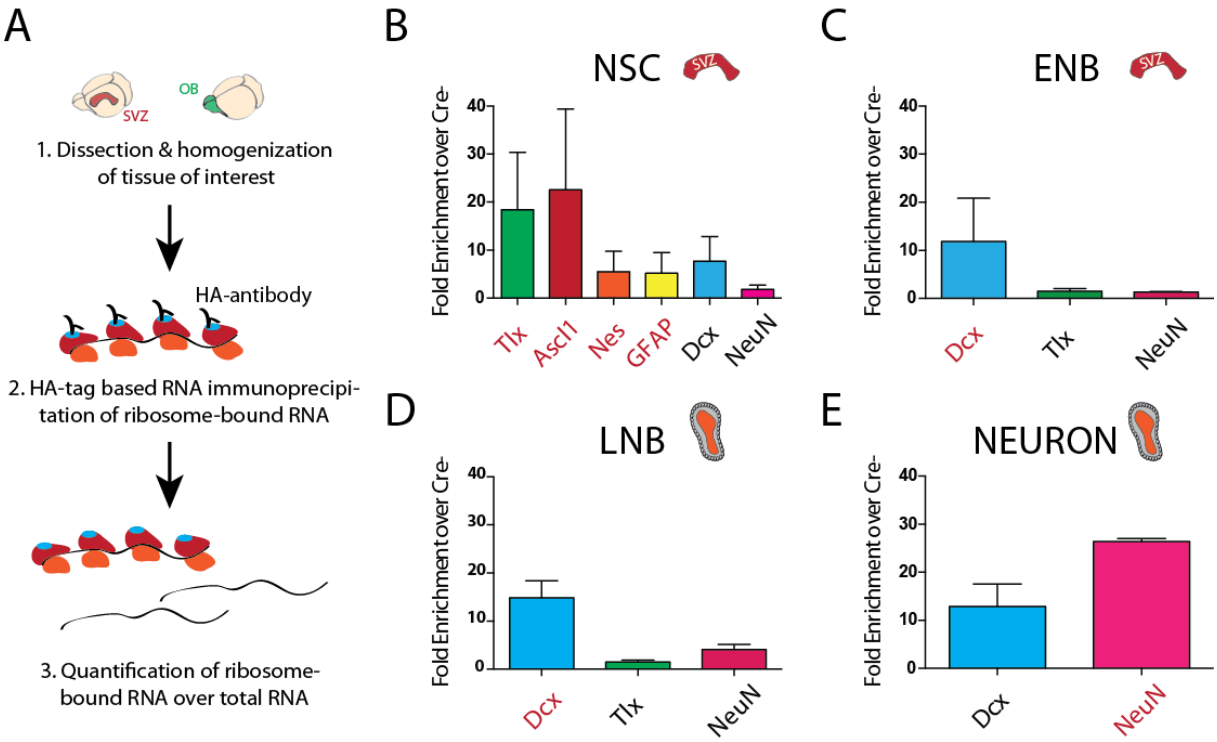

Figure 20: Evaluation of HA-tag based RNA-IP by enrichment analysis **A** Experimental setup. Tissue harboring NSC, ENBs, LNBs or Neurons (SVZ or OB) is isolated at specific timepoints after labeling. After homogenization lysate is incubated with HA-antibody and ribosome-RNA-HA complexes are isolated by affinity beads. RNA is released and compared to total RNA (input RNA). **B-E** Enrichment of cell type specific transcripts for NSC **(B)**, ENB **(C)**, LNB **(D)** and Neuron **(E)** by fold enrichment of HA-IP RNA (RIBO) over input RNA of Cre+ mice compared to Cre- mice, assessed by qPCR. Genes expected to be enriched after successful immunoprecipitation are labeled in red.

Enrichment was compared between HA-tag+ (RIBO+) and HA-tag- mice (RIBO-) to assess background-binding normalized net enrichment of target transcripts. NSC RIBO+ samples expectedly enriched for transcripts including Tlx (expressed in NSCs and astrocytes), Ascl1 (expressed in NSCs and NPCs), Nestin (expressed in NSCs and ependymal cells) and GFAP (expressed in NSCs and astrocytes). On top, also the neuroblast marker Dcx was enriched in RIBO+ samples, in contrast to the neuronal marker NeuN (Figure 20E). Enrichment of Dcx might come by the fraction of cells that started differentiation at the timepoint of the experiment as described earlier (see paragraph 3.2.2). Assessment for correct enrichment of NSCs is challenging since these cells share many common transcripts with astrocytes (e.g. Tlx, GFAP). Ascl1 is more characteristic for the actively proliferating fraction of NSCs and neural progenitor cells (NPCs). The enrichment of both astrocyte/NSCs transcripts together with Ascl1 indicated correct enrichment for NSCs. Interestingly, Nestin, a transcript shared by NSCs and ependymal cells, was not enriched in the previous analysis of sorted cells (see paragraph before) but was slightly enriched in the enrichment analysis of HA-tag based isolation of target populations. Samples showing similar enrichment values were further processed into sequencing libraries. Analysis of ENBs and LNBs was more conclusive showing high enrichment for the neuroblast marker DCX. The astrocyte/NSC transcript Tlx showed very little enrichment in both sets of samples, while enrichment of the neuronal transcript NeuN became more apparent in LNBs, which contained some neurons based on previous histological analyses (see paragraph 3.2.2). In neurons, the neuronal marker NeuN was highly enriched. However, also the neuroblast marker Dcx showed enrichment. This was rather surprising, since at the timepoint of the experiment (4wpi), all HA-tag positive cells should be mature neurons that do not express Dcx based on previous histology (Figure 16). Nevertheless, samples were converted to sequencing libraries and assessed later in greater detail based on sequencing information.

The described experiments represented a screening for successful immunoprecipitations. Some samples did not show any enrichment for cell-type specific transcripts and were excluded from further analysis. Again, two to three replicate samples of each population were produced for sequencing. In order to normalize for background binding, samples of mock immunoprecipitation using Cre-negative animals with no HA-tag expression (RIBO-, each one set for SVZ and OB) were introduced.

3.2.6 Assessment of transcriptome and translatome by next generation sequencing

Libraries with strong enrichment for cell type specific marker genes over mixed control population (transcriptome, RNAseq) or total input RNA (translatome, RIBOseq) were sequenced to an average depth of 30 million reads on a HiSeq2000 platform of Illumina. Samples went through a stringent pipeline of quality control measures based on technical parameters including unique mapping rate and gene body coverage, essentially following the standards of the ENCODE Consortium. Samples with unique mapping rates under 50% or obvious signs of degradation (bias for 5' end of transcripts) were excluded from further analysis.

Sequencing results confirmed high enrichment for cell type specific transcripts both at the level of transcriptome (RNAseq) and translatome (RIBOseq, Figure 21A,B). While NSC transcripts were mostly restricted to NSCs in the SVZ, neuroblast genes already started to get expressed at the level of NSCs (RNA- and RIBOseq, Figure 21A) gradually increased between ENBs and LNBs and finally reduced at the neuronal stage (Figure 21B), demonstrating that some genes have an expression spectrum broader than previously thought. Similarly, neuronal genes started to get expressed at the immature level of LNBs.

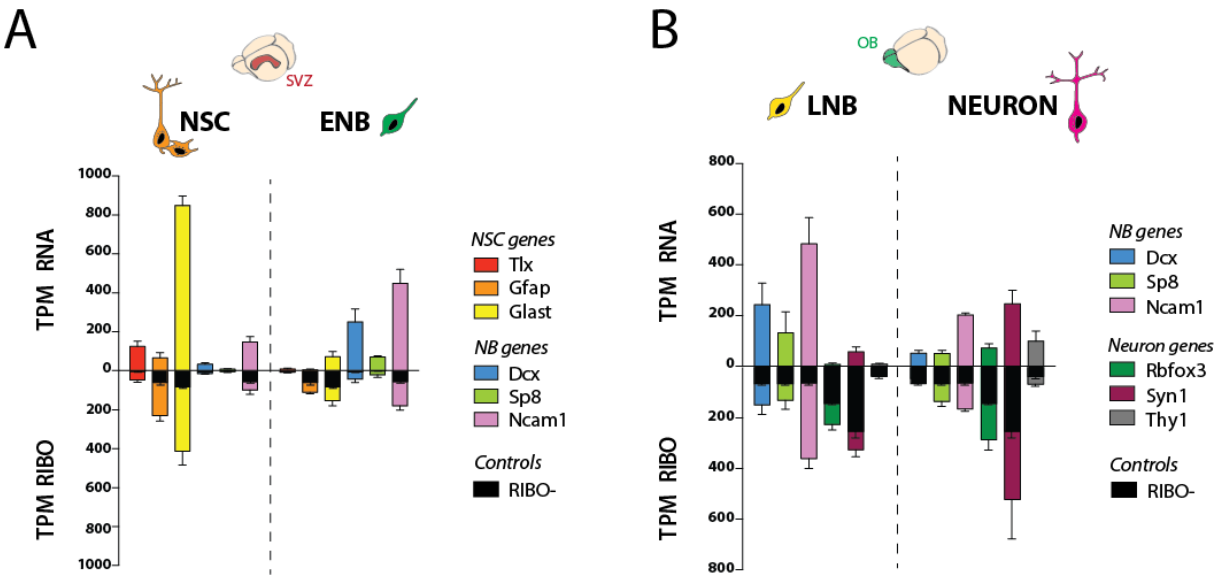

Figure 21: Analysis of transcriptome and translatome based on single marker genes **A** Expression of stage-specific marker genes for SVZ populations at the level of transcriptome (top) and translatome (bottom). **B** Expression of stage-specific marker genes for OB populations at the level of transcriptome (top) and translatome (bottom). Expression values based on tags per million (TPM) reads after Trimmed Mean of M-values (TMM) normalisation. Black bars in RIBOseq base on mock immunoprecipitation using Cre- mice (no HA-tag expression, RIBO-) representing average expression in the respective tissue corresponding to background binding (=noise).

Unspecific binding of RNAs to antibody and/or beads accounted for a significant amount of the signal in this assay (Figure 18B). Sequencing control samples (RIBO-, Figure 21A,B) allowed estimation of background binding and correction in downstream analyses. RIBO- samples represented a mix of transcripts expressed by the entire tissue (SVZ or OB). Transcripts, which were more specific to rare cell types (e.g. Tlx in NSCs) showed almost no expression in RIBO- since the signal was highly diluted by more abundant transcripts. In contrast, in the OB, which is densely populated by neurons, neuronal transcripts (e.g. Syn1) contribute highly to the background binding in RIBOseq samples (Figure 21B).

Next, differential expression analysis was performed for stage transitions solely based on RNAseq or RIBOseq data, respectively (Figure 21A,B). This allowed estimation of successful enrichment for target populations, as well as assessment to which level background binding covers biological differences. When comparing ENBs to NSCs more genes were up- or downregulated at the level of RNAseq when compared to RIBOseq (RNAseq: 2785/3452, RIBOseq: 1257/1598). Interestingly, this ratio changed when comparing ENBs to LNBs, which were pulled down from different brain regions. Now more genes seemed to be differentially expressed at the RIBOseq level (RNAseq: 1395/679, RIBOseq: 3450/3341). Since the average gene expression differs significantly between the SVZ and the OB, large RIBOseq differences most likely represented changes in background binding (RIBO-). Therefore RIBO- control samples were implemented in all further downstream analyses for assessing the overall correlation of the transcriptome and translatome.

When comparing LNBs and neurons of the OB, a similar number of genes were differentially expressed between RNAseq and RIBOseq (RNAseq: 1788/1426, RIBOseq: 1614/1827) already indicating that control at the level of ribosome binding plays an important role for neurons.

To investigate whether key molecular features between populations are maintained in the combined analysis of RNAseq and RIBOseq commonly up- and downregulated genes in RNA- and RIBOseq were identified and analyzed by gene ontology (GO) analysis without considering RIBO- controls. This analysis revealed 447 genes that were upregulated in ENBs and were enriched for processes including central nervous development, neuron projection development and regulation of microtubuli, processes which are highly characteristic for migrating neuroblasts (Figure 21C).

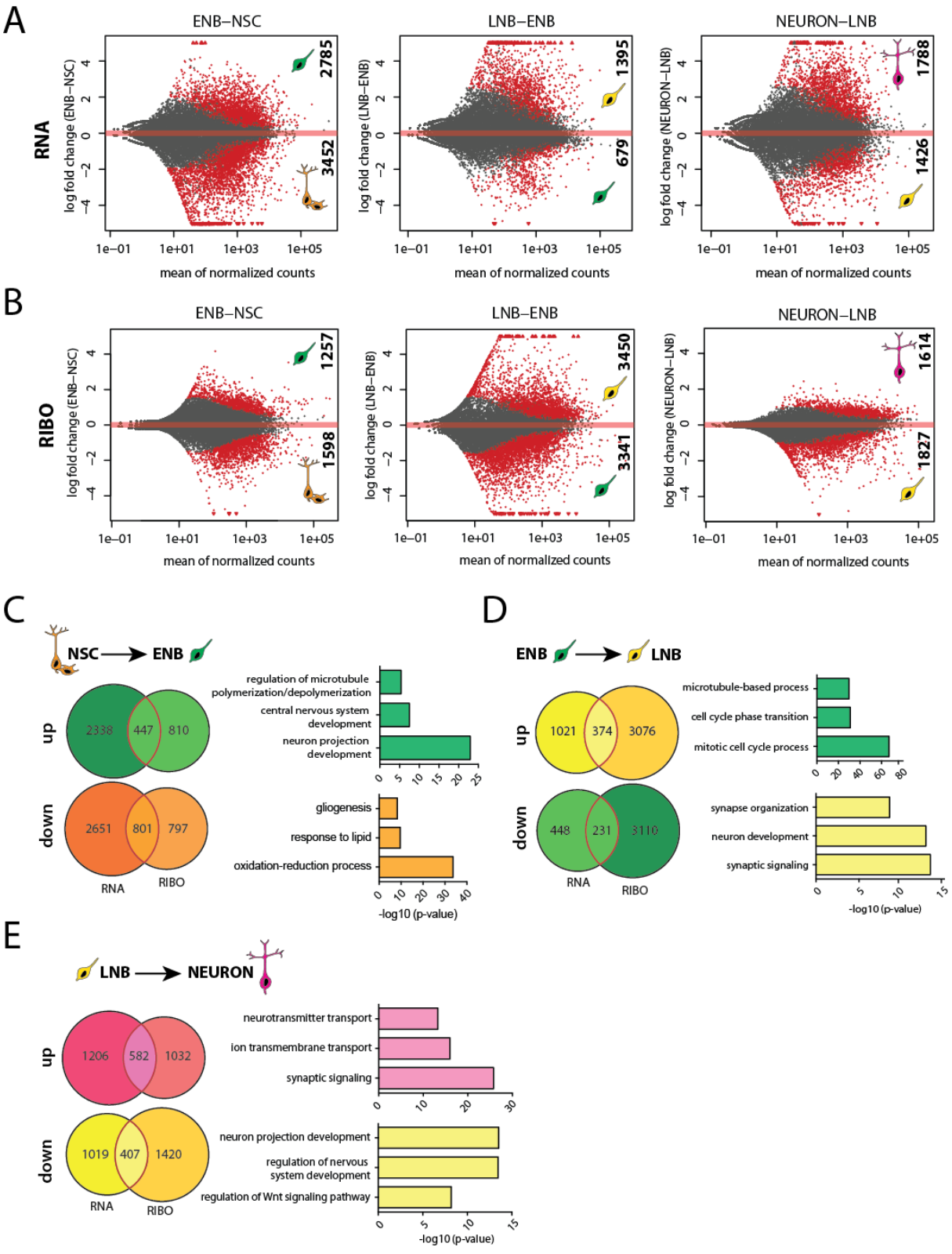

Figure 22: Differential expression analysis for RNAseq & RIBOseq over stage-transitions **A** Differential gene expression based on RNAseq. Subsequent populations were compared and significantly changing genes marked in red (FDR: 10%). **B** Differential gene expression based on RIBOseq without normalization for RIBO-. Subsequent populations were compared and significantly changing genes marked in red (FDR: 10%). **C-E** Overlap of differentially expressed genes between RNAseq and RIBOseq for transition of NSC to ENB (C), ENB to LNB (D) and LNB to NEURON (E, FDR=10%). Only protein coding genes are considered. Gene ontology analysis based on MetaScape on shared genes (marked in red) confirms enrichment of stage specific gene ontologies. Analyses performed in collaboration with Bernd Fischer (Computational Genome Biology, DKFZ, Heidelberg).

In the same line, 801 genes were downregulated that were enriched for processes that are more characteristic for the glial nature of NSCs (e.g. gliogenesis, response to lipid). When looking at the ENB-LNB transition, 374 genes were upregulated in RNAseq and RIBOseq, enriched for processes including neuron development and synapse organization, indicating establishment of neuronal characteristics (Figure 21D). Downregulated genes were mostly related to cell cycle, since olfactory bulb neuroblasts are much less proliferative compared to earlier stages in the SVZ/RMS. In neurons, neuronal properties were further enhanced, while developmental categories were reduced indicating that the differentiation process is complete (Figure 22E). Interestingly, gene ontologies related to Wnt signaling were downregulated from immature to mature stages of neurons.

Together, this paragraph demonstrates that this system, after appropriate background subtraction, can be used for integrated and stage-specific transcriptome and translatome analysis.

3.2.7 Integrated Analysis of Transcriptome vs. Translatome During Lineage Progression

Storage of mRNA for temporal and local control of its translation is of particular importance in highly compartmentalized neurons (Jung et al., 2012). To which level similar mechanisms are already acting at earlier stages of neuronal differentiation remains elusive. The RiboTag strategy was next used to compare RNAseq and RIBOseq data in order to identify transcripts, which are post-transcriptionally controlled at the four stages of differentiation in an unbiased manner. To this end, a linear model that integrates RNAseq, RIBOseq and RIBO- for each stage of interest has been applied (Figure 23A). To identify targets with high confidence, the analysis was restricted to protein coding, highly abundant transcripts (read count > 1000 in RNAseq). Transcripts abundant in RNAseq but not RIBOseq (after correction by RIBO-) were entitled „repressed“, suggesting that active mechanisms prevent these from ribosome association and therefore protein production. In contrast, transcripts with higher ribosome association than expected based on RNAseq data were entitled „enhanced“, suggesting that their ribosome association is actively promoted. Our analysis revealed that only few transcripts showed repression (33/4502) or enhancement (9/4502) in NSCs indicating that, at least during homeostasis, abundant transcripts are proportionally translated at this stage (Figure 23B,C). Interestingly, onset of differentiation initiated divergence of the transcriptome and translatome. ENBs featured a

fraction of genes, which were translationally repressed (275/3418) or enhanced (62/3418). LNBs displayed higher divergence of transcriptome and translatome.

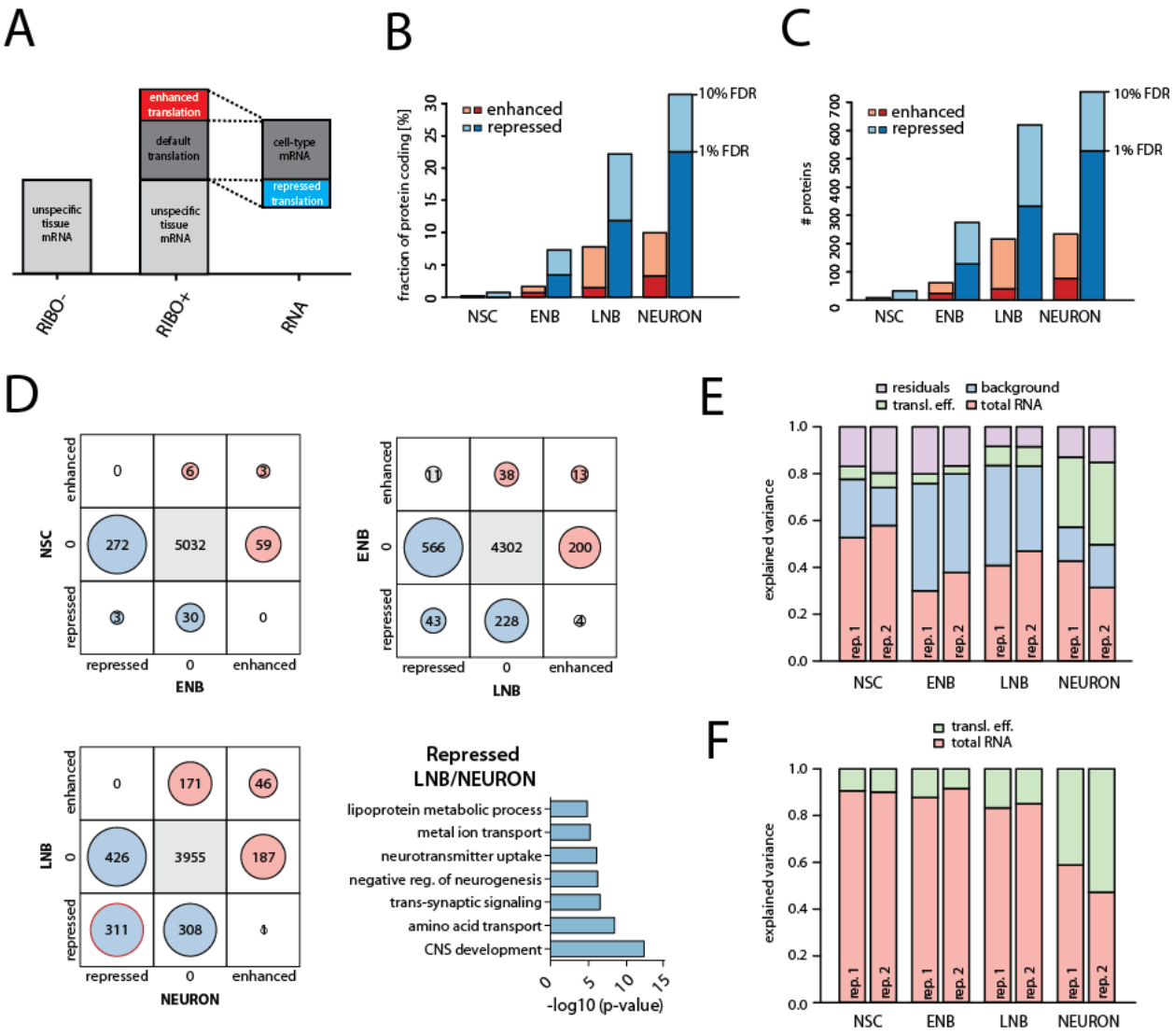

Figure 23: Stage-specific repression and enhancement of transcripts **A** Scheme describing the three datasets, which are implemented into analysis of translation efficiency. RIBO- sample resembles mock immunoprecipitation with HA-tag negative mice to assess background binding. **B** Summary of the fraction of genes, which are repressed or enhanced in each population (only protein coding). **C** Summary of the absolute number of genes, which are repressed or enhanced in each population (only protein coding). **D** Comparison of repressed- and enhanced genes over stages reveals increasing overlap with progression of cells. LNBs and neurons feature high overlap of repressed genes (n=311). Gene ontology analysis (by Metascape) for shared genes that are repressed in LNBs and neurons enrich for neuronal processes. **E** Explained variance analysis (EVA) scoring the contribution of background (RIBO-), total RNA (RNAseq), translation efficiency (RIBOseq over RNAseq and RIBO-) and residual noise to the gene expression of each population. **F** EVA reduced to the contribution of overall RNA abundance (total RNA from RNAseq) and translation efficiency (RIBOseq over RNAseq and RIBO-) indicating increased importance of translational regulation in neurons. Analyses performed in collaboration with Bernd Fischer (Computational Genome Biology, DKFZ, Heidelberg).

Repressed transcripts (n=620/1957) were related to cell adhesion and proliferation while enhanced transcripts (n=217/1957) were rather functionally unrelated but included markers of immature (e.g. Cd24a) and mature neurons (e.g. Tubb3). Neurons showed the highest degree of variation between RNAseq and RIBOseq (Figure 23B,C, Figure 24). In fact, most of the analyzed genes showed either repression (n=737/1373) or enhancement (n=234/1373).

The analysis of explained variance also confirmed that a significantly higher fraction of the RIBOseq data can be explained by translation efficiency and not only by RNA abundance in neurons (Figure 23E,F).

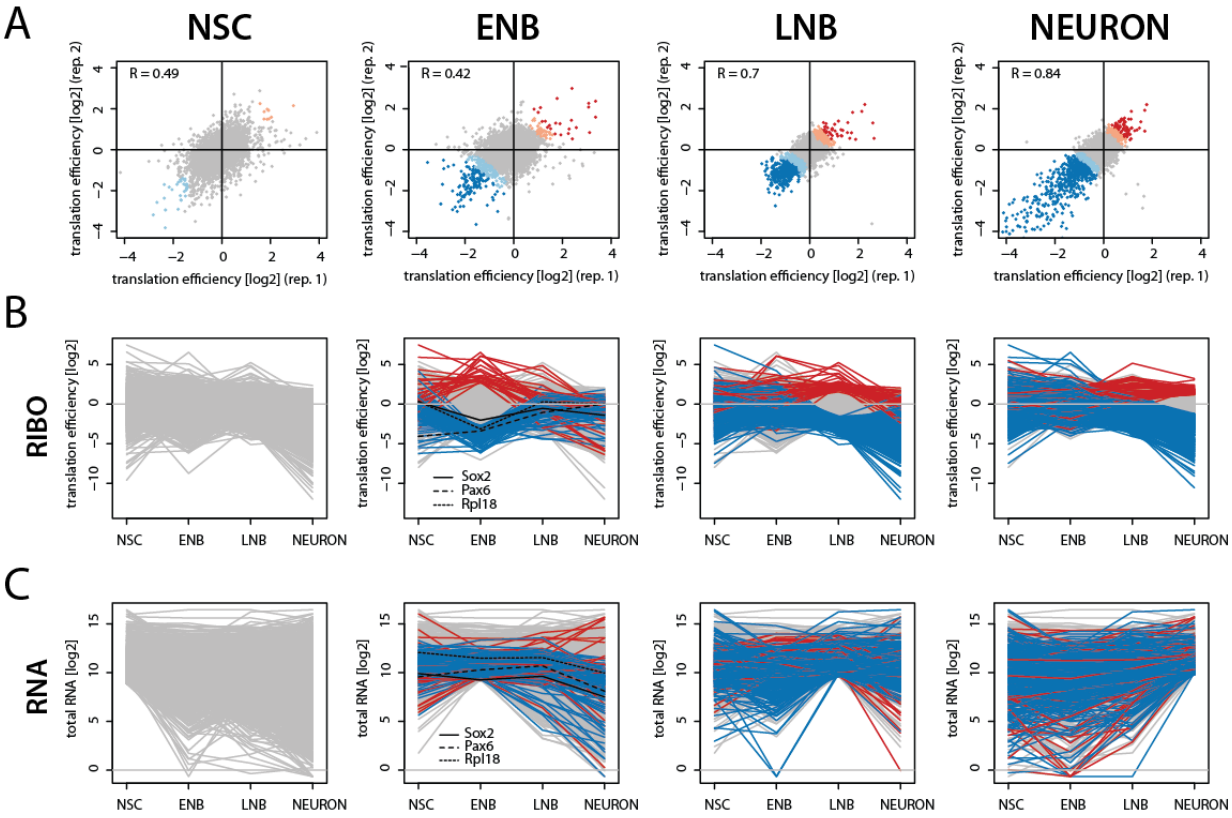

Figure 24: Temporal interplay of transcription & translation during lineage progression **A** Scatter plots for each population showing translation efficiency. Grey dots: genes with linear ratio between transcription (RNA) and translation (RIBO), blue dots: genes which are translationally repressed (dark: 1% FDR, light: 10% FDR), red dots: genes with enhanced translation (red: 1% FDR, orange: 10% FDR). Increasing number of genes with enhanced or repressed translation with further differentiation. **B** Matched plots to the order of scatter plots in (A) illustrating temporal changes in translation efficiency of genes being significantly repressed or enhanced in the respective population. Only highly significant genes marked here in color (FDR=1%), Sox2 marked in black as an example for genes that are translationally repressed at the ENB stage. **C** Matched plots to the order of scatter plots in (A) illustrating temporal changes in transcription of genes being significantly repressed or enhanced in the respective population. Only highly significant genes marked here in color (FDR=1%), Sox2 marked in black as an example for genes that are translationally repressed at the ENB stage. Analyses performed in collaboration with Bernd Fischer (Computational Genome Biology, DKFZ, Heidelberg).

Next, the interplay between transcriptional- and translational regulation was investigated (Figure 24). Transcripts with repression or enhancement were marked for every stage (Figure 24A) and how translation efficiency and transcription vary between different stages of differentiation was examined.

Doing so, different modes of repression and enhancement became apparent. Transcripts with repression at later stages (LNB and neurons) displayed a gradual decrease of translation efficiency from NSCs to neurons. However, many transcripts that were repressed at the ENB stage only showed a stage-specific repression and released the translational block with further differentiation (Figure 24B). Interestingly, many of these transcripts only showed minor differences at the total RNA level indicating a high dependency on post-transcriptional control (Figure 24C).

Clustering of enhanced- and repressed transcripts showed a developmental association where uncoupled genes were rather unique in ENBs, whereas LNBs and neurons shared a large amount of repressed and enhanced transcripts (Figure 23D). This indicates that with progressive differentiation to neurons, cells enter a mode of increasing dependency on translational control. Together, this data showed that while NSCs display a highly linear relationship between RNA levels and ribosome binding, this relation progressively diverges in their progeny, reaching maximum uncoupling in mature neurons.

3.2.8 SOX2 expression is post-transcriptionally repressed in ENBs

The screening for repressed and enhanced transcripts revealed pervasive transcript-specific regulation across the multiple stages. Further analyses focused on the ENB stage, since this is the first stage that shows substantial differences in total RNA abundance and ribosome binding. Repressed transcripts included multiple ribosomal genes as well as the prominent transcription factors Paired box protein 6 (Pax6) and sex determining region Y-box 2 (Sox2) (Figure 24B).

SOX2 is a widely known stemness factor and its deficiency leads to impaired generation of neurons *in vitro*, neurodegeneration and impaired neurogenesis in the adult brain (Cavallaro et al., 2008; Ferri, 2004). Further experiments focused on closer characterization of SOX2 expression. Sox2 mRNA is highly abundant in NSCs (TPM: 65.3±1.3) and only slightly reduced in ENBs (TPM: 41.5±7.9). However, ribosome binding, which is highly over background binding in NSCs, is entirely abolished in ENBs (Figure 25A). To confirm this,

parallel *in situ* hybridization and immunohistochemistry for Sox2 mRNA and protein was applied in the adult brain. To better visualize mRNA molecules in fine cell processes, TiCROMATO mice (Tlx-CreER-tdTomato, labels NSCs by a red fluorescent protein) were used for these experiments. Staining for doublecortin (DCX) as a neuroblast marker allowed simultaneous assessment of Sox2 RNA and protein abundance in NSCs and ENBs (Figure 25B). While both NSCs and ENBs showed substantial levels of Sox2 mRNA, protein abundance was mostly limited to NSCs. RNA molecules per cell and the respective protein expression was quantified for 289 cells (Figure 25C,D). At similar RNA levels, NSCs almost always produced higher protein levels indicating higher translation efficiency (Figure 25C).

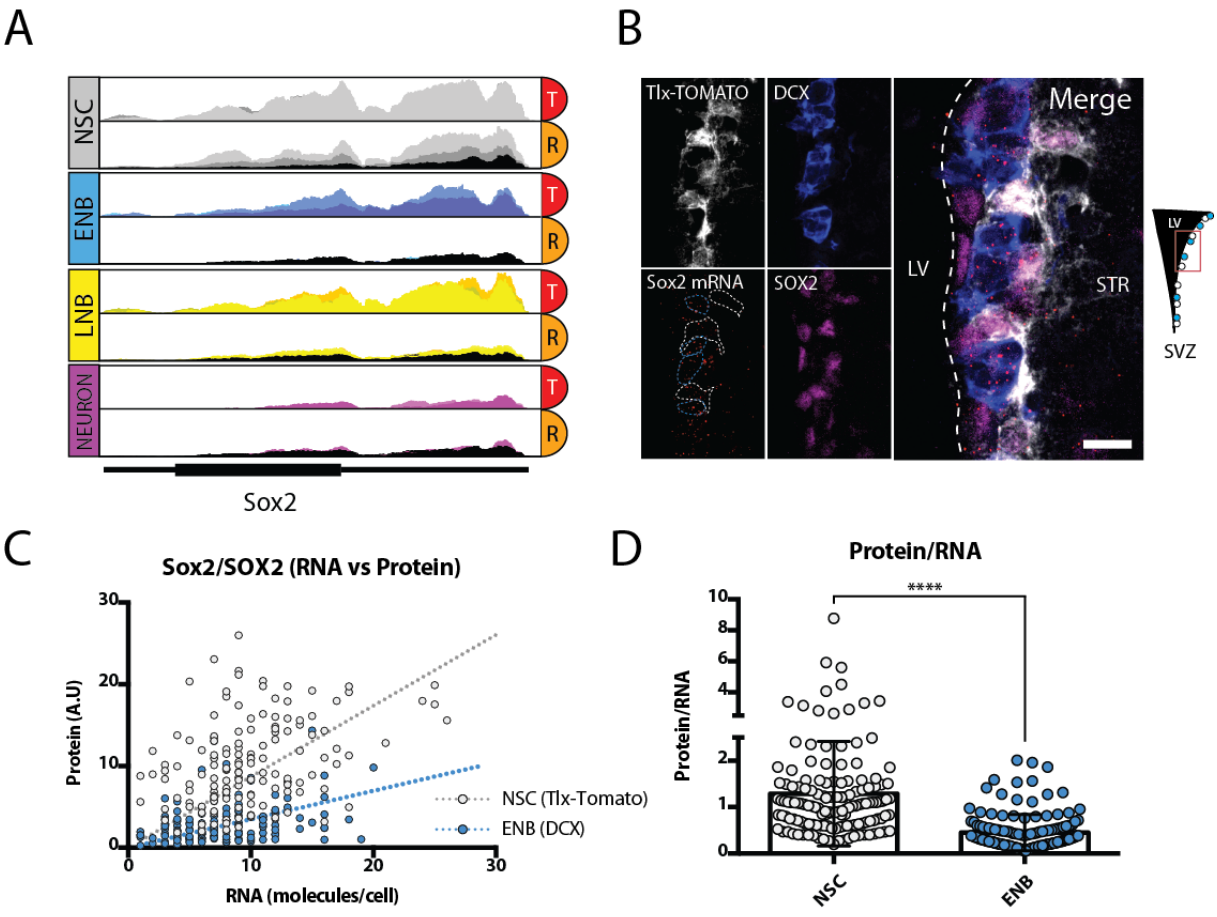

Figure 25: SOX2 is post-transcriptionally repressed in ENBs **A** Sox2 locus in the integrated genome viewer (IGV) both of total RNA (T) and ribosome-bound RNA (R) for populations of interest, histogram shows abundance of reads. Different color hues mark biological replicates. Black histogram indicates background binding (RIBO-). Sox2 shows no ribosome binding specifically at ENB stage indicating post-transcriptional repression. **B** Representative image for parallel *in situ* hybridization and immunohistochemistry for Sox2 protein/RNA in NSCs (marked by Tlx-TOMATO) and ENBs (marked by DCX) validating Sox2 repression event. Scale bar: 10µm. **C** Quantification or Sox2 RNA (molecules per cell) and protein expression (total fluorescence) by manual segmentation. Regression line indicates different translation efficiency. Quantified 144 NSCs and 145 ENBs from two mice. **D** Ratio of protein expression to RNA abundance indicates greatly reduced translation efficiency of SOX2 in ENBs. Significance by students t-test (Mann-Whitney).

Interestingly, ENBs performed poorly in producing SOX2 protein even when containing high levels of its RNA. Comparison of protein expression to RNA abundance revealed a 2,8-fold reduction of Sox2 translation efficiency from NSCs (Protein/RNA=1.3±1.1) to ENBs (Protein/RNA=0.5±0.4) confirming the RIBOseq data.

Since, quantification within the densely packed SVZ can be challenging, Sox2 translation efficiency was independently addressed in freshly sorted cells of the SVZ (Figure 26). Shortly after plating, cells were fixed and assessed for Sox2 mRNA and protein as described in the tissue. Also in this *ex vivo* paradigm, NSCs exhibited the highest Sox2 translation efficiency when compared to NPCs and ENBs (Figure 26B,C). Interestingly, NPCs, which are developmentally positioned between NSCs and ENBs, showed an intermediate efficiency for Sox2 translation (see regression lines), even if they displayed the highest absolute levels of Sox2 mRNA and protein (Figure 26B).

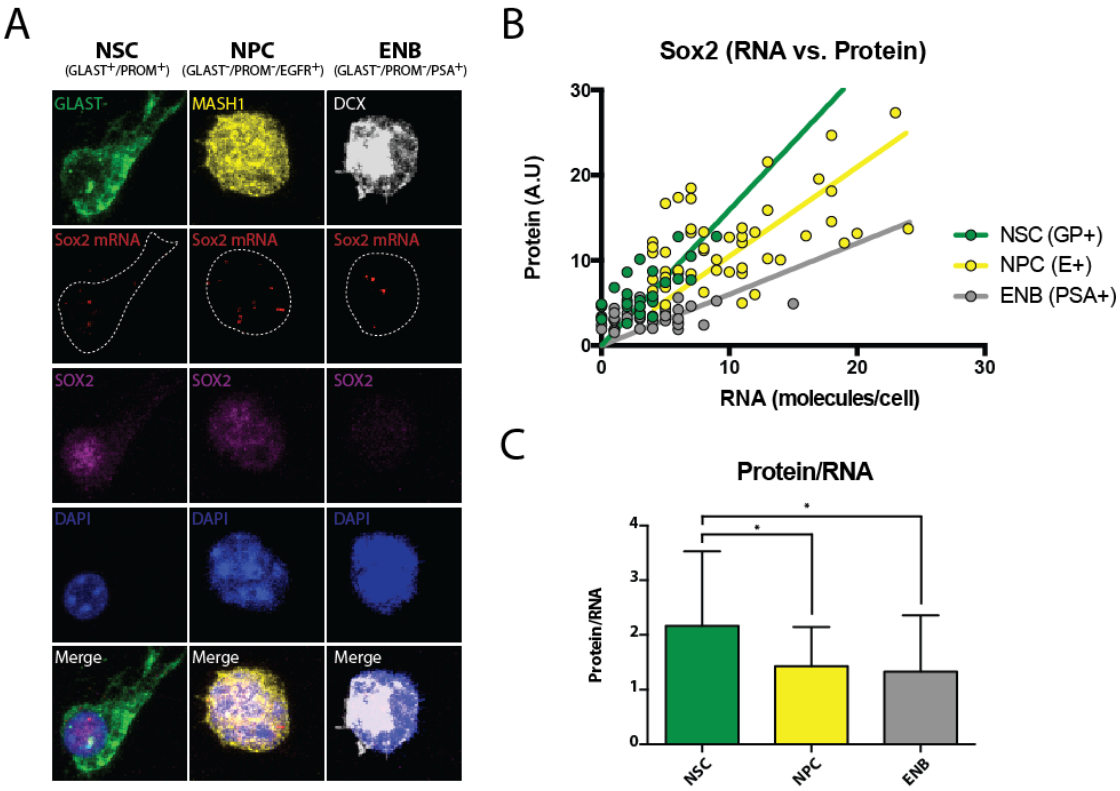

Figure 26: SOX2 translation effiency progressively drops from NSCs over NPCs to ENBs **A** Representative images for parallel *in situ* hybridization (ISH) and immunocytochemistry of freshly sorted cells of the SVZ. Comparison of NSCs (GLAST+PROM+), neural progenitor cells (NPCs, GLAST-PROM-EGFR+) and ENBs (GLAST-PROM-PSA-NCAM+). Stained for cell type specific marker proteins and SOX2. ISH for Sox2 mRNA. Scale bar: 5µm. **B** Quantification of SOX2 protein and RNA expression in NSCs, NPCs and ENBs. Regression line indicates most efficient translation in NSCs. **C** Ratio of protein expression to RNA abundance indicates higher translation efficiency of SOX2 in NSCs when compared to NPCs or ENBs. Significance by students t-test (Mann-Whitney).

Interestingly, Sox2 ribosome binding was over background binding at later stages (LNBs and neurons), which was surprising since Sox2 is mostly known to be expressed in immature cells (Figure 25A). To further investigate this, DiCRY mice were used to label neuroblasts and newborn neurons were investigated in the olfactory bulb four weeks after induction. While, adult born neurons in the granular cell layer (GCL) did not show any SOX2 expression, periglomerular neurons exhibited high levels of SOX2 protein. Co-staining with multiple neuronal markers identified Calretinin-positive neurons of the PGL as the only neurons in the OB to express SOX2 protein (Figure 27A).

To investigate whether these neurons are adult-born with SVZ origin two timepoints were compared after labeling. Migration of cells from the SVZ to the olfactory bulb can take up to 15 days (Lois and Alvarez-Buylla, 1994). Consequently, an early timepoint after recombination was chosen (3dpi), when labeled cells of SVZ and RMS are still migrating, and a late timepoint (4wpi), when all labeled cells reached their final OB destination.

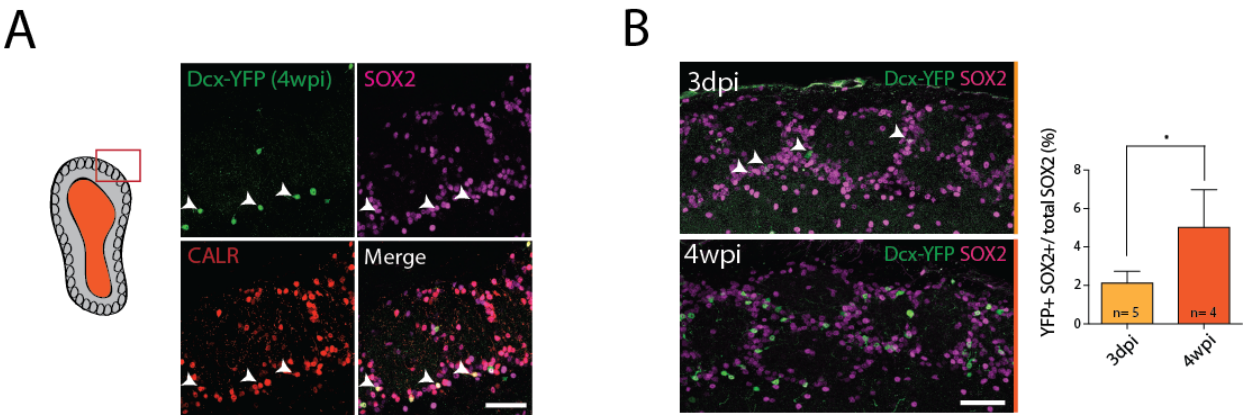

Figure 27: SOX2 is highly expressed in a subpopulation of olfactory bulb interneurons **A** Staining of olfactory bulb periglomerular layer showing Dcx-eYFP traced cells (4wpi), which coexpress SOX2 and the neuronal marker Calretinin. Scale bar: 50µm. **B** Comparison of short (3dpi) and long (4wpi) tracing of Dcx-eYFP cells shows increase of $eYFP^+SOX2^+$ cells with time indicating contribution of migrating, newborn neurons to the pool of $SOX2^+$ neurons in the periglomerular layer. n=9. Significance by students t-test (Mann-Whitney). Scale bar: 50µm.

This analysis showed that significantly more $SOX2^+eYFP^+$ cells are present at the later timepoint indicating contribution of newborn, migrating neuroblasts to this layer (Figure 27B). This is in line with the RIBOseq data, which showed that ribosome binding of Sox2 transcript is increased at olfactoy bulb neuroblasts and neurons (Figure 25A).

Together, these experiments showed that Sox2 transcripts are transiently repressed in ENBs, presumably to shutdown the NSC program. Surprisingly, these dormant Sox2 transcripts become re-expressed in a subset of olfactory bulb neurons.

3.2.9 Temporal repression is mediated by 5′ pyrimidine-rich motifs and mTORC1 activity

ENBs featured a defined set of 275 translationally repressed genes. The question arised whether these genes would share features that distinguish them from thousands of non-repressed genes that were assessed in parallel. In order to screen for common sequence features, *de novo* motif analysis was applied on both untranslated regions (UTRs) as well as the coding region of repressed transcripts. While hits in the coding region and 3′ UTRs where more divergent and varying in their composition (see Table S1), enriched motifs in the 5′ UTR were clearly composed of a stretch of pyrimidines (TCTTTC/CTCTTT, Figure 28A).

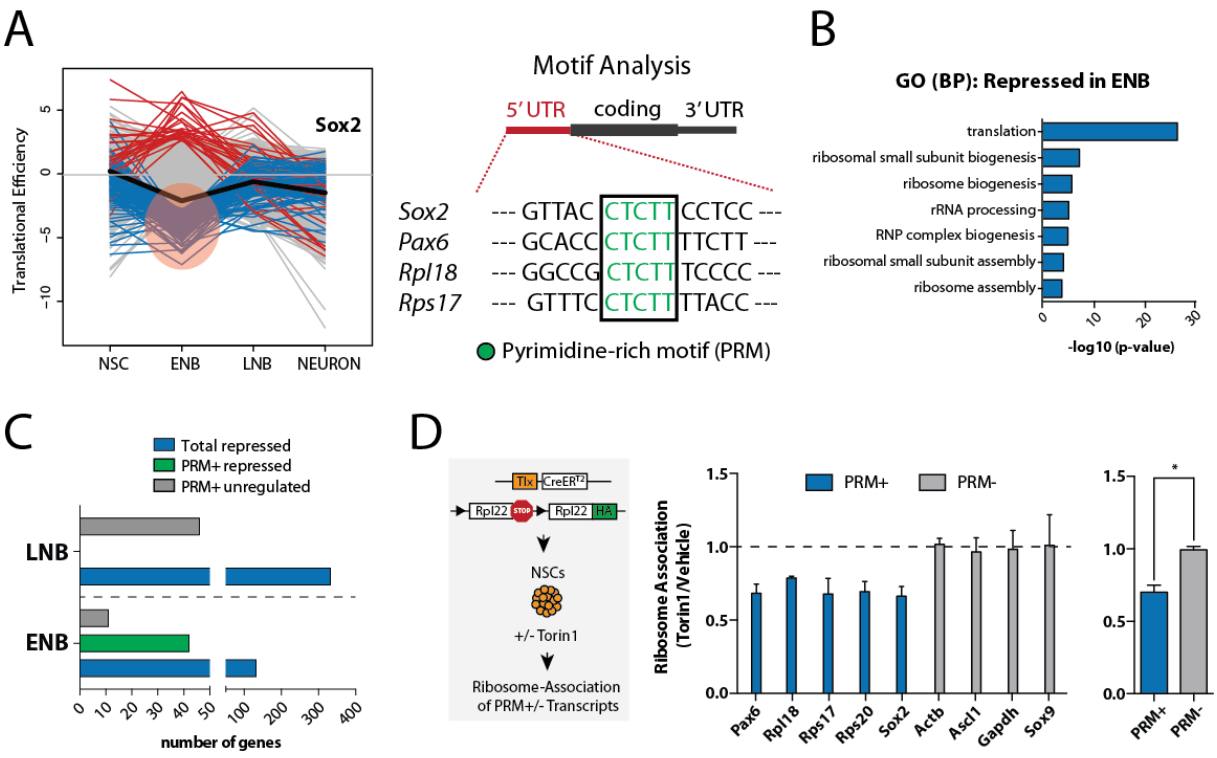

Figure 28: Pyrimidine-rich motifs in the 5′ UTR predict translational repression **A** Motif analysis reveals enrichment of pyrimidine-rich motif (PRM) CTCTT in the 5′ untranslated region (UTR) of genes, which are repressed at the ENB stage. **B** Gene ontology analysis for genes, which are repressed at the ENB stage are mostly related to the protein synthesis machinery. **C** Relation of containing a 5′ PRM and repression at the ENB or LNB stage indicates stage-specific repression of 5′ PRM containing transcripts in ENBs independent of the total number of repressed genes (1% FDR). **D** Investigation of ribosome association under Torin1-induced inhibition of mammalian target of rapamycin (mTOR). Ribosome association by RNA immunoprecipitation using Rpl22-HA+ NSCs. PRM-containing transcripts reduce ribosome association after Torin1 treatment (2h), while PRM- transcripts maintain their ribosome association. Significance by students t-test (Mann-Whitney). Analyses performed in collaboration with Bernd Fischer (Computational Genome Biology, DKFZ, Heidelberg).

Similar motifs were previously shown to mediate mTORC1-dependent translation. These, so-called 5′ terminal oligopyrimidine (TOP) motifs feature multiple ribosomal proteins and translational regulators, which are found to be particularly sensitive to mTORC1 activity (Thoreen et al., 2012). Similarly, the list of repressed genes in ENBs enriched highly for

translational regulators including several ribosomal subunit proteins (e.g. Rpl18, Rps17, Rps20) but also transcription factors important for neurogenesis (e.g. Sox2, Pax6, Figure 28A,B). Many of these transcripts harbored a stretch of pyrimidines, that unlike the traditional TOP motifs, were not always situated at the terminal end of the untranslated region (UTR).

The presence of pyrimidine rich motifs (PRMs) sensitizes transcripts for mTORC1 activity and therefore PRM-containing transcripts would be particularly repressed during a mTORC1 mediated global shutdown of protein synthesis in ENBs. Indeed, over eighty percent of PRM containing transcripts showed stage-specific translational repression in ENBs (Figure 28C). Interestingly, no PRM-containing transcripts were repressed at the LNB stage, although this population featured many more genes with translational repression. This suggests, that PRMs mediate translation efficiency in a highly stage-specific manner.

To prove that PRM-containing transcripts behave differently to others under mTORC1 inhibition, NSCs were isolated from TiCRY mice, which express Rpl22-HA and can be used to isolate and analyze ribosome-bound mRNAs (Figure 28D). Cells were acutely treated with the mTOR inhibitor Torin1, which unlike rapamycin fully inhibits mTORC1 (Thoreen et al., 2012; 2009)(Figure 29A). RNA immunoprecipitation using HA antibody and subsequent conversion of ribosome-bound mRNAs into cDNA allowed analysis per qPCR. Based on the hypothesis, transcripts that contain PRMs would be more sensitive to mTORC1 inhibition than others. Ribosome association of transcripts from the list of repressed genes that contained PRMs (PRM+: Pax6, Rpl18, Rps17, Rps20 and Sox2) were compared to transcripts that do not contain PRMs (PRM-: Actb, Ascl1, Gapdh, Sox9) after Torin1 treatment. Indeed, PRM-containing transcripts showed an average of 32% reduction of ribosome association upon Torin1 treatment, while control genes (PRM-) did not show any change in ribosome association (Figure 28D).

To further support that ribosome association after mTORC1 inhibition is dependent on the presence of PRMs, sucrose gradient fractionation of primary NSCs was performed following Torin1 treatment. Torin1 had only minor impact on global translation, as assessed by the shape of the rRNA absorption curve (Figure 29B). Next, the change in the ribosome association of PRM- transcripts (Actb, Ascl1) and PRM+ transcripts (Rpl18, Rps17) upon Torin1 treatment was assessed by quantitative PCR of individual ribosomal fractions. In this assay, later fractions correspond to association to polysomes (multiple ribosomes)

indicating high translation efficiency. Again, PRM+ transcripts showed higher sensitivity to the Torin1 treatment than PRM- transcripts shown by a shift of a subset of transcripts to earlier fractions (Figure 29C,D). However, replicate samples showed a higher degree of variation, which might be due to technical variability of the assay.

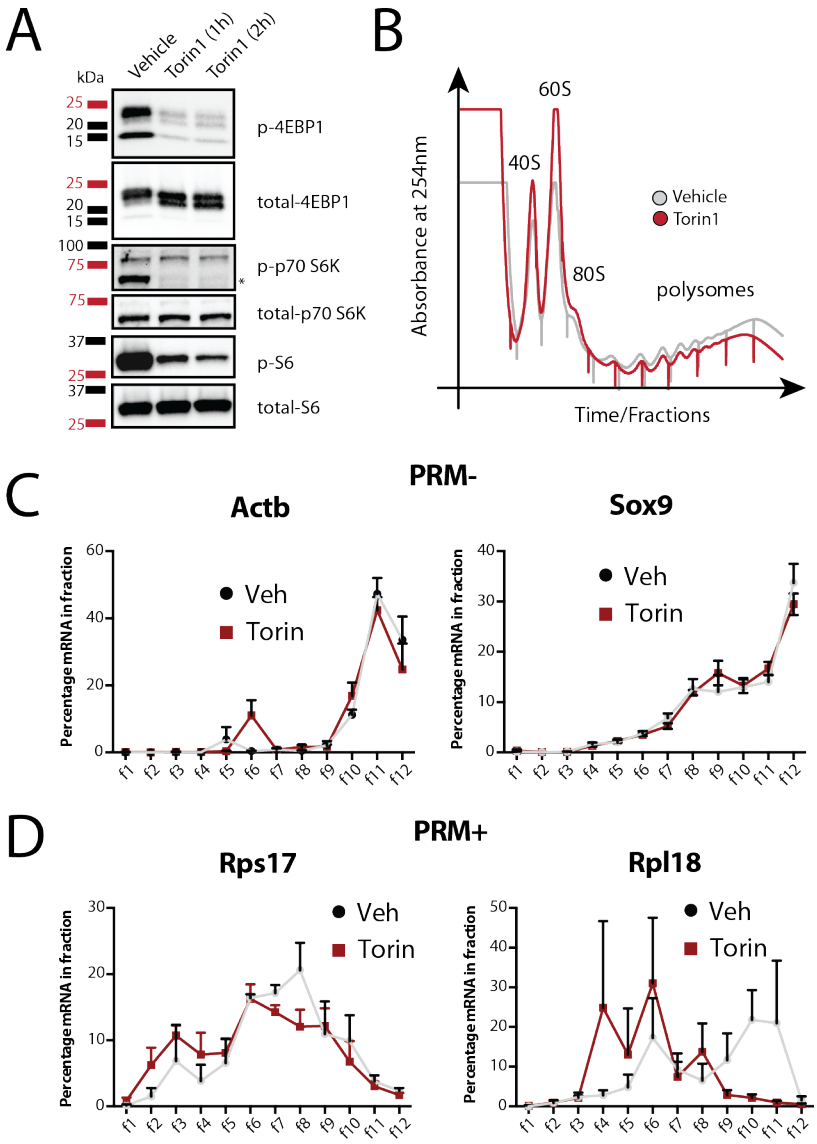

Figure 29: Sucrose gradient fractionation of NSCs after Torin1 treatment **A** Western blot after Torin1 treatment (100mM) of primary NSCs shows inhibition of 4EBP1-, p70 S6 kinase- and S6 phosphorylation, all indicators of mTORC1 activity. Star pinpoints correct band. **B** Representative absorption profiles for vehicle- and Torin1-treated NSCs (2h) after sucrose gradient fractionation indicate little changes in global translation. **C** Quantitative PCRs from RNA fractions show that PRM- transcripts do not shift to lighter fractions. **D** Quantitative PCRs from RNA fractions show that PRM+ transcripts are more sensitive to Torin1 treatment, indicated by shift to lighter fractions. Variability of biological replicates (n=3) indicated by standard error (SEM). Experiments performed in collaboration with Yonglong Dang (Molecular Neurobiology, DKFZ, Heidelberg).

This data demonstrates a clear correlation between presence of a 5' PRM and sensitivity to mTORC1 inhibition, which would explain the translational repression of a number of transcripts at the ENB stage.

The hypothesis that inhibition of mTOR signaling might be the reason for stage-specific repression of PRM-containing transcripts arose by the fact that transition from NSC stages to ENBs is characterized by a global reduction in protein synthesis as assessed by OPP incorporation, which is often accompanied with activity of the mTOR signaling pathway (Figure 12). To prove that mTORC1 activity indeed drops during stage transition of NSCs to ENBs, SVZ brain sections were stained for phosphorylation of ribosomal protein S6 (pS6), a downstream indicator of PI3K-mTORC1 pathway activity. A transgenic mouse line was used where induced Cre-recombinase activity under the Tailless (Tlx) promoter labeled NSCs with enhanced yellow fluorescent protein (Tlx-CreERT2-eYFP, (Liu et al., 2008)).

In combination with DCX immunofluorescence, this mouse model allowed comparison of rpS6 phosphorylation in NSCs and ENBs. Phosphorylation of rpS6 was low in all ENBs (DCX expressing cells), which was in accordance with the global translation (Figure 30A). Interestingly, eYFP-labeled NSCs showed heterogeneity in their rpS6 phosphorylation, reflecting their different activation status.

A similar heterogeneity of rpS6 phosphorylation could also be found within the olfactory bulb. Strikingly, mitral cells featured by far the highest levels of rpS6 phosphorylation (Figure 30B). When comparing late stages of neurogenesis, LNBs showed higher levels of rpS6 phosphorylation than neighboring neurons (Figure 30C). Interestingly, there was no specific repression of PRM+ transcript in neurons, suggesting that other mechanisms might act in this population.

Together, this data further supports that repression of mTORC1 activity in ENBs particularly affects PRM-containing transcripts including components of the translation machinery, as well as key stemness-associated transcription factors.

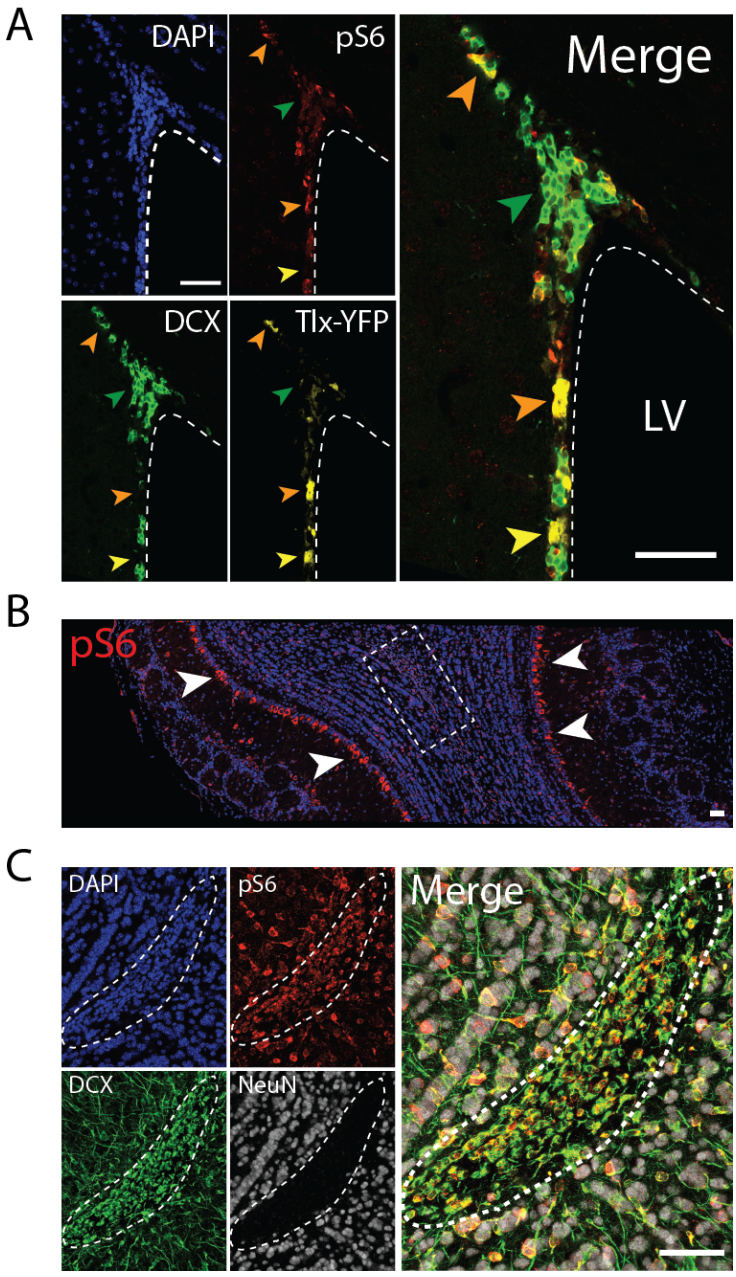

Figure 30: IHC for phosphorylation of ribosomal protein S6 indicating mTORC1 activity **A** Comparison of NSCs (Tlx-eYFP$^+$) and ENBs (DCX$^+$) in the subventricular zone. All ENBs show low levels of pS6 (green arrow), while some NSCs show high pS6 (orange arrows) and others show low levels of pS6 (yellow arrow). **B** Overview of the olfactory bulb. Mitral cells (marked by arrows) show highest level of pS6. **C** Inset from (B)**.** Comparison of LNBs and neurons in the olfactory bulb (OB). The core of the OB (marked with dashed line) which contains only LNBs (DCX$^+$) is enriched for high pS6, while only few neurons (NeuN$^+$DCX$^-$) have high levels of pS6. Scale bars: 50µm.

3.2.10 Translational uncoupling in NSCs upon brain injury

During homeostasis, only few transcripts showed specific translational regulation in NSCs (Figure 23,24). It is known that cellular stress can cause a shutdown of transcriptional regulation favoring regulation of protein levels based on the translation of existing transcripts. To test, whether stress-response in NSCs is partially mediated by translational

regulation, an ischemic brain injury was applied to TiCRY mice. Animals were subjected to bilateral common carotid artery occlusion (BCCAO, Figure 31A) which causes striatal and white matter injury affecting NSCs of the subventricular zone (Llorens-Bobadilla et al., 2015; Yoshioka et al., 2011). As before, transcriptome and translatome was analyzed dissecting the different levels of response to brain injury. Differential expression analysis of RNAseq between homeostatic and injured NSCs resulted in 293 genes, which are up-, and 278 genes, which are downregulated after injury, respectively. Upregulated genes enriched highly for biological processes related to the response to cytokines including interferons, which play a critical role in the innate immune response against viral infections (Figure 31B).

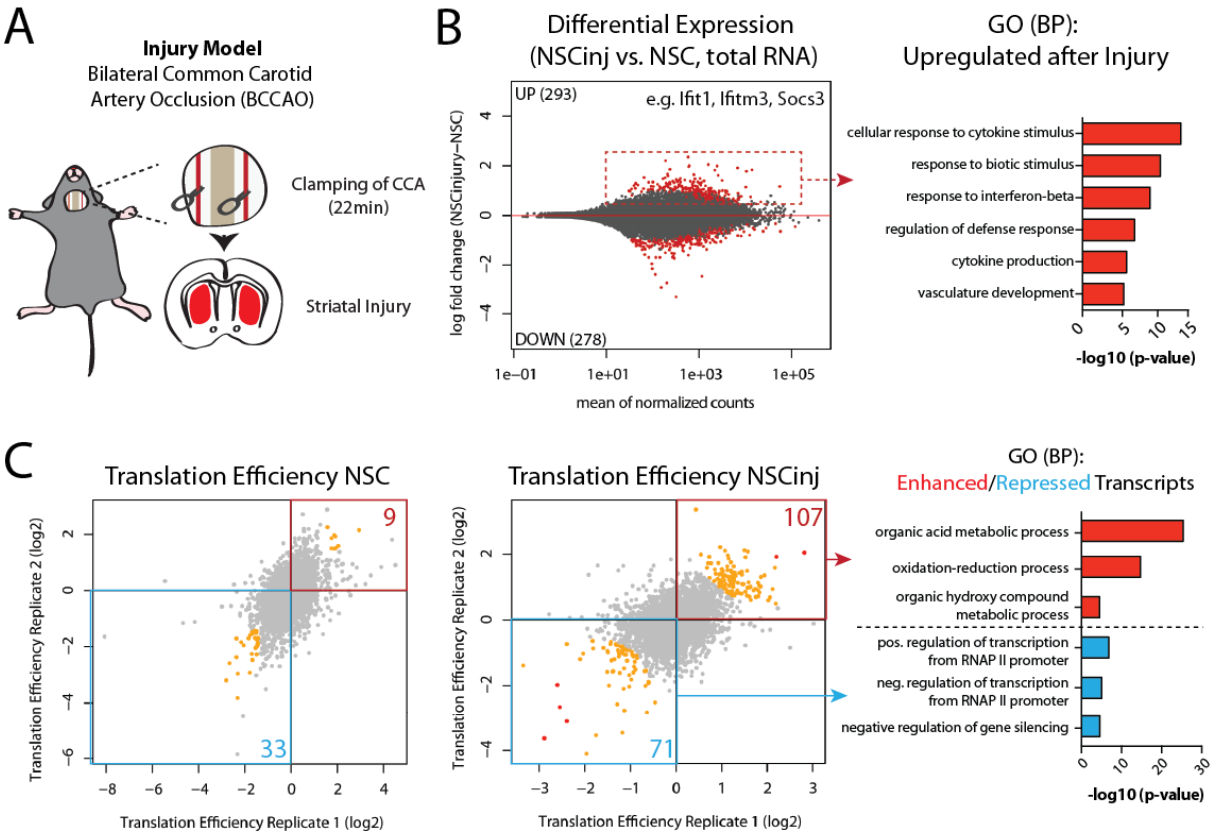

Figure 31: Transcriptional and translational response of NSCs to brain injury **A** Bilateral common carotid artery occlusion (BCCAO) model for brain injury. **B** Differential gene expression based on total RNA changes in NSCs after brain injury (FDR: 1%). Upregulated genes enrich for multiple gene ontology categories related to cellular response to cytokines including interferon-beta. **C** Changes of translational efficiency in NSCs upon brain injury. Injury promotes increased number of enhanced and repressed genes. Enhanced genes enrich for several metabolic processes, while repressed genes are highly related to transcriptional regulation of gene expression (red dots: 1% FDR/orange dots: 10% FDR). Numbers of enhanced and repressed transcripts in boxes base on 10% FDR. All gene ontologies by Metascape. Analyses performed in collaboration with Bernd Fischer (Computational Genome Biology, DKFZ, Heidelberg).

The efficiency of induction of an ischemic injury was further demonstrated by the upregulation of the interferon-induced protein with tetratricopeptide repeats 1 (Ifit1) and

suppressor of cytokine signaling 3 (Socs3), whose expression is known to be induced through brain ischemia. Next, translational efficiency was investigated as before comparing NSCs during homeostasis and brain injury. Strikingly, brain injury promoted the divergence of the transcriptome and translatome known as translation uncoupling. While homeostatic NSCs featured 42 transcripts that were uncoupled (9 enhanced/33 repressed), this number significantly increased after injury (107 enhanced/71 repressed, Figure 31C). Uncoupled transcripts did not overlap between homeostatic- and injured NSCs indicating that different mechanisms act upon brain injury. While enhanced transcripts enriched for multiple metabolic processes, repressed transcripts comprised multiple regulators of transcription. Together, this experiment supports the concept of increased translational regulation after cellular stress, exemplified by NSCs, which are subjected to an inflammatory environment caused by ischemic brain injury.

3.2.11 Contribution of RNA-binding proteins to translational uncoupling

RNA-binding proteins (RBPs) are major regulators of posttranscriptional control. They are involved in processes including alternative splicing, RNA processing and modification, nuclear export, transcript stability as well as directly in translation of mRNAs by recruiting ribosomes and initiation factors (Ye and Blelloch, 2014).

In order to investigate the potential contribution of RBPs to the translational regulation during neurogenesis as well as after brain injury, clusters of repressed and enhanced transcript sequences were compared to binding sites of multiple RBPs. A recently published dataset comprising the binding sites of 73 RBPs in two cell lines (HepG2 and K562), which were identified using a modified, enhanced crosslinking immunoprecipitation (ECLIP) protocol, was used for this analysis (Van Nostrand et al., 2016). The cluster of translationally repressed transcripts in ENBs featured binding sites for almost all RBPs in the ECLIP study, which was mostly due to the overrepresentation of ribosomal transcripts in this cluster (Figure 32A). Interestingly, multiple ribosomal subunit transcripts were targets of the majority of RBPs in this study, suggesting that RBPs are closely related to the regulation of the translation machinery (data not shown). The correlation with binding sites of RBPs was more specific in the other clusters of translational regulation.

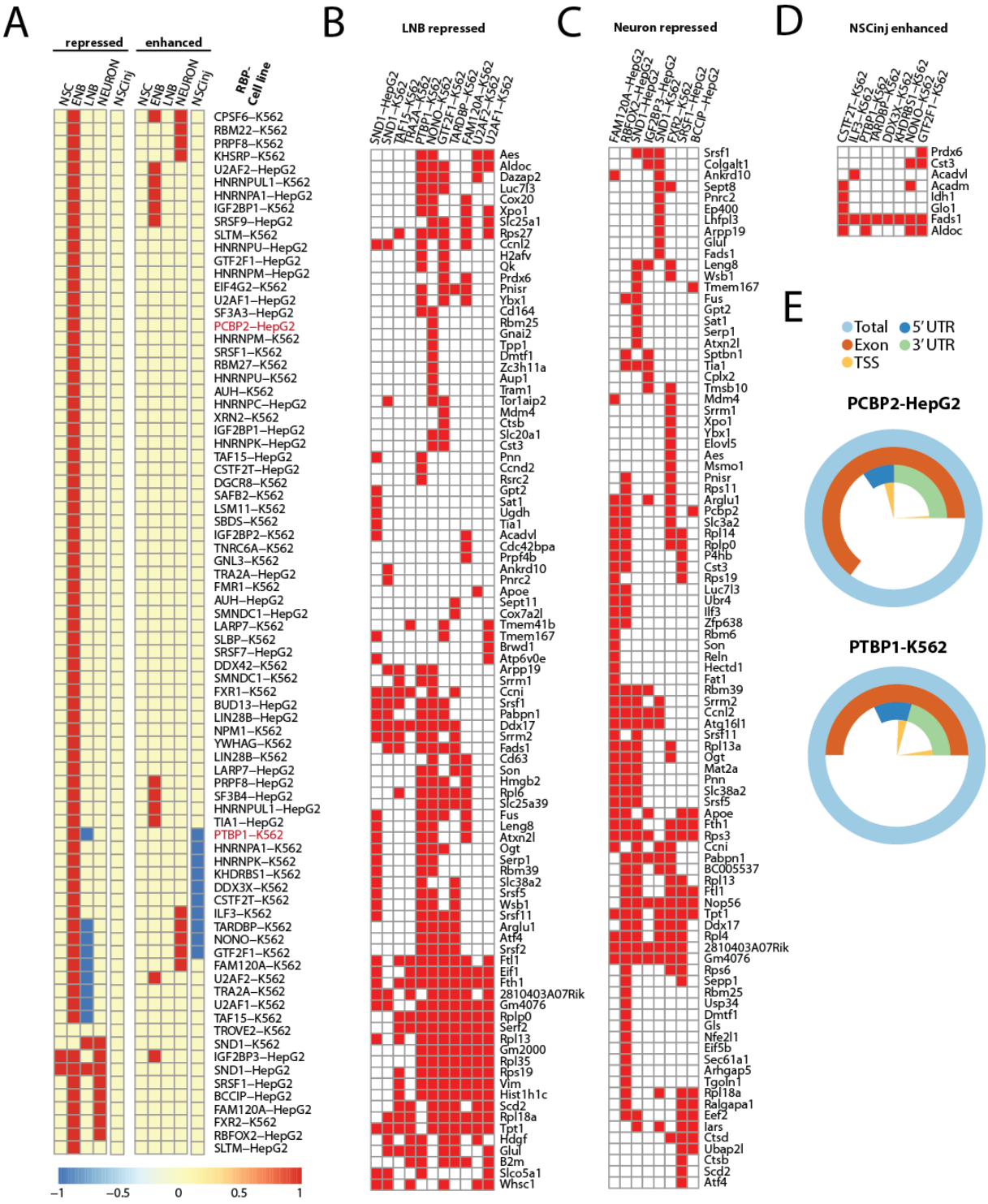

Figure 32: Correlation of translational regulation and presence of RBP-binding sites **A** Summary of the comparison of ECLIP dataset (Nostrand et al., 2016) covering the mRNA-binding sites of 73 RBPs in two cell lines (HepG2 and K562) to the different clusters of translational regulation at different stages. Red boxes indicate overrepresentation (correlation=1), while blue boxes indicate underrepresentation (correlation=-1). **B** RBPs and their corresponding target mRNAs, which are translationally repressed at the stage of LNBs. **C** Same as in (B) for the cluster of transcripts, which are translationally repressed in neurons. **D** RBPs and their target mRNAs, which are translationally enhanced in NSCs after brain injury, no correlation could be found in NSCs without injury. **E** Genomic position of mapped peaks in ECLIP data (indicating RBP-binding) for two representative RBPs. While large proportion of the binding is in intronic regions, some peaks correspond to untranslated regions and might have regulatory potential. Analyses performed in collaboration with Bernd Fischer (Computational Genome Biology, DKFZ, Heidelberg).

Transcripts repressed in LNBs showed an overrepresentation of SND1 binding sites (in both cell lines), while binding sites of multiple other RBPs (including U2AF2 and NONO) were underrepresented in this cluster indicating the latter ones might act as translational activators. The target transcripts comprised again multiple ribosomal proteins (e.g. Rps27 and Rpl18a) as well as RNA-helicase Ddx17 and polyadenylate-binding protein 2 (Pabpn1, Figure 32B).

Interestingly, transcripts repressed in LNBs and neurons showed an overlap of RBP binding sites, in part linked to the shared set of commonly regulated transcripts between these stages (see Figure 23). Further, multiple transcripts including the eukaryotic elongation factor 2 (Eef2) are potential binding partners of RBPs in neurons but not LNBs (Figure 32C).

While a significant portion of translationally regulated transcripts could originate in regulation by binding of RBPs, the translational regulation in NSCs after brain injury can barely be explained by RBP activity. While no repressed transcripts showed over- or underrepresentation of RBP binding sites, 8 of the enhanced transcripts featured binding sites for one or more RBPs (Figure 32A,D). Interestingly, Fatty acid desaturase 1 (Fads1), an enzyme that regulates unsaturation of fatty acids, featured binding sites for a number of RBPs, indicating translational regulation of metabolic activity after injury (Figure 32D).

The binding of RBPs to untranslated regions often regulates translation of transcripts. Some RBPs, including the splicing regulator polypyrimidine tract binding protein 1 (PTBP1), have been previously shown to bind almost exclusively to intronic regions (Linares et al., 2015). This way, a contribution to translational regulation would be unlikely. To test whether PTBP1 and the poly(rC) binding protein 2 (Pcbp1) also bind to exonic regions, particularly the 5'- and 3' UTRs, the genomic position of mapped peaks was determined. While approximately half of PTBP1 binding sites were positioned in exons, almost three quarters of binding sites of PCBP2 could be located to exons (Figure 32E). This suggests that previous publications might have underestimated the exonic binding of RBPs, potentially due to technical reasons. Further, a fraction of RBP binding sites might be highly cell type specific. For both investigated RBPs, a large fraction of binding sites were situated in untranslated regions of the transcripts. Association to these binding sites might have a prominent role in recruitment of translational regulators to these mRNAs affecting their protein synthesis.

Together, comparison of the ECLIP dataset covering binding sites of 73 RBPs to clusters of enhanced and repressed transcripts from the RiboTag analysis provided insights to the contribution of individual RBPs to the stage- and injury dependent translational regulation. Further dissection of individual binding sites, their nucleotide composition as well as genomic environment will help to identify crucial sites of RBP activity.

4. Discussion

4.1 Global protein synthesis in stem cells and their progeny

4.1.1 Cellular differences in protein synthesis – what does it matter?

Proteins are major players of biological systems and account for about 20% of the human's bodyweight (Widdowson et al., 1951). A large proportion of cellular resources is dedicated to the synthesis of proteins from mRNAs, a process which is known as translation. In fact, it is the most energy consuming process within mammalian cells what makes it even more remarkable that its impact was underestimated until recently (Buttgereit and Brand, 1995; Rolfe and Brown, 1997). Much of what we know about protein synthesis was learned from simple model organisms including yeast and mammalian cell cultures (Hinnebusch and Lorsch, 2012). The forthcoming of novel tools, including the use of O-Propargyl-Puromycin (OPP), also gave researchers outside the "field" opportunity to study cellular differences in protein synthesis and potential consequences. Thus, within the last years multiple studies focused on the potential role of translational regulation in various systems.

Using OPP incorporation, we have observed that stages of high proliferation (active NSCs and neurogenic progenitor cells) as well as the late stage of neuronal differentiation (LNBs) feature increased levels of protein synthesis. The dependency of cell division on active protein synthesis was already demonstrated early on and is nowadays heavily used as a therapeutic target, particularly by making use of differences in prokaryotic and eukaryotic translation as well as healthy and malignant cells (Bhat et al., 2015; Taylor, 1963). In contrast, the question whether differentiation promotes protein synthesis is more elusive. The differentiation of embryonic stem cells to embryonic bodies is accompanied by a global increase in protein synthesis (Sampath et al., 2008). Similarly, differentiating germ cells in *Drosophila* present an increased protein synthesis when compared to germline stem cells (Sanchez et al., 2015). In line, the germline knockdown of ribosome assembly- and translation initiation leads to accumulation of stem cell cysts, clusters of undifferentiated cells, indicating that active translation maintains the differentiation program. Interestingly, the increased protein synthesis in germ cells seems to be independent of transcription of ribosomal RNA, which usually correlates with global levels of protein synthesis (Sanchez et al., 2015). A similar observation has been made in the hematopoietic stem cell system, where activation drives protein synthesis but not rRNA transcription, suggesting that the dogma of correlation of these processes might need to

be reconsidered (Signer et al., 2014). It is possible that during differentiation other, not yet defined mechanisms, act on protein synthesis, which do not play a role during maintenance.

Parallel to differentiation, newborn neurons need to integrate into existing neuronal circuits. Without feedback signals from neighboring neurons, cells fail to integrate and die, which in fact happens for the majority of neuroblast after arrival in the olfactory bulb (Petreanu and Alvarez-Buylla, 2002). Modification of local activity by enriched odor environment stimulates survival of newborn neurons, while sensory deprivation during a critical time window further increases neuronal death (Rochefort et al., 2002; Yamaguchi and Mori, 2005). To be fully integrated into the olfactory bulb network, newborn neurons need to form multiple synaptic connections (Nissant and Pallotto, 2011). The formation of synapses is highly dependent on active protein synthesis, as demonstrated in rat cerebellar cultures after treatment with the translation inhibitor cycloheximide (Burry, 1985). The formation of long-term memories, in contrast to short-term memories, is highly dependent on active protein synthesis during a critical time window after the stimulus (Costa-Mattioli et al., 2009). Memory formation is a highly complex process, which depends on the proper integration of neural circuits. Neuroblasts of the olfactory bulb might produce more protein than their more immature counterpart in the SVZ, since signals from the environment activate them for synapse formation, a process that requires the synthesis of new proteins. It would be interesting to study whether increase of protein synthesis within a fraction of olfactory bulb neuroblasts, for example by genetic manipulation of translational repressors, would result in a higher proliferation-independent integration of these neuroblasts as compared to wild-type ones.

The data regarding global levels of protein synthesis was exclusively collected in *ex vivo* experiments, where cells were freshly isolated from their natural environment. This was unavoidable since OPP did not cross the blood-brain barrier after intraperitoneal or intravenous injection and featured low diffusion after cisterna magna- and intraventricular injection. For future experiments investigating protein synthesis within the brain it will be crucial to improve existing tools, potentially by chemical alterations of puromycins or packaging into vesicles that allow efficient uptake and homogenous distribution.

4.1.2 Proliferation and protein synthesis – like the chicken and the egg?

The level of protein synthesis is very much linked to the proliferative nature of cells – but does increased protein synthesis cause proliferation or vice versa? Quiescent stem cells are characterized by extremely low levels of protein synthesis (Llorens-Bobadilla et al., 2015; Signer et al., 2014). It is known that active NSCs heavily increase protein synthesis, in part by increased transcription of ribosomal proteins (Llorens-Bobadilla et al., 2015). Our data suggests that neurogenic progenitor cells produce even more protein than active NSCs, which is noteworthy since active NSCs are already highly proliferative. The question arises whether a higher fraction of NPCs are proliferating in comparison to active NSCs or the higher protein levels are linked to other features. In the same line, we showed that LNBs, the neuroblasts of the olfactory bulb, produce more protein than ENBs, the neuroblasts residing within the SVZ. This is rather surprising, since LNBs are, in contrast to their earlier counterpart, largely postmitotic. Notably, in skin stem cells, which similar to NSCs and HSCs produce less protein than their proliferative progeny, the activation of protein synthesis is linked to activation of differentiation and not only of proliferation (Blanco et al., 2016). These data support the idea that in stem cells activation of differentiation, and not of proliferation, dictates the level of protein synthesis. In addition, low levels of protein synthesis seem to be essential for stem cell maintenance, as in both HSCs and NSCs, increasing protein synthesis by deletion of PTEN, leads to exhaustion of the stem cell pool (Bonaguidi et al., 2011; Signer et al., 2014). To which level protein synthesis of differentiating cells at later stages needs to be maintained for proper integration in the neuronal network remains elusive and would need to be addressed by stage-specific manipulation of the protein synthesis rate.

4.1.3 Translational arrest in neuroblast – initiating differentiation?

We observed that differentiation of NSCs into early neuroblasts, the immature neurons within the SVZ, features a dramatic decrease of protein synthesis, which cannot be solely explained by reduced proliferation. The question arises whether this drop is part of a predetermined cellular program, which allows coordinated differentiation and migration of these cells. The study of HSCs showed that protein synthesis is tightly regulated and both reduction as well as increase in protein synthesis abrogate the stem cell function (Signer et al., 2014). Similarly, eIF2-phosphorylation keeps satellite cells, the stem cells within muscles, quiescent (Zismanov et al., 2016). Considering the homogenous low levels

of OPP incorporation in early neuroblasts, it could well be that protein synthesis needs to be maintained within a defined range during critical stages of differentiation. In fact, it has been shown that postnatal PTEN deletion, which is known to increase protein synthesis, causes premature termination of migration and differentiation of neuroblasts, resulting in an enlarged SVZ and rostral migratory stream (Zhu et al., 2012). Interestingly, this phenotype is not based on defective migration of neuroblasts but ectopic differentiation. A reduced cell density in the olfactory bulb, the original destination of migrating neuroblasts, accompanies the increased cell number in the SVZ. Inhibition of mTORC1 by rapamycin fully rescues these phenotypes demonstrating the importance of the mTOR pathway for proper differentiation of NSCs. While showing that mTORC1-dependent regulation of protein synthesis might have a crucial impact on neurogenesis, this study leaves it open whether there is a critical stage where mTOR activity (and probably protein synthesis) needs to get regulated. The authors use an inducible mouse model, which targets Nestin-positive progenitor cells. It is likely that this way active NSCs, neurogenic progenitor cells and, some days after recombination, neuroblasts are affected by the PTEN deletion. Therefore it is difficult to predict, which of the mentioned populations contribute to the observed phenotype. Similar experiments conducted in a mouse line where the mutation is specifically induced in neuroblasts could demonstrate whether manipulation of protein synthesis at this stage is critical for proper differentiation. Further, PTEN is a negative regulator of PI3K-AKT signaling, which has various functions including direct effects on NSC proliferation and differentiation (Peltier et al., 2007). More specific manipulation of protein synthesis for example by promotion of ribosome biosynthesis, rRNA transcription and translation initiation would help to exclude secondary effects of manipulations and pinpoint key regulatory components.

4.1.4 Protein synthesis in neurons – subtype dependent?

Neurons showed very low level of protein synthesis in our system. Since OPP does not enter the brain after systemic exposure, direct *in situ* assessment of protein synthesis was not possible. We cannot exclude that these cells are more sensitive to the experimental conditions and behave differently to their *in vivo* setting. However, low phosphorylation status of ribosomal protein S6 (rpS6), a downstream indicator of mTORC1, supports rather low activity of the majority of olfactory bulb interneurons *in vivo*. Interestingly, neurons of the mitral cell layer in the OB showed by far the highest levels of rpS6 phosphorylation,

suggesting variability between different neuronal subtypes regarding mTOR activity, which might translate into protein synthesis rates. This variability was not obvious in our OPP experiments. Granular cells, which are situated in the most central layer of the OB, represent the vast majority of OB interneurons (Nissant and Pallotto, 2011). Thus, it is likely that the neurons, which were assessed in OPP experiments, mostly originate in this layer, particularly considering the fact that a relatively small number of neurons have been assessed in our experiments. Further, NeuN-expression was used as an identifier of mature neurons and several classes of olfactory bulb neurons outside the granular cell layer, including mitral cells, do not feature NeuN-expression. In future experiments, a more widespread marker of neurons (e.g. Tuj1) would allow the analysis of all types of olfactory bulb interneurons.

Different odor receptors within the olfactory epithelium receive odor information and transmit the signal via sensory neurons to the glomeruli of the olfactory bulb. The primary dendrites of up to 20 mitral cells innervate glomeruli. In contrast to neurons of the granular cell layer, which function as inhibitory interneurons, mitral cells represent output neurons with long axons and constant activity, which is essential for signal transmission to the olfactory cortex (Mori et al., 1999). To which level elevated protein synthesis contributes to mitral cell function remains elusive. However, infusion of the translation inhibitor anisomycin interfered with long-term odor memory suggesting that intact protein synthesis is important for proper signal transmission to the olfactory cortex (Grimes et al., 2011).

4.2 Transcript-specific regulation of protein synthesis

4.2.1 Advanced RiboTag strategy unveils translational control

RiboTag experiments so far were conducted using constitutively active Cre driver lines recombining in terminally differentiated cell types (Sanz et al., 2009; 2013; Shigeoka et al., 2016). They were primarily designed for cell types that are difficult to assess via FACS, either because cells feature complex morphology (like neurons) or are highly sensitive to isolation from their natural environment. We adapted this method for the first time to study a dynamic system *in vivo.* Studies based on ribosomal tags focused so far mostly on the fraction of mRNAs that bind to ribosomes. Here we combined ribotagging with the analysis of the corresponding total mRNA, which allowed evaluation of the transcript-

specific translation efficiency. This revealed an unexpectedly instable relationship between total RNA abundance and ribosome binding. While in NSCs total RNA resembles the ribosome-bound fraction, this linear relation becomes entirely disrupted at later stages of neurogenesis. This highly cell-type specific relation between total- and ribosome-bound RNA raises the question to which level RNAseq-based comparison of cell types recapitulates real biological differences. It might happen that lower expression on the total RNA level is compensated by higher translation efficiency in a cell type-specific manner. Combination of sophisticated mouse models with FACS identification of specific cell types, novel sequencing technologies as well as improved mass spectrometery-based technologies will help to uncover the complex relationship between the transcriptome, translatome and proteome.

While offering key advantages over bacTRAP lines (Doyle et al., 2008; Heiman et al., 2008) the usage of RiboTag mouse lines introduced challenges of mixed populations. We spent significant efforts to minimize these and restricted our analyses to abundant, protein-coding transcripts. This way we gained high confidence in finding correct hits, at the risk of underestimating the absolute degree of uncoupling. More sophisticated mathematical models will help to uncover whether additional transcripts potentially involved in proper development and function of neurons are under translational control. Further, modification of current protocols should allow ribosome profiling (Ingolia et al., 2009) of defined cell populations to study not only ribosome-association, but also investigate the current position of ribosomes on the transcript of interest at a given time. In addition, mRNAs can under certain conditions be associated to translationally inactive ribosomes, a process known as ribosome stalling. Ribosome profiling would help to identify these cases, since ribosome stalling usually happens close to the translation start site (Ingolia et al., 2011).

4.2.2 Translation in NSCs – homeostasis vs. brain injury

To our surprise, we did not find significant translational regulation at the level of NSCs. Similarly, a combined analysis of proteome, transcriptome and methylome of HSCs showed a similar overall correlation indicating little post-transcriptional regulation taking place in homeostatic HSCs (Cabezas-Wallscheid et al., 2014). There has been long-standing discussion about the overall correlation of transcript- and protein abundance with contradicting conclusions from identical datasets (Li et al., 2014; Schwanhäusser et al.,

2011). However, with the forthcoming of refined mathematical models and latest technologies for quantitation, it is believed that mRNA levels largely explain protein abundance during steady state (Li and Biggin, 2015). The study of developmental lineage transitions *in vivo* in our neurogenesis paradigm, has allowed us to uncover that the concordance between transcription and translation is highly dynamic and stage-specific. It is predicted that short-term adaptations (e.g. stress-conditions) cause alterations between the total abundance of mRNAs and their ribosome association, even in cells that show high concordance such as NSCs (Liu et al., 2016).

To this end, we applied global forebrain ischaemia, an injury model that results in striatal and white matter damage which was shown to cause activation of quiescent NSCs in the SVZ (Llorens-Bobadilla et al., 2015; Yoshioka et al., 2011). Indeed, the previously observed linearity between transcript abundance and ribosome-association is partially abolished after brain injury, which is in line with literature describing the importance of posttranscriptional control of gene expression during cellular stress (Liu et al., 2016). Many transcripts related to metabolic processes show enhanced translation after injury, which might help to quickly adapt to the inflammatory environment. This concept of "translation on demand" is often found in more simple systems as in budding yeast, where for example the Gcn4p mRNA is constitutively expressed but its translation is only activated upon amino acid starvation (Hinnebusch and Natarajan, 2002). Repressed transcripts are highly related to transcription suggesting that cells might shut down transcriptional control to save cellular resources and fine-tune gene expression temporarily via translational control. This is rather surprising since it was shown that transcription factors are in particular subject to "translation on demand" (Lee et al., 2013).

The detailed analysis of regulated transcripts will be key to understand the underlying molecular mechanisms. RNA-binding proteins resemble one regulatory component, which might be involved in translational control after brain injury. Interferon induced protein with tetratricopeptide repeats 1 (Ifit1) is an RNA-binding protein that is specifically expressed in NSCs after brain injury and resembles therefore a potential candidate (Llorens-Bobadilla et al., 2015). However, its function in NSCs, as well its mRNA targets are so far poorly characterized.

4.2.3 Progressive uncoupling with maturation – translational control as a neuronal feature?

We have shown that while homeostatic NSCs show a high overall correlation of RNA abundance and ribosome association, this relation becomes progressively uncoupled with ongoing differentiation, peaking at the stage of mature neurons, where finally transcript abundance becomes a poor indicator for protein synthesis. The question arises whether the dependence on regulation at the translational level is a neuronal feature that cells establish with ongoing differentiation. In fact, the concept of translational uncoupling is most evident when talking about local mRNA translation in polarized cells like neurons (Jung et al., 2012). It has been shown that local translation is important for synaptic plasticity in dendritic spines upon extrinsic signals (Sutton and Schuman, 2006). In the same line, both guidance cue-based outgrowths as well as regeneration of growth cones require local protein synthesis (Campbell and Holt, 2001; Verma et al., 2005).

However, translational control does not seem to be directly linked to neuronal function, but instead represents a way for cells to generate protein gradients. Protein gradients are important to determine polarity of cells. These gradients emanate from a specific position within the cell, which can be the synapse of a neuron that translates proteins upon signals from the environment. Gradients of proteins generated by selective translation are of particular importance during development. Oocytes, the prime model to study translation, are transcriptionally silent and use local protein synthesis for pattern formation (Richter and Lasko, 2011).

Similar gradients have been shown to control proliferation- versus differentiation decisions in neural progenitors during embryonic development. The RNA-binding protein Staufen2 is distributed asymmetrically during progenitor divisions preferentially segregating into neuronally committed daughter cells taking along a subset of associated mRNAs (Kusek et al., 2012). In the same line, a complex of eIF4E1 and its binding partner 4E-T coordinately repress translation of proteins of the neurogenin-family that determine neurogenesis (Yang et al., 2014). These examples illustrate that gradients of mRNAs (which translate into proteins) accomplished by local repression and release can have significant impact on cell fate decisions.

4.2.4 Definitive exit from pluripotency – by mTORC1 and PRMs?

Our motif analysis demonstrated that transcripts that are translationally repressed at the early stage of differentiation in ENBs (including Sox2, Pax6 and multiple ribosomal proteins) share a common pyrimidine rich motif (PRM) in their 5′ untranslated region. Transcripts harboring similar motifs (termed terminal oligopyrimidine-/TOP motifs) were previously shown to be highly sensitive to mTOR inhibition (Thoreen et al., 2012). Indeed, we could show that transcripts, which feature PRMs not necessarily in a terminal position, are highly sensitive to Torin1-mediated inhibition of translation. We and others have further shown, using pS6 as a readout, that mTORC1 activity is low in quiescent NSCs, high in active NSCs and progenitors and drops when neurogenic differentiation becomes more apparent (Paliouras et al., 2012). This follows the dynamics of protein synthesis, as assessed here by OPP incorporation. Taken together, our data suggests that mTORC1 activity drops in parallel to global protein synthesis in ENBs and transcripts carrying a 5′ PRMs are more repressed in their translation than PRM-free counterparts. It is likely that this is mediated in part by the mTORC1 downstream effector eiF4E-binding proteins (4EBPs) as suggested earlier (Thoreen et al., 2012). Several RNA binding proteins were proposed to contribute additionally to the regulation of TOP containing transcripts, including LA-related protein 1 (LARP1) which associates with mTORC1 and stimulates the translation of 5′ TOP containing transcripts (Tcherkezian et al., 2014) as well as the stress granule proteins TIA1 and TIAR (Damgaard and Lykke-Andersen, 2011). However, none of these proteins was differentially expressed between NSCs and ENBs. Specific deletion of PRMs in reporter constructs would help to understand whether this motif is essential for mTORC1 sensitivity or alternatively, whether the presence of PRMs coincides with further properties, such as a special structure of the UTR that allows binding of regulatory components.

Noteworthy, not all repressed transcripts featured 5′ PRMs but the majority of PRM-containing transcripts were repressed, indicating that there must be additional mechanisms that control repression. Altogether, we propose that a drop in mTORC1 activity in early neuroblasts causes a transient arrest in translation in these cells during their migration towards the olfactory bulb. Through the presence of PRMs, shared by ribosomal genes and key stemness-associated transcription factors, this translation arrest selectively promotes the definitive exit from the stem cell state and might be instrumental

to prevent malignant transformation. In this line it was shown that the mTOR pathway is hyperactivated in 90% of high-grade glioma brain tumors (Wei et al., 2016).

Noteworthy, the transition of LNBs to neurons is characterized by a similar drop in mTORC1 activity as seen for the NSC-ENB transition. However, PRM-containing transcripts did not show repression in neurons, indicating that other cellular mechanisms are more dominant at this stage.

4.2.5 Translational block and release of Sox2 – roles outside of stem cells?

We showed that SOX2, a major stemness-associated transcription factor, is consistently detected at the RNA level in early neuroblasts (ENBs), however its expression is repressed by posttranscriptional mechanisms. Interestingly, this translational block is released at later stages resulting in high SOX2 protein expression in a subset of neurons in the olfactory bulb which are situated in the periglomeruli and feature Calretinin-expression, a calcium-binding protein involved in calcium signaling.

SOX2 is one of the famous Yamanaka factors whose overexpression together with Oct4, Klf4 and c-Myc leads to the generation of induced pluripotent (iPS) cells from somatic cells (Takahashi and Yamanaka, 2006). Similarly, SOX2 maintains pluripotency in embryonic and adult neural stem cells and its deficiency leads to impaired generation of neurons (Cavallaro et al., 2008; Ferri, 2004; Graham et al., 2003). In hippocampal NSCs, this was shown to be partly controlled by an autocrine mechanism where SOX2 deficiency causes loss of soluble factors, including sonic hedgehog (SHH) and WNT3A, and SHH agonists partially rescue the hippocampal defect (Favaro et al., 2009).

The expression of SOX2 in a subset of terminally differentiated neurons challenges its widespread view as a pluripotency factor and questions which alternate functions SOX2 may have in a different cellular context. It has been reported earlier that SOX2 is expressed by a small proportion of neurons, particularly in the thalamus, striatum and septum (Ferri, 2004). Reduction of SOX2 levels in these neurons causes abnormalities common to diverse neurodegenerative diseases including cerebral malformations with parenchymal loss, ventricle enlargement and epilepsy-like syndrome (Ferri, 2004). Also on the cellular level, these neurons showed signs of degeneration. Neurons were smaller in size, had a hyperchromatic cell body, nuclear and cytoplasmic condensation, membrane irregularities as well as perinuclear inclusions. Degenerating neurons featured protein aggregates,

indicating defects in clearing excess (potentially harmful) proteins, which is again characteristic for several neurodegenerative diseases including Alzheimer's disease.

Taken together, SOX2 appears to have multiple functions within the cell. In stem- and progenitor cells SOX2 guards pluripotency and controls coordinated proliferation and differentiation, whereas in terminally differentiated neurons it is involved in keeping neuronal function and morphology intact in part by preventing the accumulation of detrimental protein aggregates. Whereas its function in pluripotency is well studied in a number of systems, the exact mechanisms behind its functions in neurons remain elusive. Strikingly, we discovered a mechanism, which allows SOX2 expression to be repressed during early neuronal differentiation, to exit from pluripotency and allows de-repression later on when SOX2 is likely important for neuronal function in periglomerular neurons. Inducible and stage specific depletion of SOX2 would uncover whether it is involved in multiple parallel cellular networks with different functions or whether the same networks can control different processes based on the activity of cofactors.

4.2.6 The role of RNA-binding proteins within the neural lineage

RNA-binding proteins (RBPs) are important post-transcriptional regulators of gene expression, particularly in polarized cells like neurons where RBPs help to successfully integrate environmental signals (Jung et al., 2012). To which level RBPs contribute to regulation of protein synthesis in NSCs as well as their role in stage transitions during stem cell differentiation remains elusive and has been addressed only to a limited degree, mostly due to technical reasons. The binding partners of RBPs are commonly identified by crosslinking immunoprecipitation and subsequent sequencing (CLIP-seq), where the binding of RBPs and their target mRNAs is stabilized and the complexes are isolated and target mRNAs analyzed by deep sequencing (Darnell, 2010). While this technique offers great potential, its application has been limited by poor specificity of antibodies as well as a low success rate. An enhanced CLIP (eCLIP) protocol massively improved specificity and discovered authentic binding sites of 73 RBPs from 102 eCLIP experiments in two cell lines (Van Nostrand et al., 2016). We have used this dataset to compare target mRNAs of individual RBPs to transcripts that are enhanced- or repressed in their translation at different stages of neurogenesis.

Transcripts repressed in early neuroblasts correlated with binding sites for almost all RBPs analyzed in the study, which was highly related to the enrichment for ribosomal transcripts within this cluster. Interestingly, according to the eCLIP database multiple ribosomal transcripts are targets of a number of RBPs suggesting that RBPs might be involved in ribosome biogenesis and composition. The fact that only subsets of ribosomal subunit mRNAs are targets implies that some parts of the ribosome are under special regulation. In this line it was suggested that distinct composition of ribosomal proteins yields specialized ribosomes with tissue-specific regulatory functions (Shi and Barna, 2015). It is exciting to speculate that RBPs might be involved in customizing ribosomes to increase affinity for a subset of mRNAs. However, a lot more work has to be done to change the dogma of ribosomes as highly uniform housekeeping machinery.

No RBPs showed binding sites in the transcripts regulated in NSCs, mostly due to the low total number. Interestingly, this did not change much after injury, where many more transcripts displayed translational regulation indicating that the translational uncoupling might be mediated by other RBPs than the 73 covered in the eCLIP study. In LNBs and neurons, a defined set of RBPs displayed binding sites for translationally regulated transcripts, suggesting that later stages of neurogenesis might be under more specific control of RBPs. This is in line with previous work demonstrating key roles of RBPs in neurons (Jung et al., 2012).

The eCLIP dataset provides a powerful library of RBP binding sites that allows systematic analysis for correlation with multiple clusters of transcripts, which we have found to be regulated in a specific way. However, it also has limitations. While some RBPs have very conserved binding sites, for example members of the cytoplasmic polyadenylation element binding proteins (CPEBs)(Richter, 1999), others like the fragile X mental retardation protein FMRP recognize mRNAs based on secondary structures (Melko and Bardoni, 2010). There is no certainty that binding is conserved over systems and takes place in neuronal cells. This would need to be addressed by CLIP experiments, ideally from defined cell populations *in vivo*, which is highly challenging since these experiments usually require high input material.

4.3 Concluding remarks

In summary, our data offers a comprehensive genomic view on translational control during neuron generation in the adult brain, adding a novel layer of regulation of stem cell differentiation (Figure 33). It will be important to further dissect the underlying mechanisms to fully understand how the final levels of protein expression are accomplished, to which extent these mechanisms contribute to cellular function and whether their targeted manipulation can help to counteract pathological states.

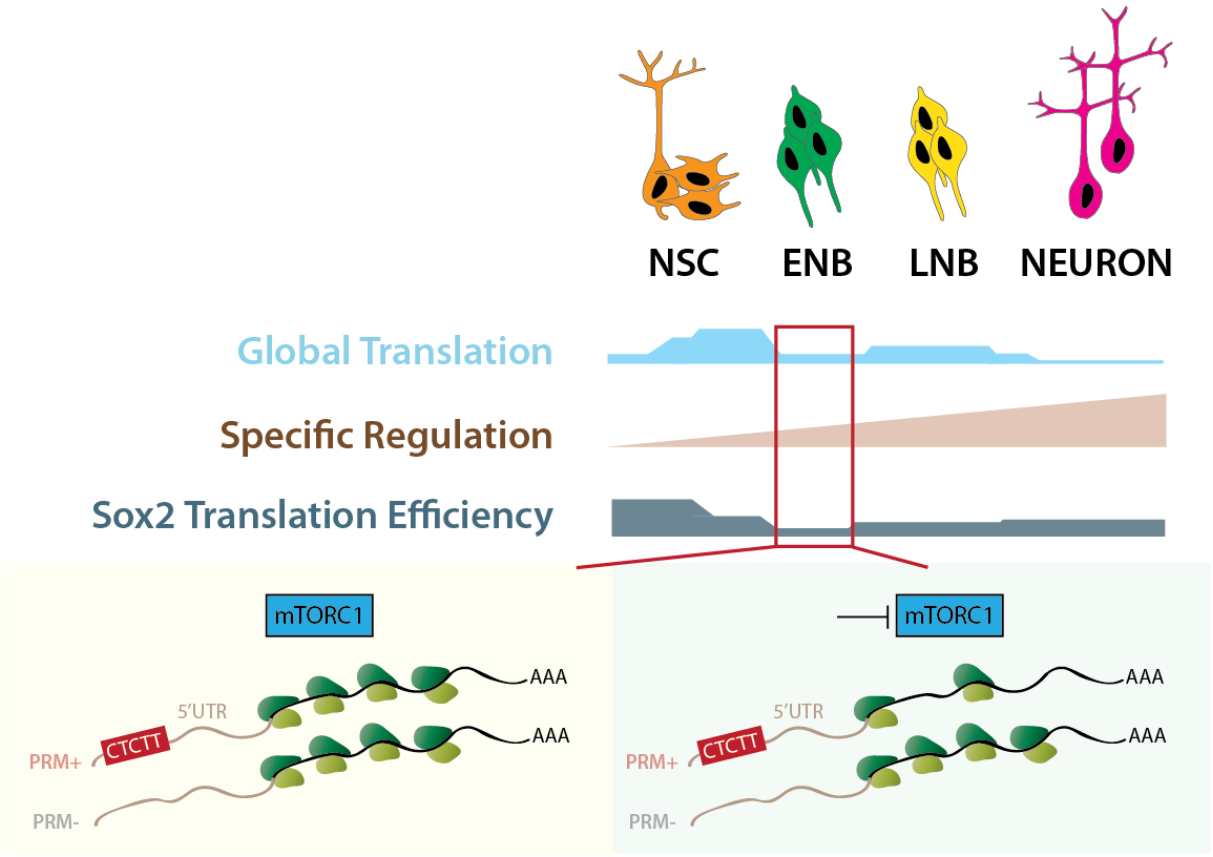

Figure 33: Summary of global- and transcript-specific translation during neurogenesis. Global protein synthesis peaks at stages of high proliferation and neuronal integration, while (transcript-) specific regulation progressively increases with neurogenic differentiation. Interestingly, the pluripotency-associated transcription factor Sox2 is translationally repressed at the stage of early neuroblasts (ENBs) together with a number of translation factors, a cluster that features 5' pyrimidine-rich motifs (PRMs) that sensitize them for repression of mTORC1 activity. This temporal translational arrest is released at later stages, illustrated by Sox2 protein expression in a subset of olfactory bulb neurons.

5. Supplements

5.1 *De novo* motif analysis

Table S1 contains all sequence motifs (6-mer nucleotide sequences), which are overrepresented (Oddsratio>1) in transcripts that are repressed in ENBs (FDR=10%).

Table S1: Overrepresented motifs in transcripts repressed in ENBs. Related to Figure 28.

Region	Motif	Pvalue	Padj	OddsRatio
coding	AAGCGC	1,38E-06	0,002825562	2,050534649
coding	CGCAAG	9,00E-07	0,002825562	2,063369368
coding	GGCGCC	5,77E-06	0,004538333	1,92250725
coding	CCGCAA	5,50E-06	0,004538333	2,062277219
coding	TCCCGC	6,95E-06	0,004538333	2,086819718
coding	CGGTCG	7,76E-06	0,004538333	2,933011765
coding	TTCGCG	6,70E-06	0,004538333	3,204130275
coding	TGCGCG	1,36E-05	0,006948711	2,526120578
coding	GCGCCC	2,16E-05	0,009843091	1,962224592
coding	ACCCGG	2,61E-05	0,010680577	1,884348779
coding	GCCGCG	6,85E-05	0,025523368	1,985042697
coding	GCGCGG	8,98E-05	0,030637982	2,069005507
coding	GCCCAA	0,000156305	0,031386527	1,633298702
coding	CGGAAG	0,000158327	0,031386527	1,649224384
coding	CCCGTG	0,000102954	0,031386527	1,782271819
coding	ACCCGC	0,000133018	0,031386527	1,918815879
coding	GCGCCG	0,000116174	0,031386527	1,919707538
coding	TTCGAC	0,000160917	0,031386527	1,940963448
coding	AACCCG	0,000155204	0,031386527	1,975184051
coding	CGCCCG	0,000148208	0,031386527	2,013122505
coding	CGCGCC	0,000115163	0,031386527	2,048552017
coding	GAAGCG	0,000174666	0,031440344	1,671571256
coding	GGCCGC	0,000185028	0,031440344	1,678894916
coding	CCGCCG	0,000180953	0,031440344	1,782184419
coding	CCGCGC	0,000191897	0,031440344	2,009415387
coding	CGAAAA	0,000261999	0,041274904	1,832724239
coding	CCCGCA	0,000275784	0,041837412	1,780890561
coding	CCGCGT	0,000305239	0,044652043	2,259800835
coding	CCGGAA	0,000347392	0,049066169	1,659537513
coding	CCGCGG	0,000395244	0,050591247	1,853123555
coding	GTCCGG	0,00038236	0,050591247	1,864262099
coding	CGCGGG	0,000395102	0,050591247	1,957523212
coding	CCGCAG	0,0004542	0,053038841	1,635557514
coding	GGCCCG	0,000466162	0,053038841	1,679768787
coding	CGAAGG	0,0004287	0,053038841	1,731900709
coding	GTCGCA	0,000485019	0,053692871	1,998957571
coding	TCCGCA	0,000549381	0,059217445	1,754073876
coding	GCGTCG	0,000723385	0,075974006	2,14137932
coding	CCAAGA	0,000839236	0,080658312	1,496541762
coding	GGCTAA	0,000857593	0,080658312	1,749022625
coding	CGCGGA	0,000866447	0,080658312	1,946931934
coding	GGCGCG	0,000866447	0,080658312	1,946931934
coding	GCGAAG	0,00093206	0,084838145	1,711474495
coding	CGCAAA	0,001082889	0,096424163	1,839909751
3′ UTR	ATAAAG	1,16E-08	4,75E-05	2,021943628
3′ UTR	AATAAA	1,32E-06	0,002706685	2,096907719
3′ UTR	TAATAA	2,76E-06	0,003770774	1,81458933
3′ UTR	TACGAT	3,00E-05	0,030730983	3,364823081
3′ UTR	CAATAA	4,56E-05	0,031145614	1,728814644
3′ UTR	CGTCGG	4,08E-05	0,031145614	5,022286143

continued

3′ UTR	TAAAGT	0,000106317	0,062210378	1,647370392
5′ UTR	CTCTTT	1,14E-06	0,004677545	2,391075318
5′ UTR	TCTTTC	3,32E-05	0,067986943	2,152585165

6. References

Adiconis, X., Borges-Rivera, D., Satija, R., DeLuca, D.S., Busby, M.A., Berlin, A.M., Sivachenko, A., Thompson, D.A., Wysoker, A., Fennell, T., et al. (2013). Comparative analysis of RNA sequencing methods for degraded or low-input samples. Nat Meth *10*, 623–629.

Alain, T., Morita, M., Fonseca, B.D., Yanagiya, A., Siddiqui, N., Bhat, M., Zammit, D., Marcus, V., Metrakos, P., Voyer, L.-A., et al. (2012). eIF4E/4E-BP ratio predicts the efficacy of mTOR targeted therapies. Cancer Res. *72*, 6468–6476.

Altman, J., and Das, G.D. (1965). Autoradiographic and histological evidence of postnatal hippocampal neurogenesis in rats. J. Comp. Neurol. *124*, 319–335.

Arvidsson, A., Collin, T., Kirik, D., Kokaia, Z., and Lindvall, O. (2002). Neuronal replacement from endogenous precursors in the adult brain after stroke. Nat. Med. *8*, 963–970.

Baser, A., Skabkin, M., and Martin-Villalba, A. (2017). Neural Stem Cell Activation and the Role of Protein Synthesis. Brain Plasticity. 1–15.

Beckervordersandforth, R., Tripathi, P., Ninkovic, J., Bayam, E., Lepier, A., Stempfhuber, B., Kirchhoff, F., Hirrlinger, J., Haslinger, A., Lie, D.C., et al. (2010). In Vivo Fate Mapping and Expression Analysis Reveals Molecular Hallmarks of Prospectively Isolated Adult Neural Stem Cells. Stem Cell *7*, 744–758.

Bhat, M., Robichaud, N., Hulea, L., Sonenberg, N., Pelletier, J., and Topisirovic, I. (2015). Targeting the translation machinery in cancer. Nat Rev Drug Discov *14*, 261–278.

Blanco, S., Bandiera, R., Popis, M., Hussain, S., Lombard, P., Aleksic, J., Sajini, A., Tanna, H., Cortés-Garrido, R., Gkatza, N., et al. (2016). Stem cell function and stress response are controlled by protein synthesis. Nature *534*, 335–340.

Bonaguidi, M.A., Wheeler, M.A., Shapiro, J.S., Stadel, R.P., Sun, G.J., Ming, G.-L., and Song, H. (2011). In vivo clonal analysis reveals self-renewing and multipotent adult neural stem cell characteristics. Cell *145*, 1142–1155.

Bond, A.M., Ming, G.-L., and Song, H. (2015). Adult Mammalian Neural Stem Cells and Neurogenesis: Five Decades Later. Cell Stem Cell *17*, 385–395.

Brichta, L., Shin, W., Jackson-Lewis, V., Blesa, J., Yap, E.-L., Walker, Z., Zhang, J., Roussarie, J.-P., Alvarez, M.J., Califano, A., et al. (2015). Identification of neurodegenerative factors using translatome-regulatory network analysis. Nat Neurosci *18*, 1325–1333.

Burry, R.W. (1985). Protein synthesis requirement for the formation of synaptic elements. Brain Res. *344*, 109–119.

Buttgereit, F., and Brand, M.D. (1995). A hierarchy of ATP-consuming processes in mammalian cells. Biochem. J. *312 (Pt 1)*, 163–167.

Cabezas-Wallscheid, N., Klimmeck, D., Hansson, J., Lipka, D.B., Reyes, A., Wang, Q., Weichenhan, D., Lier, A., Paleske, von, L., Renders, S., et al. (2014). Identification of Regulatory Networks in HSCs and Their Immediate Progeny via Integrated Proteome, Transcriptome, and DNA Methylome Analysis. Stem Cell 1–16.

Cai, X., Gao, L., Teng, L., Ge, J., Oo, Z.M., Kumar, A.R., Gilliland, D.G., Mason, P.J., Tan, K., and Speck, N.A. (2015). Runx1 Deficiency Decreases Ribosome Biogenesis and Confers Stress Resistance to Hematopoietic Stem and Progenitor Cells. Cell Stem Cell *17*, 165–177.

Calzolari, F., Michel, J., Baumgart, E.V., Theis, F., Götz, M., and Ninkovic, J. (2015). Fast clonal expansion and limited neural stem cell self-renewal in the adult subependymal zone. Nat Neurosci *18*, 490–492.

Campbell, D.S., and Holt, C.E. (2001). Chemotropic responses of retinal growth cones mediated by rapid local protein synthesis and degradation. Neuron *32*, 1013–1026.

Candelario, K.M., Shuttleworth, C.W., and Cunningham, L.A. (2013). Neural stem/progenitor cells display a low requirement for oxidative metabolism independent of hypoxia inducible factor-1alpha expression. J. Neurochem. *125*, 420–429.

Cardinali, B., Carissimi, C., Gravina, P., and Pierandrei-Amaldi, P. (2003). La protein is associated with terminal oligopyrimidine mRNAs in actively translating polysomes. J. Biol. Chem. *278*, 35145–35151.

Cavallaro, M., Mariani, J., Lancini, C., Latorre, E., Caccia, R., Gullo, F., Valotta, M., DeBiasi, S., Spinardi, L., Ronchi, A., et al. (2008). Impaired generation of mature neurons by neural stem cells from hypomorphic Sox2 mutants. Development *135*, 541–557.

Codega, P., Silva-Vargas, V., Paul, A., Maldonado-Soto, A.R., Deleo, A.M., Pastrana, E., and Doetsch, F. (2014). Prospective identification and purification of quiescent adult neural stem cells from their in vivo niche. Neuron *82*, 545–559.

Costa-Mattioli, M., Sossin, W.S., Klann, E., and Sonenberg, N. (2009). Translational Control of Long-Lasting Synaptic Plasticity and Memory. Neuron *61*, 10–26.

Damgaard, C.K., and Lykke-Andersen, J. (2011). Translational coregulation of 5'TOP mRNAs by TIA-1 and TIAR. Genes & Development *25*, 2057–2068.

Darnell, R.B. (2010). HITS-CLIP: panoramic views of protein-RNA regulation in living cells. Wiley Interdiscip Rev RNA *1*, 266–286.

Dibble, C.C., and Manning, B.D. (2013). Signal integration by mTORC1 coordinates nutrient input with biosynthetic output. Nature Cell Biology *15*, 555–564.

Dobin, A., Davis, C.A., Schlesinger, F., Drenkow, J., Zaleski, C., Jha, S., Batut, P., Chaisson, M., and Gingeras, T.R. (2013). STAR: ultrafast universal RNA-seq aligner. Bioinformatics *29*, 15–21.

Dowling, R.J.O., Topisirovic, I., Alain, T., Bidinosti, M., Fonseca, B.D., Petroulakis, E., Wang, X., Larsson, O., Selvaraj, A., Liu, Y., et al. (2010). mTORC1-mediated cell proliferation, but not cell growth, controlled by the 4E-BPs. Science *328*, 1172–1176.

Doyle, J.P., Dougherty, J.D., Heiman, M., Schmidt, E.F., Stevens, T.R., Ma, G., Bupp, S., Shrestha, P., Shah, R.D., Doughty, M.L., et al. (2008). Application of a Translational Profiling Approach for the Comparative Analysis of CNS Cell Types. Cell *135*, 749–762.

Encinas, J.M., Michurina, T.V., Peunova, N., Park, J.-H., Tordo, J., Peterson, D.A., Fishell, G., Koulakov, A., and Enikolopov, G. (2011). Division-coupled astrocytic differentiation and age-related depletion of neural stem cells in the adult hippocampus. Cell Stem Cell *8*, 566–579.

Favaro, R., Valotta, M., Ferri, A.L.M., Latorre, E., Mariani, J., Giachino, C., Lancini, C., Tosetti, V., Ottolenghi, S., Taylor, V., et al. (2009). Hippocampal development and neural stem cell maintenance require Sox2-dependent regulation of Shh. Nat Neurosci *12*, 1248–1256.

Ferri, A.L.M. (2004). Sox2 deficiency causes neurodegeneration and impaired neurogenesis in the adult mouse brain. Development *131*, 3805–3819.

Fischer, J., Beckervordersandforth, R., Tripathi, P., Steiner-Mezzadri, A., Ninkovic, J., and tz, M.G.O. (2011). Prospective isolation of adult neural stem cells from the mouse subependymal zone. Nat Protoc *6*, 1981–1989.

Fuentealba, L.C., Obernier, K., and Alvarez-Buylla, A. (2012). Adult neural stem cells bridge their niche. Cell Stem Cell *10*, 698–708.

Furlan, R., Pluchino, S., Marconi, P.C., and Martino, G. (2003). Cytokine gene delivery into the central nervous system using intrathecally injected nonreplicative viral vectors. Methods Mol. Biol. *215*, 279–289.

Furutachi, S., Miya, H., Watanabe, T., Kawai, H., Yamasaki, N., Harada, Y., Imayoshi, I., Nelson, M., Nakayama, K.I., Hirabayashi, Y., et al. (2015). Slowly dividing neural progenitors are an embryonic origin of adult neural stem cells. Nat Neurosci *18*, 657–665.

Gonzalez, C., Sims, J.S., Hornstein, N., Mela, A., Garcia, F., Lei, L., Gass, D.A., Amendolara, B., Bruce, J.N., Canoll, P., et al. (2014). Ribosome Profiling Reveals a Cell-Type-Specific Translational Landscape in Brain Tumors. J. Neurosci. *34*, 10924–10936.

Graham, V., Khudyakov, J., Ellis, P., and Pevny, L. (2003). SOX2 functions to maintain neural progenitor identity. Neuron *39*, 749–765.

Grimes, M.T., Smith, M., Li, X., Darby-King, A., Harley, C.W., and McLean, J.H. (2011). Neurobiology of Learning and Memory. Neurobiology of Learning and Memory *95*, 385–391.

Heiman, M., Schaefer, A., Gong, S., Peterson, J.D., Day, M., Ramsey, K.E., Suárez-Fariñas, M., Schwarz, C., Stephan, D.A., Surmeier, D.J., et al. (2008). A Translational Profiling Approach for the Molecular Characterization of CNS Cell Types. Cell *135*, 738–748.

Hinnebusch, A.G., and Lorsch, J.R. (2012). The mechanism of eukaryotic translation initiation: new insights and challenges. Cold Spring Harb Perspect Biol *4*.

Hinnebusch, A.G., and Natarajan, K. (2002). Gcn4p, a master regulator of gene expression, is

controlled at multiple levels by diverse signals of starvation and stress. Eukaryotic Cell *1*, 22–32.

Holt, C.E., and Schuman, E.M. (2013). The Central Dogma Decentralized: New Perspectives on RNA Function and Local Translation in Neurons. Neuron *80*, 648–657.

Holz, M.K., Ballif, B.A., Gygi, S.P., and Blenis, J. (2005). mTOR and S6K1 mediate assembly of the translation preinitiation complex through dynamic protein interchange and ordered phosphorylation events. Cell *123*, 569–580.

Hornstein, N., Torres, D., Sharma, Das, S., Tang, G., Canoll, P., and Sims, P.A. (2016). Ligation-free ribosome profiling of cell type-specific translation in the brain. Genome Biol. 1–15.

Hutchison, C.A., Chuang, R.-Y., Noskov, V.N., Assad-Garcia, N., Deerinck, T.J., Ellisman, M.H., Gill, J., Kannan, K., Karas, B.J., Ma, L., et al. (2016). Design and synthesis of a minimal bacterial genome. Science *351*, aad6253.

Ingolia, N.T., Brar, G.A., Stern-Ginossar, N., Harris, M.S., Talhouarne, G.J.S., Jackson, S.E., Wills, M.R., and Weissman, J.S. (2014). Ribosome profiling reveals pervasive translation outside of annotated protein-coding genes. Cell Reports *8*, 1365–1379.

Ingolia, N.T., Ghaemmaghami, S., Newman, J.R.S., and Weissman, J.S. (2009). Genome-wide analysis in vivo of translation with nucleotide resolution using ribosome profiling. Science *324*, 218–223.

Ingolia, N.T., Lareau, L.F., and Weissman, J.S. (2011). Ribosome profiling of mouse embryonic stem cells reveals the complexity and dynamics of mammalian proteomes. Cell *147*, 789–802.

Isaacs, W.B., and Fulton, A.B. (1987). Cotranslational assembly of myosin heavy chain in developing cultured skeletal muscle. Proc. Natl. Acad. Sci. U.S.a. *84*, 6174–6178.

Jefferies, H.B., Reinhard, C., Kozma, S.C., and Thomas, G. (1994). Rapamycin selectively represses translation of the "polypyrimidine tract" mRNA family. Proc. Natl. Acad. Sci. U.S.a. *91*, 4441–4445.

Jung, H., Yoon, B.C., and Holt, C.E. (2012). Axonal mRNA localization and local protein

synthesis in nervous system assembly, maintenance and repair. Nat Rev Neurosci *13*, 308–324.

Kapeli, K., and Yeo, G.W. (2012). Genome-wide approaches to dissect the roles of RNA binding proteins in translational control: implications for neurological diseases. Front Neurosci *6*.

Khacho, M., Clark, A., Svoboda, D.S., Azzi, J., MacLaurin, J.G., Meghaizel, C., Sesaki, H., Lagace, D.C., Germain, M., Harper, M.-E., et al. (2016). Mitochondrial Dynamics Impacts Stem Cell Identity and Fate Decisions by Regulating a Nuclear Transcriptional Program. Cell Stem Cell *19*, 232–247.

Kiebler, M.A., and Bassell, G.J. (2006). Neuronal RNA granules: movers and makers. Neuron *51*, 685–690.

Kolb, H.C., Finn, M.G., and Sharpless, K.B. (2001). Click Chemistry: Diverse Chemical Function from a Few Good Reactions. Angew. Chem. Int. Ed. Engl. *40*, 2004–2021.

Kusek, G., Campbell, M., Doyle, F., Tenenbaum, S.A., Kiebler, M., and Temple, S. (2012). Asymmetric segregation of the double-stranded RNA binding protein Staufen2 during mammalian neural stem cell divisions promotes lineage progression. Cell Stem Cell *11*, 505–516.

Lee, M.T., Bonneau, A.R., Takacs, C.M., Bazzini, A.A., DiVito, K.R., Fleming, E.S., and Giraldez, A.J. (2013). Nanog, Pou5f1 and SoxB1 activate zygotic gene expression during the maternal-to-zygotic transition. Nature.

Li, B., and Dewey, C.N. (2011). RSEM: accurate transcript quantification from RNA-Seq data with or without a reference genome. BMC Bioinformatics *12*, 323.

Li, J.J., and Biggin, M.D. (2015). Gene expression. Statistics requantitates the central dogma. Science *347*, 1066–1067.

Li, J.J., Bickel, P.J., and Biggin, M.D. (2014). System wide analyses have underestimated protein abundances and the importance of transcription in mammals. PeerJ *2*, e270.

Linares, A.J., Lin, C.H., Damianov, A., and Adams, K.L. (2015). The splicing regulator PTBP1

controls the activity of the transcription factor Pbx1 during neuronal differentiation. Elife.

Lindvall, O., Kokaia, Z., and Martinez-Serrano, A. (2004). Stem cell therapy for human neurodegenerative disorders-how to make it work. Nat. Med. *10 Suppl*, S42–S50.

Liu, H.K., Belz, T., Bock, D., Takacs, A., Wu, H., Lichter, P., Chai, M., and Schutz, G. (2008). The nuclear receptor tailless is required for neurogenesis in the adult subventricular zone. Genes & Development *22*, 2473–2478.

Liu, J., Xu, Y., Stoleru, D., and Salic, A. (2012). Imaging protein synthesis in cells and tissues with an alkyne analog of puromycin. Proc. Natl. Acad. Sci. U.S.a. *109*, 413–418.

Liu, L., and Duff, K. (2008). A technique for serial collection of cerebrospinal fluid from the cisterna magna in mouse. JoVE.

Liu, Y., Beyer, A., and Aebersold, R. (2016). On the Dependency of Cellular Protein Levels on mRNA Abundance. Cell *165*, 535–550.

Livingstone, M., Atas, E., Meller, A., and Sonenberg, N. (2010). Mechanisms governing the control of mRNA translation. Phys Biol *7*, 021001.

Llorens-Bobadilla, E., Zhao, S., Baser, A., Saiz-Castro, G., Zwadlo, K., and Martin-Villalba, A. (2015). Single-Cell Transcriptomics Reveals a Population of Dormant Neural Stem Cells that Become Activated upon Brain Injury. Cell Stem Cell *17*, 329–340.

Lois, C., and Alvarez-Buylla, A. (1994). Long-distance neuronal migration in the adult mammalian brain. Science *264*, 1145–1148.

Love, M.I., Huber, W., and Anders, S. (2014). Moderated estimation of fold change and dispersion for RNA-seq data with DESeq2. Genome Biol. *15*, 550.

Ma, X.M., and Blenis, J. (2009). Molecular mechanisms of mTOR-mediated translational control. Nature Publishing Group *10*, 307–318.

Melko, M., and Bardoni, B. (2010). The role of G-quadruplex in RNA metabolism: involvement of FMRP and FMR2P. Biochimie *92*, 919–926.

Merkle, F.T., Mirzadeh, Z., and Alvarez-Buylla, A. (2007). Mosaic Organization of Neural Stem

Cells in the Adult Brain. Science *317*, 381–384.

Merkle, F.T., Fuentealba, L.C., Sanders, T.A., Magno, L., Kessaris, N., and Alvarez-Buylla, A. (2014). Adult neural stem cells in distinct microdomains generate previously unknown interneuron types. Nat Neurosci *17*, 207–214.

Meyuhas, O. (2000). Synthesis of the translational apparatus is regulated at the translational level. Eur. J. Biochem. *267*, 6321–6330.

Ming, G.-L., and Song, H. (2011). Adult Neurogenesis in the Mammalian Brain: Significant Answers and Significant Questions. Neuron *70*, 687–702.

Mirzadeh, Z., Doetsch, F., Sawamoto, K., Wichterle, H., and Alvarez-Buylla, A. (2010). The subventricular zone en-face: wholemount staining and ependymal flow. JoVE.

Mirzadeh, Z., Merkle, F.T., Soriano-Navarro, M., Garcia-Verdugo, J.M., and Alvarez-Buylla, A. (2008). Neural Stem Cells Confer Unique Pinwheel Architecture to the Ventricular Surface in Neurogenic Regions of the Adult Brain. Cell Stem Cell *3*, 265–278.

Mori, K., Nagao, H., and Yoshihara, Y. (1999). The olfactory bulb: coding and processing of odor molecule information. Science *286*, 711–715.

Nandagopal, N., and Roux, P.P. (2015). Regulation of global and specific mRNA translation by the mTOR signaling pathway. Translation *3*, e983402.

Nathans, D. (1964). Puromycin inhibition of protein synthesis: incorporation of puromycin into peptide chains. Proc. Natl. Acad. Sci. U.S.a. *51*, 585–592.

Nissant, A., and Pallotto, M. (2011). Integration and maturation of newborn neurons in the adult olfactory bulb - from synapses to function. Eur J Neurosci *33*, 1069–1077.

Okano, H., Kawahara, H., Toriya, M., Nakao, K., Shibata, S., and Imai, T. (2005). Function of RNA-binding protein Musashi-1 in stem cells. Experimental Cell Research *306*, 349–356.

Paliouras, G.N., Hamilton, L.K., Aumont, A., Joppe, S.E., Barnabe-Heider, F., and Fernandes, K.J.L. (2012). Mammalian Target of Rapamycin Signaling Is a Key Regulator of the Transit-Amplifying Progenitor Pool in the Adult and Aging Forebrain. J. Neurosci. *32*, 15012–15026.

Pause, A., Belsham, G.J., Gingras, A.C., Donzé, O., Lin, T.A., Lawrence, J.C., and Sonenberg, N. (1994). Insulin-dependent stimulation of protein synthesis by phosphorylation of a regulator of 5'-cap function. Nature *371*, 762–767.

Peltier, J., O'Neill, A., and Schaffer, D.V. (2007). PI3K/Akt and CREB regulate adult neural hippocampal progenitor proliferation and differentiation. Dev Neurobiol *67*, 1348–1361.

Perrière, N., Demeuse, P., Garcia, E., Regina, A., Debray, M., Andreux, J.-P., Couvreur, P., Scherrmann, J.-M., Temsamani, J., Couraud, P.-O., et al. (2005). Puromycin-based purification of rat brain capillary endothelial cell cultures. Effect on the expression of blood-brain barrier-specific properties. J. Neurochem. *93*, 279–289.

Petreanu, L., and Alvarez-Buylla, A. (2002). Maturation and death of adult-born olfactory bulb granule neurons: role of olfaction. J. Neurosci. *22*, 6106–6113.

Picelli, S., Faridani, O.R., rklund, A.S.K.B.O., Winberg, G.O.S., Sagasser, S., and Sandberg, R. (2014). Full-length RNA-seq from single cells usingSmart-seq2. Nat Protoc *9*, 171–181.

Pierfelice, T., Alberi, L., and Gaiano, N. (2011). Notch in the vertebrate nervous system: an old dog with new tricks. Neuron *69*, 840–855.

Retz, K.C., and Steele, W.J. (1980). Ribosome turnover in rat brain and liver. Life Sci. *27*, 2601–2604.

Richter, J.D. (1999). Cytoplasmic polyadenylation in development and beyond. Microbiol. Mol. Biol. Rev. *63*, 446–456.

Richter, J.D., and Lasko, P. (2011). Translational control in oocyte development. Cold Spring Harb Perspect Biol *3*, a002758.

Ritchie, M.E., Phipson, B., Wu, D., Hu, Y., Law, C.W., Shi, W., and Smyth, G.K. (2015). limma powers differential expression analyses for RNA-sequencing and microarray studies. Nucleic Acids Research *43*, e47.

Rochefort, C., Gheusi, G., Vincent, J.-D., and Lledo, P.-M. (2002). Enriched odor exposure increases the number of newborn neurons in the adult olfactory bulb and improves odor memory. J. Neurosci. *22*, 2679–2689.

Rolfe, D.F., and Brown, G.C. (1997). Cellular energy utilization and molecular origin of standard metabolic rate in mammals. Physiological Reviews *77*, 731–758.

Sakakibara, S.-I., Nakamura, Y., Yoshida, T., Shibata, S., Koike, M., Takano, H., Ueda, S., Uchiyama, Y., Noda, T., and Okano, H. (2002). RNA-binding protein Musashi family: roles for CNS stem cells and a subpopulation of ependymal cells revealed by targeted disruption and antisense ablation. Proc. Natl. Acad. Sci. U.S.a. *99*, 15194–15199.

Sampath, P., Pritchard, D.K., Pabon, L., Reinecke, H., Schwartz, S.M., Morris, D.R., and Murry, C.E. (2008). A Hierarchical Network Controls Protein Translation during Murine Embryonic Stem Cell Self-Renewal and Differentiation. Cell Stem Cell *2*, 448–460.

Sanchez, C.G., Teixeira, F.K., Czech, B., Preall, J.B., Zamparini, A.L., Seifert, J.R.K., Malone, C.D., Hannon, G.J., and Lehmann, R. (2015). Regulation of Ribosome Biogenesis and Protein Synthesis Controls Germline Stem Cell Differentiation. Cell Stem Cell.

Sanz, E., Evanoff, R., Quintana, A., Evans, E., Miller, J.A., Ko, C., Amieux, P.S., Griswold, M.D., and McKnight, G.S. (2013). RiboTag Analysis of Actively Translated mRNAs in Sertoli and Leydig Cells In Vivo. PLoS ONE *8*, e66179.

Sanz, E., Yang, L., Su, T., Morris, D.R., McKnight, G.S., and Amieux, P.S. (2009). Cell-type-specific isolation of ribosome-associated mRNA from complex tissues. Proc. Natl. Acad. Sci. U.S.a. *106*, 13939–13944.

Schmidt, E.K., Clavarino, G., Ceppi, M., and Pierre, P. (2009). SUnSET, a nonradioactive method to monitor protein synthesis. Nat Meth *6*, 275–277.

Schwanhäusser, B., Busse, D., Li, N., Dittmar, G., Schuchhardt, J., Wolf, J., Chen, W., and Selbach, M. (2011). Global quantification of mammalian gene expression control. Nature *473*, 337–342.

Shi, Z., and Barna, M. (2015). Translating the Genome in Time and Space: Specialized Ribosomes, RNA Regulons, and RNA-Binding Proteins. Annu. Rev. Cell Dev. Biol. *31*, 31–54.

Shigeoka, T., Jung, H., Jung, J., Turner-Bridger, B., Ohk, J., Lin, J.Q., Amieux, P.S., and Holt, C.E. (2016). Dynamic Axonal Translation in Developing and Mature Visual Circuits. Cell *166*, 181–192.

Shin, J., Berg, D.A., Zhu, Y., Shin, J.Y., Song, J., Bonaguidi, M.A., Enikolopov, G., Nauen, D.W., Christian, K.M., Ming, G.-L., et al. (2015). Single-Cell RNA-Seq with Waterfall Reveals Molecular Cascades underlying Adult Neurogenesis. Cell Stem Cell *17*, 360–372.

Signer, R.A.J., Magee, J.A., Salic, A., and Morrison, S.J. (2014). Haematopoietic stem cells require a highly regulated protein synthesis rate. Nature *509*, 49–54.

Starck, S.R., Green, H.M., Alberola-Ila, J., and Roberts, R.W. (2004). A General Approach to Detect Protein Expression In Vivo Using Fluorescent Puromycin Conjugates. Chemistry & Biology *11*, 999–1008.

Sutton, M.A., and Schuman, E.M. (2006). Dendritic protein synthesis, synaptic plasticity, and memory. Cell *127*, 49–58.

Takahashi, K., and Yamanaka, S. (2006). Induction of pluripotent stem cells from mouse embryonic and adult fibroblast cultures by defined factors. Cell *126*, 663–676.

TAYLOR, E.W. (1963). Relation of protein synthesis to the division cycle in mammalian cell cultures. J. Cell Biol. *19*, 1–18.

Tcherkezian, J., Cargnello, M., Romeo, Y., Huttlin, E.L., Lavoie, G., Gygi, S.P., and Roux, P.P. (2014). Proteomic analysis of cap-dependent translation identifies LARP1 as a key regulator of 5'TOP mRNA translation. Genes & Development *28*, 357–371.

Thoreen, C.C., Chantranupong, L., Keys, H.R., Wang, T., Gray, N.S., and Sabatini, D.M. (2012). A unifying model for mTORC1-mediated regulation of mRNA translation. Nature *485*, 109–113.

Thoreen, C.C., Kang, S.A., Chang, J.W., Liu, Q., Zhang, J., Gao, Y., Reichling, L.J., Sim, T., Sabatini, D.M., and Gray, N.S. (2009). An ATP-competitive mammalian target of rapamycin inhibitor reveals rapamycin-resistant functions of mTORC1. J. Biol. Chem. *284*, 8023–8032.

Turner, P.V., Brabb, T., Pekow, C., and Vasbinder, M.A. (2011). Administration of substances to laboratory animals: routes of administration and factors to consider. J. Am. Assoc. Lab. Anim. Sci. *50*, 600–613.

Van Nostrand, E.L., Pratt, G.A., Shishkin, A.A., Gelboin-Burkhart, C., Fang, M.Y.,

Sundararaman, B., Blue, S.M., Nguyen, T.B., Surka, C., Elkins, K., et al. (2016). robust transcriptome-wide discovery of rnA-binding protein binding sites with enhanced cliP (ecliP). Nat Meth 1–9.

Verma, P., Chierzi, S., Codd, A.M., Campbell, D.S., Meyer, R.L., Holt, C.E., and Fawcett, J.W. (2005). Axonal protein synthesis and degradation are necessary for efficient growth cone regeneration. J. Neurosci. *25*, 331–342.

Vessey, J.P., Amadei, G., Burns, S.E., Kiebler, M.A., Kaplan, D.R., and Miller, F.D. (2012). An asymmetrically localized Staufen2-dependent RNA complex regulates maintenance of mammalian neural stem cells. Cell Stem Cell *11*, 517–528.

Wang, X., Li, W., Williams, M., Terada, N., Alessi, D.R., and Proud, C.G. (2001). Regulation of elongation factor 2 kinase by p90(RSK1) and p70 S6 kinase. The EMBO Journal *20*, 4370–4379.

Wei, W., Shin, Y.S., Xue, M., Matsutani, T., Masui, K., Yang, H., Ikegami, S., Gu, Y., Herrmann, K., Johnson, D., et al. (2016). Single-Cell Phosphoproteomics Resolves Adaptive Signaling Dynamics and Informs Targeted Combination Therapy in Glioblastoma. Cancer Cell *29*, 563–573.

Widdowson, E.M., McCance, R.A., and Spray, C.M. (1951). The chemical composition of the human body. Clin Sci *10*, 113–125.

Yamaguchi, M., and Mori, K. (2005). Critical period for sensory experience-dependent survival of newly generated granule cells in the adult mouse olfactory bulb. Proc. Natl. Acad. Sci. U.S.a. *102*, 9697–9702.

Yang, G., Smibert, C.A., Kaplan, D.R., and Miller, F.D. (2014). An eIF4E1/4E-T Complex Determines the Genesis of Neurons from Precursors by Translationally Repressing a Proneurogenic Transcription Program. Neuron *84*, 723–739.

Ye, J., and Blelloch, R. (2014). Regulation of pluripotency by RNA binding proteins. Cell Stem Cell *15*, 271–280.

Yoshioka, H., Niizuma, K., Katsu, M., Sakata, H., Okami, N., and Chan, P.H. (2011). Consistent Injury to Medium Spiny Neurons and White Matter in the Mouse Striatum after Prolonged

Transient Global Cerebral Ischemia. Journal of Neurotrauma *28*, 649–660.

Zhang, K.X., Tan, L., Pellegrini, M., Zipursky, S.L., and McEwen, J.M. (2016). Rapid Changes in the Translatome during the Conversion of Growth Cones to Synaptic Terminals. CellReports *14*, 1258–1271.

Zhang, Q., Shalaby, N.A., and Buszczak, M. (2014). Changes in rRNA transcription influence proliferation and cell fate within a stem cell lineage. Science *343*, 298–301.

Zhou, P., Zhang, Y., Ma, Q., Gu, F., Day, D.S., He, A., Zhou, B., Li, J., Stevens, S.M., Romo, D., et al. (2013). Interrogating translational efficiency and lineage-specific transcriptomes using ribosome affinity purification. Proc. Natl. Acad. Sci. U.S.a. *110*, 15395–15400.

Zhu, G., Chow, L.M.L., Bayazitov, I.T., Tong, Y., Gilbertson, R.J., Zakharenko, S.S., Solecki, D.J., and Baker, S.J. (2012). Pten deletion causes mTorc1-dependent ectopic neuroblast differentiation without causing uniform migration defects. Development *139*, 3422–3431.

Zismanov, V., Chichkov, V., Colangelo, V., Jamet, S., Wang, S., Syme, A., Koromilas, A.E., and Crist, C. (2016). Phosphorylation of eIF2α Is a Translational Control Mechanism Regulating Muscle Stem Cell Quiescence and Self-Renewal. Cell Stem Cell *18*, 79–90.

Zong, Q., Schummer, M., Hood, L., and Morris, D.R. (1999). Messenger RNA translation state: the second dimension of high-throughput expression screening. Proc. Natl. Acad. Sci. U.S.a. *96*, 10632–10636.